Universidade de Aveiro Departamento de Química
2019

Pedro Miguel Oliveira Gomes

Novas moléculas para diagnóstico da doença de Alzheimer por Tomografia de Emissão de Positrões

New molecules for diagnosis of Alzheimer's disease by Positron Emission Tomography (PET)

Universidade de Aveiro Departamento de Química
2019

Pedro Miguel Oliveira Gomes

Novas moléculas para diagnóstico da doença de Alzheimer por Tomografia de Emissão de Positrões

New molecules for diagnosis of Alzheimer's disease by Positron Emission Tomography (PET)

Dissertação apresentada à Universidade de Aveiro para cumprimento dos requisitos necessários à obtenção do grau de Mestre em Bioquímica, com especialização em Bioquímica Clínica, realizada sob a orientação científica da Doutora Vera Lúcia Marques da Silva, Professora Auxiliar do Departamento de Química da Universidade de Aveiro e coorientação científica do Professor Doutor Artur Manuel Soares da Silva, Professor Catedrático do Departamento de Química da Universidade de Aveiro

o júri

presidente

Prof. Doutor Francisco Manuel Lemos Amado
professor associado c/ agregação do Departamento de Química da Universidade de Aveiro

Prof. Doutora Vera Lúcia Marques da Silva
professora auxiliar do Departamento de Química da Universidade de Aveiro

Prof. Doutora Clementina Maria Moreira dos Santos
professora adjunta da Escola Superior Agrária do Instituto Politécnico de Bragança

agradecimentos

À Doutora Vera L. M. Silva, orientadora desta dissertação, agradeço todo o apoio, dedicação e atenção prestados. Agradeço também por todos os ensinamentos, quer práticos quer teóricos, que me transmitiu ao longo deste tempo todo. Por fim, um enorme agradecimento por toda a compreensão demonstrada ao longo deste percurso. Foi sem dúvida o apoio mais importante durante esta dissertação.

Ao Professor Doutor Artur M. S. Silva, coorientador desta dissertação, agradeço a sua orientação científica.

À Doutora Susana M. Cardoso agradeço todo o apoio prestado nos estudos sobre atividade antioxidante apresentados nesta dissertação.

Ao Dr. Hilário Tavares e à Dra. Cristina Barros, agradeço por toda a disponibilidade e contributo prestados na obtenção dos espetros de RMN e espetros de massa, respetivamente.

À Dra. Maria Manuela Marques por toda a simpatia e disponibilidade em pesar quantidades mínimas dos compostos sintetizados, indispensáveis para realização dos testes de atividade antioxidante.

Agradeço também a todas as minhas colegas de laboratório por todo o apoio e boa disposição neste longo percurso.

A todos os outros elementos do grupo de Química Orgânica com quem privei, agradeço todas as palavras de apoio e sugestões que me endereçaram nesta dissertação.

Por fim agradeço à minha família, em particular aos meus pais e namorada por todo o apoio, por toda a paciência, por todas as chamadas de atenção e por toda a inspiração que me permitiram concluir esta dissertação, o fim de mais uma etapa da minha vida.

palavras-chave

Doença de Alzheimer, stress oxidativo, beta-amilóide, placas senis, tomografia de emissão de positrões, pirazóis, flúor-18, radiofármacos

resumo

A doença de Alzheimer é a mais prevalente forma de demência afetando atualmente 50 milhões de pessoas, ocorrendo um novo caso a cada 3 segundos. As previsões apontam para 152 milhões de pessoas em 2050. Existem duas formas da doença de Alzheimer: familiar ou esporádica. Quanto à forma familiar as suas principais causas são mutações genéticas, já quanto à forma esporádica sabe-se que o stress oxidativo tem um papel muito importante, sendo uma causa e consequência da doença, ativando vias de sinalização que promovem a agregação de péptidos Aβ promovendo a formação de placas senis e agregados neurofibrilares (NFTs) de proteína Tau, duas características da doença de Alzheimer. O diagnóstico destas placas pode ser feito por Tomografia de Emissão de Positrões (PET, derivado da sigla inglesa).

PET é um exame imagiológico, usado na medicina nuclear, que utiliza um radiofármaco, composto contendo um radionuclídeo, que emite um positrão no momento da sua desintegração, o qual é detetado para formar as imagens do exame. Esta técnica tem vindo a ser cada vez mais utilizada no diagnóstico e monitorização de várias doenças. Devido ao curto tempo de semi-vida do carbono-11, um dos radionuclídeos mais usados em diagnóstico, é necessário desenvolver novos radiofármacos contendo radioisótopos com maior tempo de semi-vida como o flúor-18 (^{18}F). Alguns pirazóis têm sido usados como radioligandos para detetar a atividade de certas enzimas e a concentração de recetores cerebrais através de PET com resultados encorajadores. Além disso, os pirazóis são conhecidos pelas diversas atividades biológicas que possuem, incluindo atividade antioxidante.

Assim, este trabalho teve como primeiro objetivo a síntese, do 5(3)-(4-fluorofenil)-3(5)-(2-hidroxifenil)-1*H*-pirazol, do (*E*)-5(3)-(4-fluoroestiril)-3(5)-(2-hidroxifenil)-1*H*-pirazol e do (*E*)-4-(4-fluoroestiril)-3(5)-(2-hidroxifenil)-1*H*-pirazol e a avaliação da sua atividade antioxidante. Com base nos resultados obtidos, foi selecionado o (*E*)-4-(4-fluoroestiril)-3(5)-(2-hidroxifenil)-1*H*-pirazol, o composto mais ativo, para transformação em precursores apropriados para a marcação com flúor-18 através de reações de substituição alifática nucleofílica. A preparação desses precursores envolveu reações de alquilação deste pirazol para introdução de cadeias alquílicas de 2 ou 6 átomos de carbono com um grupo hidroxilo terminal, seguido de tosilação do grupo hidroxilo. Foi ainda proposta uma metodologia para a síntese de precursores destes pirazóis apropriados para marcação com flúor-18 via reações de substituição aromática nucleofílica.

Posteriormente, foram efetuados estudos para avaliar o efeito da introdução das cadeias alquílicas na atividade antioxidante destes compostos. O estudo da atividade antioxidante dos compostos sintetizados consistiu na avaliação da capacidade de captação dos radicais ácido 2,2'-azino-bis(3-etilbenzotiazolina-6-sulfónico) ($ABTS^{+\bullet}$) e $NO^{\bullet}$. Os valores obtidos foram expressos em função da concentração de composto que promoveu 50% de captação dos radicais (IC_{50}) para serem estabelecidas algumas relações estrutura-atividade biológica.

Os novos compostos obtidos foram ainda caracterizados por técnicas de espectroscopia de ressonância magnética nuclear (RMN) mono- (^{1}H e ^{13}C) e bidimensionais (HMBC e HSQC) e, sempre que possível, por espetrometria de massa e espetrometria de massa de alta resolução.

Os resultados evidenciaram que os pirazóis sintetizados apresentam potencial como agentes antioxidantes, em particular como captadores do radical $NO^{\bullet}$ e que o tamanho da cadeia alquílica tem efeito na atividade antioxidante. Os derivados contendo cadeias alquílicas mais curtas (2 átomos de carbono) foram mais ativos. Este trabalho conduziu à obtenção de pirazóis que serão marcados com o radionuclídeo ^{18}F para serem testados no diagnóstico de agregados proteicos (placas senis) em modelos animais, com vista a avaliar o seu potencial para utilização no diagnóstico da doença de Alzheimer usando a tomografia de emissão de positrões.

keywords

Alzheimer's disease, oxidative stress, beta-amyloid, senile plaques positron emission tomography, pyrazoles, fluorine-18, radiopharmaceuticals

abstract

Alzheimer's disease is the most prevalent form of dementia currently affecting 50 million people, with a new case occurring every 3 seconds. Forecasts point to 152 million people by 2050. There are two forms of Alzheimer's disease: familial or sporadic. The main causes of familial form are genetic mutations, while for the sporadic form it is known that oxidative stress plays a key role, being a cause and consequence of the disease, activating signaling pathways that promote the aggregation of Aβ peptides promoting the formation of senile plaques and neurofibrillary aggregates (NFTs) of Tau protein, two hallmarks of Alzheimer's disease. These plaques can be diagnosed by Positron Emission Tomography (PET).

PET is a nuclear medicine functional imaging technique which uses a radiopharmaceutical, a compound containing a radionuclide, that emits a positron at the moment of its disintegration, which is detected to form the images of the analysis. This technique has been increasingly used in the diagnosis and monitoring of various diseases. Due to the short half-life of carbon-11, one of the most commonly used radionuclides in diagnosis, it is necessary to develop new radiopharmaceuticals containing longer half-life radionuclides such as fluorine-18 (^{18}F).

Some pyrazoles have been used as radioligands to detect the activity of certain enzymes and the concentration of brain receptors by PET with encouraging results. In addition, pyrazoles are known for their several biological activities, including antioxidant activity.

Thus, the first aim of this work was the synthesis of 5(3)-(4-fluorophenyl)-3(5)-(2-hydroxyphenyl)-1*H*-pyrazole, of (*E*)-5(3)-(4-fluorostyryl)-3(5)-(2-hydroxyphenyl)-1*H*-pyrazole and (*E*)-4-(4-fluorostyryl)-3(5)-(2-hydroxyphenyl)-1*H*-pyrazole and evaluation of their antioxidant activity. Based on the obtained results, the (*E*)-4-(4-fluorostyryl)-3(5)-(2-hydroxyphenyl)-1*H*-pyrazole, the most active compound, was selected for transformation into appropriate precursors for labelling with fluorine-18 through nucleophilic aliphatic substitution reactions. The preparation of such precursors involved alkylation reactions of this pyrazole for introduction of 2- or 6-carbon alkyl chains with a terminal hydroxy group, followed by tosylation of the hydroxy group. A methodology has also been proposed for the synthesis of precursors of these pyrazoles suitable for fluorine-18 labelling via nucleophilic aromatic substitution reactions.

Afterward, studies were conducted to evaluate the effect of the introduction of alkyl chains on the antioxidant activity of these compounds. The study of the antioxidant activity of the synthesized compounds consisted of the evaluation of the scavenging capacity of 2,2'-azino-bis(3-ethylbenzothiazoline-6-sulfonic acid) ($ABTS^{+\bullet}$) and nitric oxide ($NO^{\bullet}$) radicals. The values obtained were expressed as a function of the concentration of compound that promoted 50% of radical scavenging (IC_{50}) to establish some

structure-biological activity relationships.
The new obtained compounds were further characterized by mono- (^{1}H and ^{13}C) and two-dimensional (HMBC and HSQC) nuclear magnetic resonance (NMR) spectroscopy techniques and, whenever possible, by mass spectrometry and high resolution mass spectrometry.
The results showed that the synthesized pyrazoles have potential as antioxidant agents, in particular as $NO^{\bullet}$ radical scavengers and that the size of the alkyl chain has an effect on the antioxidant activity. Derivatives containing shorter alkyl chains (2 carbon atoms) were more active. This work led to the preparation of pyrazoles which will be labelled with the ^{18}F radionuclide to be tested in the diagnosis of protein aggregates (senile plaques) in animal models to assess its potential for use in the diagnosis of Alzheimer's disease using positron emission tomography.

Index

Abbreviations

δ	Chemical shift from tetramethylsilane (ppm)
^{1}H NMR	Nuclear magnetic resonance spectroscopy of hydrogen-1
^{13}C NMR	Nuclear magnetic resonance spectroscopy of carbon-13
^{19}F NMR	Nuclear magnetic resonance spectroscopy of fluorine-19
4-PPy	4-Pyrrolidinopyridine
ABTS	2,2'-Azino-bis(3-ethylbenzothiazoline-6-sulphonic acid)
AD	Alzheimer's disease
ADP	Adenosine diphosphate
AICD	Aminoterminal APP intracellular domain
APP	Amyloid precursor protein
AR	Adenosine receptor
ATP	Adenosine triphosphate
Aβ	Beta-amyloid
AβDPs	Aβ-degrading proteases
BBB	Blood-brain-barrier
br	Broad
cAMP	Cyclic adenosine monophosphate
CB1	Cannabinoid receptor type 1
CB2	Cannabinoid receptor type 2
cGMP	Cyclic guanosine monophosphate
CNS	Central nervous system
Cu-Zn SOD	Copper-zinc superoxide dismutase
CYP	Cytochrome P450
DCM	Dichloromethane
d	Doublet
dd	Doublet of doublets
DDC	Dicyclohexylcarbodiimide
ddd	Doublet of doublets of doublets
DMSO	Dimethyl sulfoxide
DNA	Deoxyribonucleic acid

dt	Doublet of triplets
EMA	European Medicines Agency
eNOS	Endothelial nitric oxide synthase
equiv	Molar equivalent
FAD	Familial Alzheimer's disease
FDA	Food and Drug Administration
FDG	Fluorodeoxyglucose
FTLD	Frontotemporal lobar degeneration
GLUT	Glucose transporter
GSH	Glutathione
GSSG	Oxidized glutathione
h	Hours
HMBC	Heteronuclear Multiple Bond Correlation
HPLC	High Pressure Liquid Chromatography
HRMS	High Resolution Mass Spectrometry
HSQC	Heteronuclear Single Bond Correlation
IC_{50}	Inhibitory concentration of 50% of activity
iNOS	Inducible nitric oxide synthase
IUPAC	International Union of Pure and Applied Chemistry
J	Coupling constant (Hz)
LDL	Low density lipoproteins
m	Multiplet
MCI	Mild-cognitive impairment
min	Minute
Mn-SOD	Manganese superoxide dismutase
MS	Mass Spectrometry
m.p	Melting point
m/z	Mass/charge ratio (mass spectrometry)
NAD^+	Nicotinamide adenine dinucleotide
NADPH	Reduced nicotinamide adenine dinucleotide phosphate
NFTs	Neurofibrillary tangles
NMDA	N-methyl-D-aspartate

nNOS	Neuronal nitric oxide synthase
NOS	Nitric oxide synthase
PARP-1	Poly(ADPribose)polymerase 1
PDE10A	Phosphodiesterase-10A
PET	Positron emission tomography
ppm	Parts per million
PP1	Protein phosphatase 1
PS-1	Presenilin-1
PS-2	Presenilin-2
PSD95	Postsynaptic density protein 95
p-TsCl	*p*-Toluenesulfonyl chloride
quint	Quintet
RF	Retention factor
RNA	Ribonucleic acid
RNS	Reactive nitrogen species
ROS	Reactive oxygen species
r.t	Room Temperature
s	Singlet
SAD	Sporadic Alzheimer's disease
SNP	Sodium nitroprusside
SOD	Superoxide dismutase
t	Triplet
TBAF	Tetra-*N*-butylammonium fluoride
t-BuOK	Potassium *tert*-butoxide
TEA	Triethylamine
THF	Tetrahydrofuran
TLC	Thin-layer chromatography
TSPO	Translocator protein

Preamble

This master's thesis is divided into six chapters. The first chapter presents a brief introduction to Alzheimer's Disease (AD) and its hallmarks and to oxidative stress and antioxidant defence system. It also includes a description of positron emission tomography, a diagnosis technique used in nuclear medicine, its historical evolution and application as a tool for AD diagnosis. It also presents the most commonly used radioisotopes and radiopharmaceuticals as diagnostic probes, to detect the AD hallmarks, with special emphasis on pyrazole-type compounds.

The second chapter presents the nomenclature of the main compounds synthetized in this work, the description of the synthetic methods adopted to prepare the target compounds and their structural characterization.

The third chapter presents the methods used for the evaluation of the free radicals ($ABTS^{+\bullet}$, $NO^{\bullet}$) scavenging activity of the target compounds, in order to assess their potential as antioxidants. The results obtained in these studies are also presented and discussed.

The fourth chapter presents the main conclusions of this work and future perspectives.

The fifth chapter, which is the experimental section, contains the detailed experimental procedures followed for the synthesis of the target compounds and for the evaluation of their free radicals scavenging activity, as well as the data of their structural characterization. The sixth chapter includes the references cited in this master's thesis.

After the introduction, in the second chapter, the numbering of compounds will start over at number 1 for sake of simplicity.

Objectives of the work

In the last two decades, some work has been developed towards the synthesis and biological evaluation of (2-hydroxyphenyl)-4/5-phenyl/styrylpyrazoles. However, their antioxidant and anti-inflammatory activities remain unexplored, as well as their potential to treat neuropathological conditions. In previous studies, these type of pyrazoles have shown promising antioxidant activity and some derivatives have presented affinity, in the nanomolar range, for CB_1 receptors which are located in higher density in the brain. [1][2]

Inspired by these previous results and based on the findings described throughout Chapter one, "Introduction", we have decided to select (2-hydroxyphenyl)pyrazoles as scaffolds for the development of new molecules for diagnosis of AD by Positron Emission Tomography (PET). Thus, the objective of this work is the synthesis and structural characterization of a series of novel fluorinated (2-hydroxyphenyl)pyrazoles (Figure 1) in order to test their radical scavenging ability towards $ABTS^{+\bullet}$ and $NO^{\bullet}$. It is known that oxidative stress is involved in the pathogenesis of AD and in this sense it is of our interest to develop compounds that have both functionalities (diagnosis and therapeutic)-theranostics. Among the synthetized compounds, the most promising will be selected to be labelled with ^{18}F to be tested as PET tracers for amyloid plaques in animal models. Labelling with ^{18}F requires the preparation of a suitable stable precursor that presents a group which can be easily replaced by ^{18}F when preparing the probe for PET imaging. Two strategies will be attempted for the synthesis of these precursors: i) alkylation of the pyrazole to introduce an alkyl chain with a terminal hydroxy group, followed by tosylation and introduction of fluorine (^{19}F, and later ^{18}F) by nucleophilic aliphatic substitution and ii) preparation of a sydnone-type precursor and introduction of fluorine by nucleophilic aromatic substitution (Figure 2). At the end of this work, a series of (2-hydroxyphenyl)pyrazole-type compounds will be available in sufficient amount for affinity and specificity studies towards proteins aggregates which should be performed before PET studies in animal models.

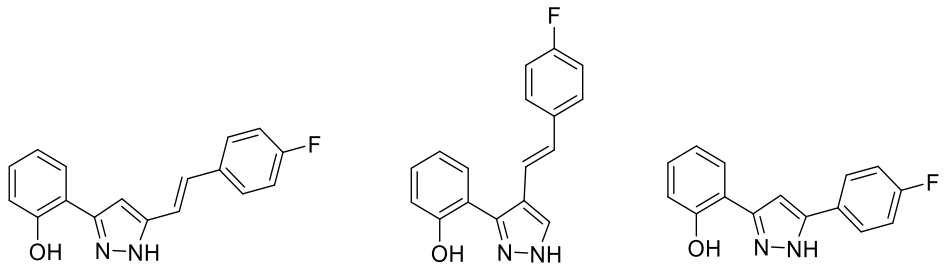

Figure 1: Fluorinated-(2-hydroxyphenyl)pyrazoles to be prepared in this work

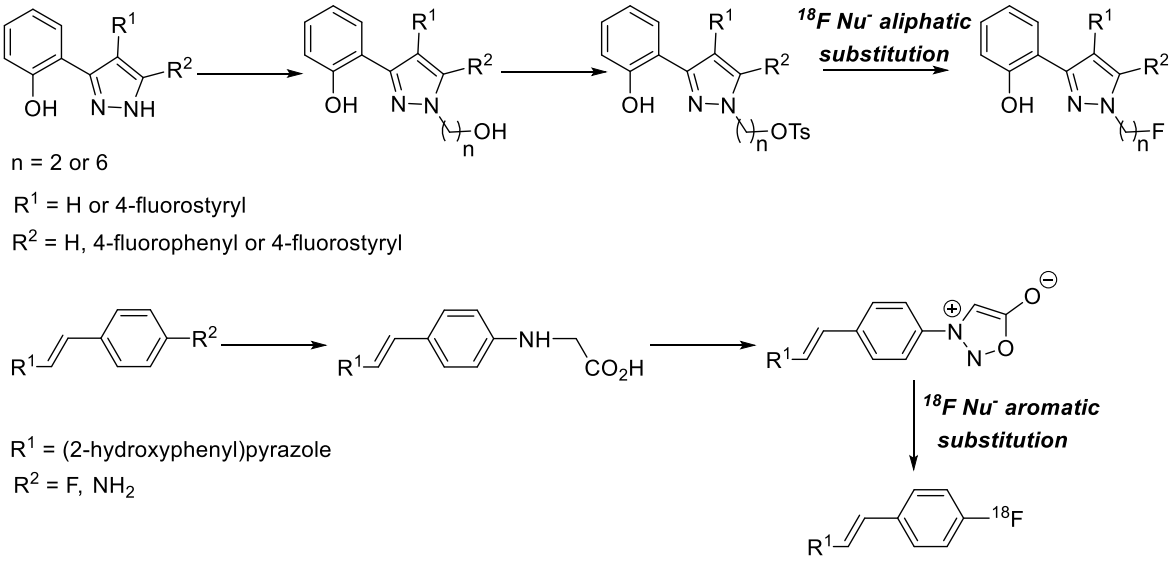

Figure 2: Strategies for the preparation of ^{18}F-pyrazoles for PET imaging

Chapter 1 - Introduction

1.1 Alzheimer's disease

According to the World Alzheimer Report of 2018, 50 million people in the world live with dementia. Alzheimer's disease (AD) is the most prevalent form of dementia, affecting two thirds of population. Forecasts indicate that, in 2050, about 152 million people will suffer from dementia. Nowadays, there's a new case of AD in the world every 3 seconds. AD is becoming America's most feared disease killing more people than breast and prostate cancer combined. It entails a cost of nearly a trillion US dollars a year. [3] AD is characterized by two aberrant structures in the brains of patients: senile plaques and neurofibrillary tangles being the latter used in the postmortem diagnosis of the disease. [4] AD can be divided in two types: familial Alzheimer's disease (FAD) and sporadic Alzheimer's disease (SAD). In the familial type the cause of the disease is the presence of mutations in one of three genes identified as amyloid precursor protein (APP) and presenilin-1 and -2 (PS-1 and PS-2). On the other hand, the knowledge about the etiology of sporadic form is very limited. Because the burden of disease in individuals increases with age, many researchers have postulated that oxidative stress may be involved in the process of aging as well as certain diseases related to advanced age, such as AD. [5]

1.1.1 Oxidative stress and Alzheimer's disease

1.1.1.1 ROS and RNS generation

Oxidative stress is the result of an imbalance between the formation of reactive oxygen species (ROS) and reactive nitrogen species (RNS), and their neutralization by the antioxidant defenses (superoxide dismutase (SOD), glutathione system, catalase, thioredoxin peroxidases, vitamins A, C and E). [6] ROS are very important in many biological processes like cell growth, cell signaling, smooth muscle relaxation, immune responses, synthesis of biological molecules, and blood pressure modulation. [7] However, the oxidative stress produced by the accumulation of ROS in the body causes modifications on several biomolecules such as proteins, lipids and DNA. [8] The mitochondria is the organelle responsible for the formation of ATP and in that process 5% of O_2 used by mitochondria on oxidative phosphorylation escapes contributing to the formation of the superoxide anion ($O_2^{-\bullet}$). [9] That radical can be converted into hydrogen peroxide (H_2O_2) in two ways: direct reduction of oxygen molecule by two electrons or by dismutation of

superoxide anion in a reaction catalyzed by several enzymes as superoxide dismutase, glucose oxidase and many others. [9] Then hydrogen peroxide can be reduced to hydroxyl radical ($HO^{\bullet}$) one of the strongest natural oxidants. [10] This reduction is a chain reaction initiated by the reduction of Fe^{3+} to Fe^{2+} by the superoxide anion (Haber-Weiss reaction). Then Fe^{2+} reacts with hydrogen peroxide to form hydroxyl radical in a reaction called Fenton reaction. The net reaction shows that superoxide anion reacts with hydrogen peroxide to form hydroxyl radical. [11] On the other hand, superoxide anion can interact with nitric oxide ($NO^{\bullet}$) producing peroxynitrite (ONO_2^-) a molecule that is not a radical but is a very powerful oxidant. [12] Nitric oxide is formed from arginine in a reaction catalyzed by nitric oxide synthase (NOS). This enzyme has three isoforms: neuronal nitric oxide synthase (nNOS), the inducible nitric oxide synthase (iNOS), and the endothelial nitric oxide synthase (eNOS). Nitric oxide has a key role on several biological processes like regulation of vascular tone, cellular adhesion, vascular permeability, inhibition of platelet adhesion and can act has an antioxidant. This anti-inflammatory and regulatory function of nitric oxide occurs when concentration of this radical is low and redox balance is present. When concentration of nitric oxide increases this chemical species inhibits enzyme function, promotes DNA damage, reduce antioxidant defenses and can react with superoxide anion to produce a strong oxidant. [13] Peroxynitrite causes deleterious effects on the mitochondria due to oxidation, nitration and nitrosation of mitochondrial components. [14] These last two reactions involve free radicals and the reaction's pathway is initiated with the reaction of peroxynitrite with carbon dioxide that leads to rapid formation of carbonate ($CO_3^{\bullet -}$) and nitrogen dioxide ($^{\bullet}NO_2$) radicals. The CO_2 concentration is higher on mitochondria due to decarboxylation reactions of Krebs cycle and reactions catalyzed by pyruvate dehydrogenase. Thus peroxynitrite/CO_2 pathway is highly relevant on mitochondria. [12] On the other hand, ROS can have an exogenous origin like the intake of some drugs (e.g. some anthracyclines such as Adriamycin and Daunorubicin, Bleomycin, and antibiotics), anesthetics, photochemical air pollutants as ozone, hyperoxia, tobacco smoke, pesticides, solvents and aromatic hydrocarbons. [9]

1.1.1.2 Antioxidant defense

To prevent accumulation of oxidant species, the body has defense mechanisms-antioxidant systems- to neutralize these reactive species. These antioxidant systems can be

divided in two groups: enzymatic (endogenous origin) and nonenzymatic (exogenous origin). The enzymatic system includes superoxide dismutase (SOD), glutathione system, catalase and thioredoxin peroxidases which have a higher reactivity with ROS when compared with nonenzymatic system but are in lower concentrations. Vitamins, Coenzyme Q10, proteins and amino acids are the nonenzymatic antioxidants. [9] In brain, catalase is practically inexistent, therefore SOD and glutathione system have a key role on oxidative balance. SOD has two different forms: copper-zinc SOD (Cu-Zn SOD) found in the cytosol and cell membrane; and manganese SOD (Mn-SOD) found in mitochondrial matrix (Figure 3). Glutathione (GSH) is a tripeptide compound of glutamic acid, cysteine and glycine and our antioxidant system is formed by reduced GSH and two enzymes: GSH reductase and GSH peroxidase. The antioxidant defense starts with the reaction of superoxide anion with SOD forming H_2O_2. Then peroxide reacts with reduced GSH in a reaction catalyzed by the enzyme GSH peroxidase resulting in oxidized GSH and water. At that point the free radical was already converted in water preventing the oxidative damage. Oxidized GSH is reduced to GSH to continue converting peroxides in water. Oxidized GSH consists in two molecules of GSH linked by a disulfide bond (GSSG). To reduce GSSG into GSH is necessary NADPH, formed in pentose phosphate pathway, and the enzyme glutathione reductase maintaining the ratio GSH /GSSG. [9]

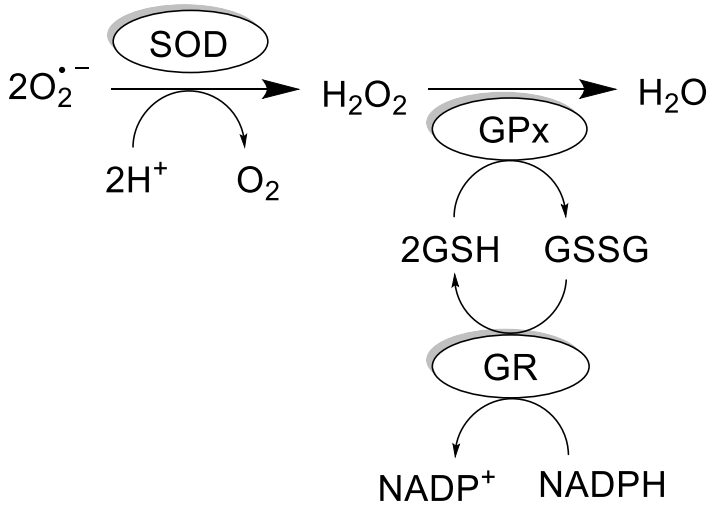

Figure 3: SOD mechanism and glutathione system.

Like ROS, antioxidant defenses can also have an exogenous origin. Vitamins A, C and E are the most significant exogenous antioxidants. Vitamin A comes from carotenes of different plants. This vitamin has a key role on the protection of LDL and its antioxidant potential prevents heart diseases. Vitamin E is a substitute lipid isoprenoid of the tocopherol

family. Its biological form is D-alpha tocopherol that has the capacity to react with lipid peroxyl radicals terminating the lipid peroxidation reactions and forming a tocopheroxyl radical which is insufficiently reactive to initiate lipid peroxidation itself. Vitamin C, also called ascorbic acid, is a glucose derivative and a free radical scavenger. This antioxidant in combination with GSH regenerates the tocopheroxyl radical formed by the action of vitamin E. Ascorbic acid has the capacity to donate an electron to a lipid radical forming one molecule of dehydroascorbate. [15]

In 2006, Barry listed 13 "brain problems" that make this organ highly vulnerable to oxidative stress: 1) the presence of excitotoxic amino acids that lead to neuronal necrosis; 2) neuronal mitochondria generates $O_2^{-\bullet}$; 3) several neurotransmitters react with $O_2^{-\bullet}$; 4) the presence of transition metals that are capable of catalyzing free radical reactions; 5) neuronal membrane lipids are rich in highly polyunsaturated fatty acid side-chains that are the main targets of free radicals; 6) brain metabolism generates high amount of H_2O_2 by the monoamine oxidases A and B, flavoprotein enzymes located in the outer mitochondrial membranes of neurons and glia; 7) modest antioxidant defenses particularly catalase; 8) microglia can become activated to produce $O_2^{-\bullet}$, H_2O_2 and cytokines such as interleukin-1, interleukin-6 and tumor necrosis factor α; 9) the presence of CYP2E1 that metabolizes ethanol, acetone, halothane and related anesthetics, and organic solvents such as CCl_4 and $CHCl_3$ producing more ROS than the other CYPs; 10) activation of matrix metalloproteinases that allow neurotoxins, endotoxin and inflammatory cells to enter the brain; 11) the presence of poly(ADPribose)polymerase-1 (PARP-1) that cleaves NAD^+ and attaches ADP-ribose residues to nuclear proteins to facilitate DNA repair (in case of overactivation of PARP-1 it can kill cells by depleting NAD^+); 12) loss of trophic support can lead to oxidative stress and apoptosis in neurons; 13) toxicity of hemoglobin that can be degraded on exposure to H_2O_2. A brief resume of the formation of reactive species responsible for oxidative stress and action of antioxidant defenses is presented in the next (Figure 4). [16]

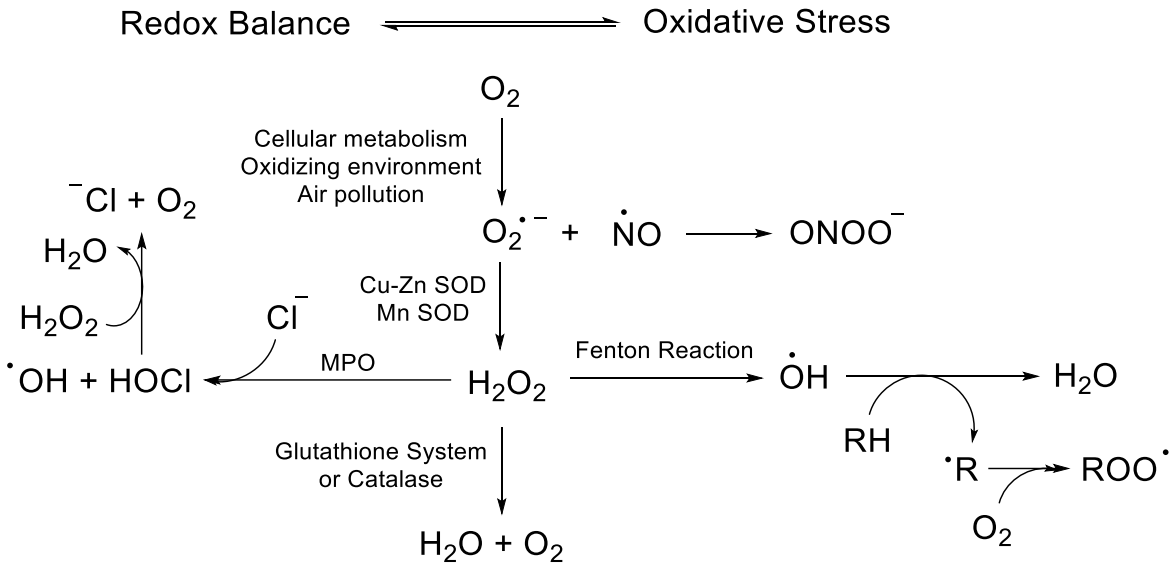

Figure 4: Resume of oxidative stress. Adapted from [9]

1.1.2 Hallmarks of Alzheimer's disease

The two principal hallmarks of AD are the presence of senile plaques and neurofibrillary tangles of Tau protein (NFTs). This protein is essential in the axonal transport of various organelles, such as mitochondria. According to the currently accepted hypothesis, the Tau protein is abnormally phosphorylated, then dissociated from the microtubules and aggregated into neurofibrillary tangles. The Tau protein has more than 45 phosphorylation sites that once phosphorylated affect the interaction of the protein with the microtubules. Phosphorylation of Tau protein is probably the earliest event of AD. In addition, evidences suggest a key role of phosphorylation of Tau protein during synaptic plasticity, specifically during long-term depression. Phosphorylated Tau protein can activate the N-methyl-D-aspartate (NMDA) receptor, through the PSD95-Fyn complex, allowing the entrance of Ca^{2+} on neurons. That excess of calcium leads to activation of protein phosphatase 1 (PP1) that increases the phosphorylation of Tau protein. This vicious cycle promotes the deposition of Tau protein that will lead to the blockade of the transport of organelles, namely mitochondria, leading to their dysfunction and subsequent energy deprivation and oxidative stress causing cell death. [17]

The senile plaques are composed mostly of a peptide called beta-amyloid (Aβ). [18] The Aβ peptide contains 43 amino acids being generated after enzymatic cleavage by β- and γ-secretases of the amyloid precursor protein (APP). This protein, a type 1 transmembrane,

is expressed mostly in the central nervous system (CNS) but is also expressed in other tissues to a shortest extent. [19] The physiological function of APP remains unknown, but this protein is thought to play a key role in brain synaptic plasticity. [20] The metabolism of APP occurs by two distinct pathways: non-amyloidogenic and amyloidogenic. In the non-amyloidogenic pathway, APP is cleaved by an α-secretase and subsequently by a γ-secretase forming the $A\beta_{17-40/42}$ peptide. On the other hand, after cleavage by α-secretase the peptide undergoes cleavage by a β-secretase forming the $A\beta_{1-16}$ peptide. In the less common route, the amyloidogenic pathway, the APP precursor is cleaved consecutively by β- and γ-secretases forming an $A\beta_{1-40/42}$ peptide. Both pathways originate, at first, aminoterminal fragments (secreted APP (sAPP), α or β), carboxyterminal fragments (respectively CTF83 or CTF99) and then the aminoterminal APP intracellular domain (AICD) (Figure 5). [21]

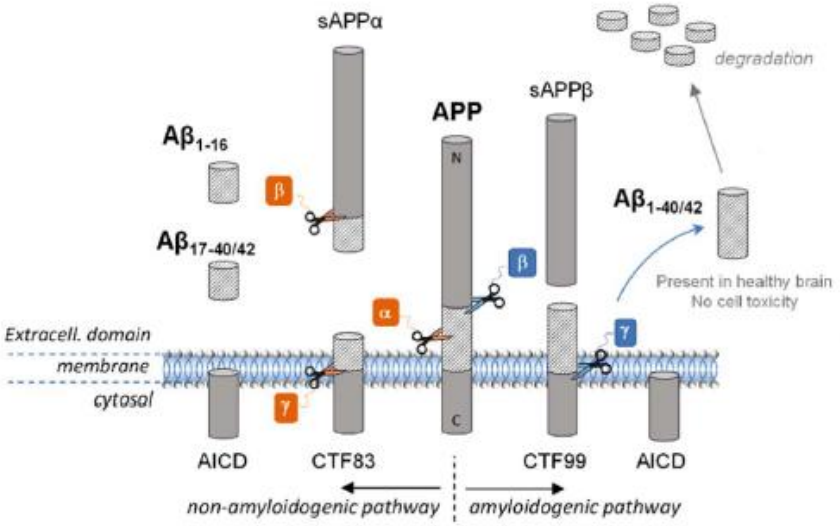

Figure 5: APP metabolism. Adapted from [18]

As previously stated, mutations in one of three genes identified as APP, PS-1 and PS-2 are the cause of FAD. These mutations increase $A\beta_{1-42}$ formation. [22] The amyloid cascade hypothesis was formulated in 1990s [23] and has become a dominant model for AD pathogenesis since Aβ was found in soluble form in healthy brain but aggregated in AD brains. [18]. According to this hypothesis, there is an abnormal increase of Aβ levels that leads to Aβ aggregation into β-sheet rich structures. The Aβ peptides, which were not degraded by Aβ-degrading proteases (AβDPs), can interact with some metals like Cu and Zn forming oligomers and then Aβ fibrils (Figure 6). These fibrils are a source of ROS due to entrapped redox-active metals present in fibrils. In addition, deposition of senile plaques starts an inflammatory response increasing the accumulation of ROS. [24] Nowadays, Aβ

plaques are used as biomarkers for detection of AD, *in vivo*, by using nuclear medicine imaging techniques such as positron emission tomography (PET). [25], [26]

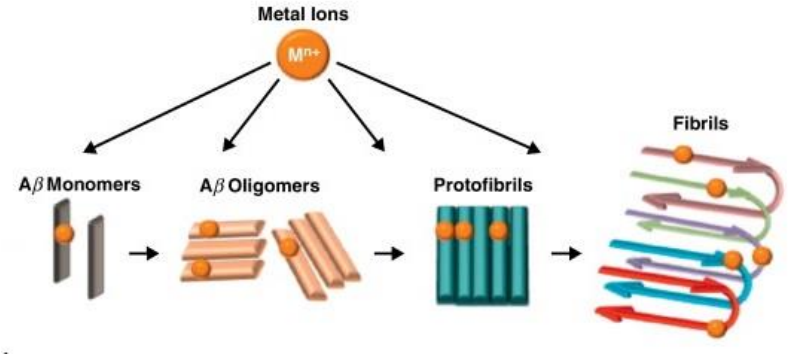

Figure 6: Role of metals in fibrils formations. Adapted from [27]

1.2 Positron emission tomography

Positron emission tomography (PET) is a nuclear medicine functional imaging technique that uses radiation - gamma rays (formed as a result of the annihilation of the positrons emitted) to provide information about the functioning of a person's specific organs. It relies on the development of sensitive and specific probes (PET tracers) coupled with imaging hardware and software to provide information about the status of a disease, at molecular and metabolic levels, in vivo, and its response to therapy, which are important aspects of disease management. Since several organs, such as thyroid, bones, heart, liver, brain, among others can be easily imaged, and disorders in their function revealed, PET has been progressively more used.

In 1968, D. E. Kuhl and R. Edwards, at the University of Pennsylvania, were the first scientists who introduced the concept of emission and transmission tomography, taking advantage of several previous works. The development of this technique was acknowledged to scientists of different fields from physics, chemistry, biology to medicine. [28] In 1930s P. Dirac, a theoretical physicist, postulated the existence of "positive electrons" – positrons – based on equations of quantum mechanics and Einstein's theory of relativity. [29] Two years later, at California Institute of Technology, C. D. Anderson observed experimentally that particles with the same mass of electrons move in a strong field along a path indicating the presence of a positive charge proving that P. Dirac was correct. These particles were named "positrons". [30] In 1930, Lawrence and co-workers created a "cyclotron", two D-shaped magnets that accelerate particles to produce progressively higher energy protons. As

Lawrence and his group improved their cyclotrons it was possible to produce and identify artificial radionuclides like carbon-11, nitrogen-13, oxygen-15, and fluorine-18 (^{11}C, ^{13}N, ^{15}O and ^{18}F, respectively). [31] In 1968, Kuhl and co-workers developed a tomographic scanner for the study of single photon emitting radiotracers. With this work, this group introduced a new form to arrange the detectors in a ring surrounding the patient's head. [32] The method of reconstruction was very primitive and mathematical algorithms used on computed tomography were later applied on PET. In 1975, Ter-Pogossian, Phelps and Hoffman design a new PET instrument which employed the filtered back projection method of reconstruction improving the primitive work made in 1968 (Figure 7). [33]

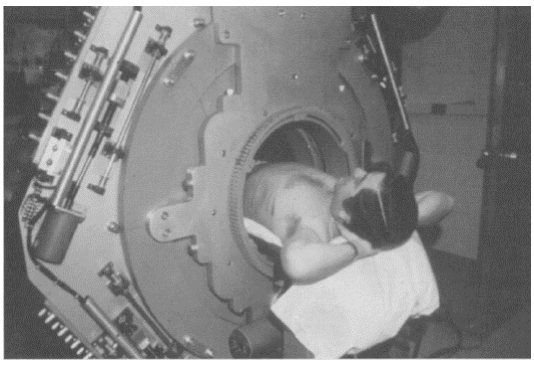

Figure 7: PET scanner developed by Ter-Pogossian and co-workers. Taken from [28]

PET is based on the detection of tiny amounts (picomolar) of biological substances labelled with a short-lived positron-emitting radionuclide (PET tracers) without perturbing biological system. PET has the advantage of being a non-invasive, functional and high sensitive technique [34]. In the last three decades the interest in PET has been growing and nowadays this technique is used in several areas as oncology [35], cardiology [36], neurology [26], drug development and evaluation [37]. Besides the several advantages of PET there are some disadvantages as: pregnant women should not undergo in PET imaging, the radioactivity of PET tracers limits the number of times one patient can undergo PET scans and finally PET imaging is a very expensive treatment. [38]

The PET tracers or probes, also known as radiopharmaceuticals, are biomolecules labelled with radionuclides such as ^{11}C, ^{13}N, ^{15}O, ^{18}F, ^{64}Cu, ^{68}Ga, ^{89}Zr and ^{124}I. Since radionuclides can replace the stable analogues, the PET probes have the same chemical structure as the drugs and biomolecules without altering their biological activity. The choice of the PET radionuclide must follow some criteria as physical and chemical characteristics, availability and timescale of the biological process in study. For different biological

processes some radionuclides are better than others. If the biological process in study gives results hours or days after the injection of PET probes, ^{64}Cu, ^{89}Zr or ^{124}I can be used because these three radionuclides have a long half-life time (12.8 h, 78.4 h and 4.17 days, respectively). Alternatively, radionuclides as ^{11}C or ^{18}F are used for labeling small organic compounds for faster biological process. [34] To avoid unnecessary irradiation it's important to choose a radionuclide with a half-life that enable the reaction of radionuclide with the carrier molecule and match the timescale of the biological process in study. ^{18}F is the ideal radionuclide for routine PET imaging because it has a short half-life (109.8 min.) but enough to allow all the process of syntheses, transport and imaging. Furthermore, it is a 97% positron-emitter and the low positron energy of ^{18}F leads to high resolution of PET imaging. [34], [39]

Once the PET probe is injected in a subject's body, it is incorporated into the normal biological processes and excreted in the usual ways. The amount of the PET probe/radionuclide given to a patient is just sufficient to obtain the required information before its decay by positron emission. [34] Thus, a radionuclide used for diagnosis must emit gamma rays of enough energy to escape from the body and it must have a half-life short enough for it to decay away soon after imaging is completed. When a positron collides with a nearby electron an annihilation reaction occurs. The energy of the positron influences the distance that positron will travel in tissue before it collides with electron. This distance is variable depending on the radionuclide; in case of ^{18}F is 1 mm, but in case of ^{15}O that distance is about 2 mm. [28] The annihilation reaction generates a pair of gamma rays, with an energy of 511 keV each, which travel in opposite directions. [40] That gamma rays are detected by two scintillation detectors which re-emitted the photon energy as visible light detected by photomultiplier tubes. In turn, this visible light is converted into an electric signal proportional to the incident photon energy. These events are reconstructed into 3D images that represent the spatial distribution of radioactive source in the studied subject (Figure 8). [34]

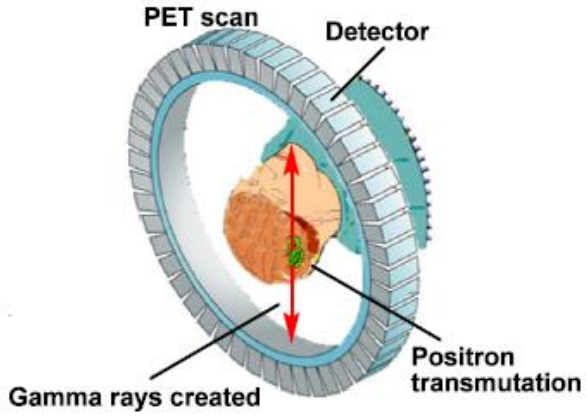

Figure 8: Detection of gamma rays in the PET scan. Taken from [34]

1.2.1 PET probes

Nowadays, there are several PET probes for diagnosis and monitoring of AD. Fluorodeoxyglucose (FDG) (Figure 9) is a glucose analogue having a fluorine atom at carbon-2 instead of the hydroxy group and was first described in 1969. [41] In 1977, FDG labelled with fluorine-18 (^{18}F), a radioactive fluorine-19 isotope, was prepared for the first time. [42] Brain uses glucose as the main source of energy and consumes about 25% of total glucose. [43] Transport of glucose across blood-brain-barrier (BBB) and intracellular catabolism are the two process that regulate cerebral glucose metabolism. Glucose transporters (GLUTs) are necessary to transport glucose. In the BBB, GLUT1 is the main glucose transporter. In case of neurons GLUT3, which has a higher affinity to glucose than GLUT1, is the main transporter on their membranes. FDG is transported to brain cells at the same rate of glucose where the hexokinase enzyme prevents the glucose and FDG from being released from the cells entering in the glycolytic process. The lack of hydroxyl group in carbon-2 blocks the progress of glycolytic process with FDG. [44] Once FDG is converted into FDG-6-phosphate cannot get out of cells until G-6-phosphatase reverse the phosphorylation or after FDG decays radioactively. Over the decay of FDG, fluorine is replaced by oxygen and after its reaction with a proton it is converted in glucose-6-phosphate and its metabolized normally. [45] The reduction of glucose metabolism is a typical finding on FDG PET in AD patients, being the posterior cingulate, hippocampus, and medial temporal regions the brains regions that first reveal that reduction. That metabolic deficit spread out across all brains structures. [46] The FDG radiopharmaceutical is also used on

treatment of ovarian cancer [47], in the clinical management of cancer [48] and infections [49].

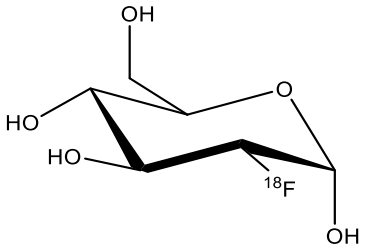

Figure 9: ^{18}F- Fluorodeoxyglucose (FDG)

1.2.1.1 Senile plaques probes

Senile plaques are one of the best biomarkers of AD. The accumulation of Aβ fibrils precedes symptoms of the disease, and therefore it is necessary to develop means of detection of those fibrils. Over the last decades, there have been developed some radiopharmaceuticals to diagnose the presence of senile plaques - amyloid PET imaging agents. These radiotracers have the ability of binding to that insoluble fibrils. [43]

The first amyloid imaging agent for PET was the ^{11}C-Pittsburgh Compound B (PiB) (Figure 10), synthetized in 2002 by Mathis and co-workers at the University of Pittsburgh. [50] PiB ($C_{14}H_{12}N_2OS$) is a fluorescent analogue of thioflavin-T labelled with the radionuclide ^{11}C, which has demonstrated a good affinity for fibrils Aβ both in mices [50] and in humans. [51] The results in mices were very promising increasing the interest in this compound. In 2004, was published the first study using PiB to detect the presence of amyloid deposits in humans. In this study, Klunk and his co-workers used 16 mild AD patients and 9 healthy patients for control. They have demonstrated discrimination between these two groups by performing PET studies using PiB as radiotracer. [51] One of the disadvantages of PiB is the radionuclide used on its synthesis. ^{11}C has a short half-life, approximately 20 minutes, limiting the access to a cyclotron and the lack of ^{11}C radiochemistry expertise. [52] To overcome this problem, ^{18}F, a radionuclide with a larger physical half-life (109.8 min) started to be used. The time of half-life of this radionuclide allowed the synthesis of several new radiopharmaceuticals but only three were approved for clinical use: ^{18}F-Florbetapir (**1**), ^{18}F-Florbetaben (**2**) and ^{18}F-Flutemetamol (**3**) (Figure 11). [43]

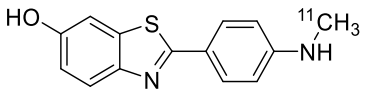

Figure 10: ^{11}C-Pittsburgh Compound B

^{18}F-Florbetapir (**1**) ($C_{20}H_{25}{}^{18}FN_2O_3$), trade name AMYViD, also known as ^{18}F-AV-45 (Figure 11), was the first ^{18}F-labelled tracer approved by the Food and Drug Administration (FDA) since FDG. This compound is a pyridyl stilbene derivative in which the terminal hydroxyl group of a triethylene glycol side-chain was replaced by ^{18}F. ^{18}F-Florbetapir like PiB, binds to beta-amyloid and accumulates significantly more in the brain of people with AD, particularly in the regions known to be associated with beta-amyloid deposits. The radiosynthesis of this PET tracer involves the nucleophilic displacement of a tosylate group of the precursor by radioactive fluoride, followed by removal of a *tert*-butoxycarbonyl protecting group by using acid. [53] PET images using this radiopharmaceutical should be acquired 30-50 minutes after its administration. ^{18}F-Florbetapir (**1**) is also used to predict progression from mild-cognitive impairment (MCI) to AD with a sensitivity of 67% and a specificity of 97%. [54]

^{18}F-Florbetaben (**2**) ($C_{21}H_{26}{}^{18}FNO_3$), trade name NeuraCeq, also known as BAY-949172 (Figure 11), was first described in 2005 by Zhang and co-workers. This radiopharmaceutical is a stilbene derivative used to detect a wide spectrum of pathologies in neurodegenerative conditions. [55] ^{18}F-Florbetaben (**2**) is very similar to ^{18}F-Florbetapir (**1**), being the only difference the presence of benzene group instead of a pyridyl group. ^{18}F-Florbetaben (**2**) binds to amyloid aggregates, with similar affinity as PiB showing the same pattern of labelling of Aβ plaques. These two radiopharmaceuticals are also metabolized by analogous pathways. ^{18}F-Florbetaben (**2**) can be used to distinguish patients with AD from patients with frontotemporal lobar degeneration (FTLD) (15-20% cases of all dementia). [52]

^{18}F-Flutemetamol (**3**) ($C_{14}H_{11}{}^{18}FN_2OS$), trade name Vizamyl (Figure 11) is the amyloid imaging tracer with more similarities with PiB. This radiopharmaceutical was approved by the FDA in 2013 and a year later by European Medicines Agency (EMA). [54] This PET tracer is currently in phase 3 clinical trials. [56]

Nowadays, there are some new ^{18}F-radiotracers undergoing clinical trials like ^{18}F-AZD4694 (**4**) (recently renamed NAV4694) and [^{18}F]MK-3328 (**5**) (Figure 11). [57], [58] In patients with AD the compound **4** showed higher radioactivity in cortical regions due the

deposition of Aβ being the regional distribution similar to other Aβ PET agents. This compound has a rapid specific binding kinetics being a short acquisition time enough to quantify Aβ load. This fact together with the half-life time of ^{18}F make the compound **4** a promising Aβ PET radioligand. [58] Studies with compound **5** performed in rhesus monkey showed a high brain uptake associated with a low binding potential in white matter and cortical grey matter and a high affinity with human amyloid plaques. A high binding potential with cerebral white matter is undesirable because it can interfere with interpretation of the results in adjacent cortical regions in human PET studies. [57]

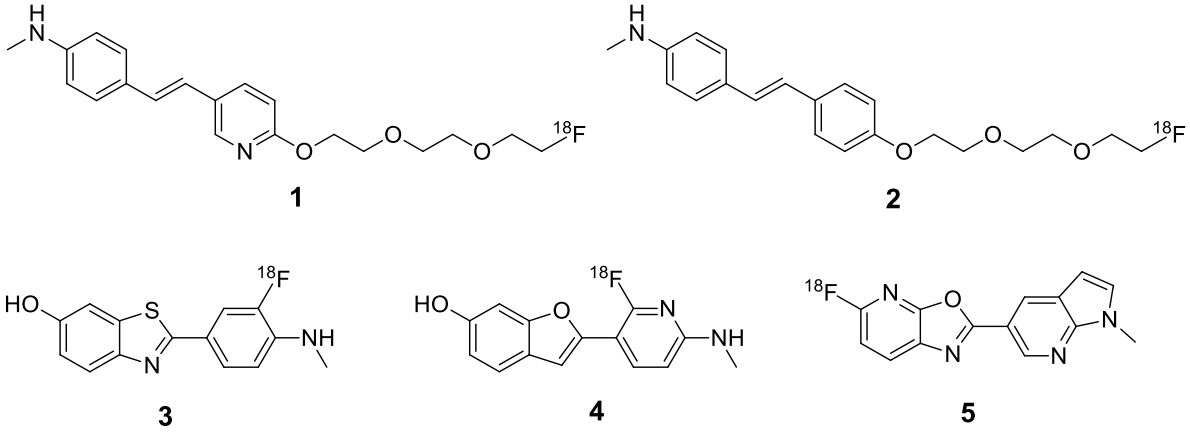

Figure 11: Amyloid ^{18}F- labelled imaging agents for PET.

1.2.1.2 Tau probes

Tau imaging is a recent addition to AD biomarkers. Tau deposition is strongly associated with AD but also with several other neurodegenerative diseases called tauopathies. [59] An early diagnosis of this condition is necessary to have a better comprehension of these neurodegenerative diseases. In the last years, several Tau-selective PET imaging probes have been developed: ^{18}F-Flortaucipir (**6**), ^{18}F-THK5351 (**7**), ^{18}F-THK5317 (**8**) and ^{11}C-PBB3 (**9**) are some examples (Figure 12). Because of the relationship of Tau deposition, cognitive impairment and neuronal injury Tau imaging can be very useful to predict progression of AD. Tau imaging results reveal that the topographical distribution of Tau in the brain is more important than the total level of Tau in the brain. In case of Aβ imaging it's the opposite. These two types of PET must be used in combination to provide better results in accurate and early diagnosis of AD, evaluation of disease staging and prediction of its progression. Tau imaging can be used to diagnose the cases of FTLD associated with hyperphosphorylated Tau. [43]

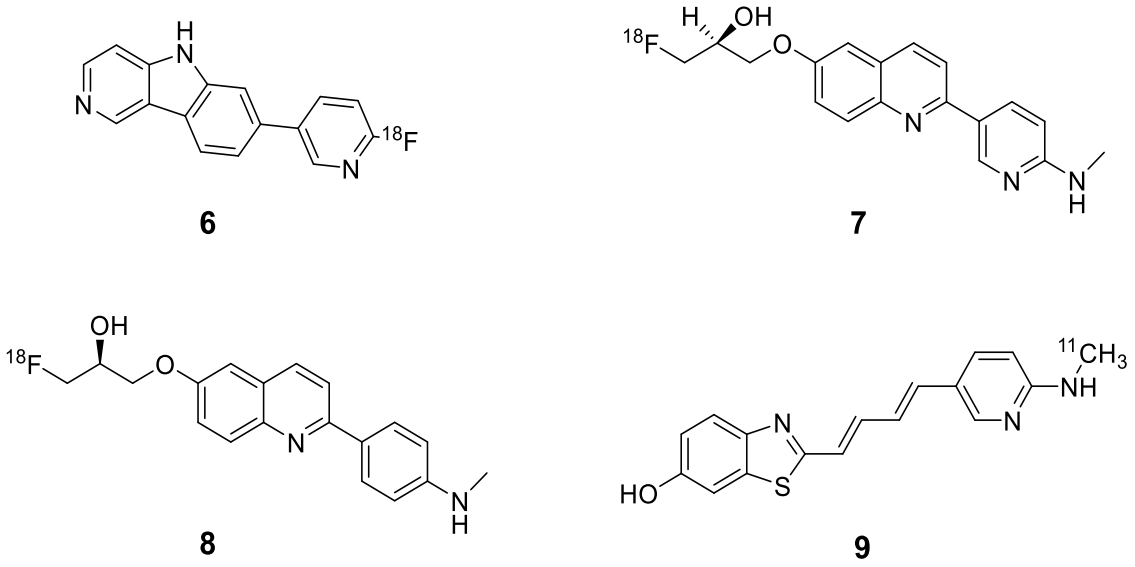

Figure 12: Tau ^{18}F- labelled imaging agents for PET

1.3 Pyrazoles

Pyrazole, 1*H*-Pyrazole (**10**), (Figure 13) is a heterocyclic compound with chemical formula $C_3H_4N_2$. L. Knorr, in 1883, was the first to introduce the name "pyrazole". [60] This family of compounds is characterized by a simple aromatic five-membered ring containing three carbon and two nitrogen atoms in adjacent positions. [61] The occurrence of the pyrazole core in nature is rare, probably due to the difficult of living organisms to make a N-N bound. [62] In 1959, a natural pyrazole derivative, 1-pyrazolyl-alanine, was isolated from seeds of watermelon by F. Noe and L. Fowden of London University. [63] Until now there are only approximately 20 natural compounds with a pyrazole core on their structures. [64] However, pyrazole and its reduced derivatives (pyrazolines, **11-13**) (Figure 13) are privileged scaffolds in medical chemistry. Pyrazole scaffold is present in several synthetic drugs being celecoxib, sildenafil, rimonabant, penthiopyrad and sulfaphenazole the most notorious. [61]

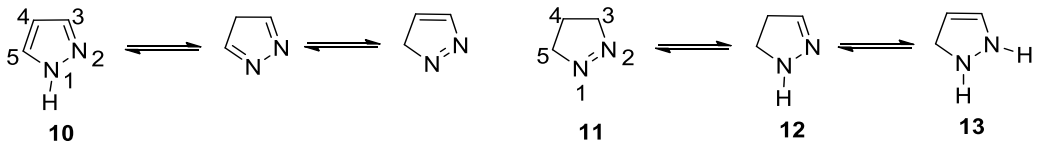

Figure 13: Chemical structures and numbering of pyrazole and dihydropyrazole (pyrazoline) tautomers 10-13. Taken from [65]

Pyrazole derivatives present a wide range of pharmaceutical activities. Mohamed and co-workers have demonstrated antitumoral activity of several compounds with a pyrazole and sulfonamide moieties; [66] antibacterial and antifungal activity of pyrazole was demonstrated by Chowdary and co-workers. [67] Pyrazoles also showed a good activity as monoamine oxidase inhibitors, BRAF inhibitors, DNA gyrase inhibitors, moderate antihepatotoxic activity, antileishmanial activity, anti-inflammatory, analgesic, cyclin-dependent kinase activity and tissue-non-specific alkaline phosphatase inhibitory activity. [68]

In 2013, Prabhu and co-workers reported the antioxidant activity of pyrazole. They demonstrated that pyrazole (1,2 diazole) can be used to prevent nephrotoxicity caused by cisplatin, a drug used to treat several cancers. Cisplatin provokes renal damage because of its toxicity to proximal tubule cells and can reduce glomerular filtration resulting in renal failure. One of the reasons of nephrotoxicity induced by cisplatin is the decreasing concentration of GSH. Pyrazole prevents nephrotoxicity induced by cisplatin by counteracting this effect, increasing the concentration of this enzyme. [69] Recently, Silva and co-workers published an extensive review concerning the antioxidant activity of more than 300 pyrazoles, showing that there are several methods to evaluate the antioxidant capacity of these compounds. [65], [70]

As stated before, oxidative stress is one of the main causes of neurodegenerative diseases as AD. Therefore, there is an increasing interest in antioxidants as drugs to prevent AD or to slow down its progression.

Besides their remarkable pharmacological properties, pyrazoles can also be used for agrochemicals purposes. For instance, Florence and co-workers described the use of fluorinated pyrazoles as herbicides, fungicides and insecticides. [71]

1.3.1 Pyrazoles for PET imaging

Recent studies have demonstrated that some pyrazoles labelled with ^{18}F can be used as PET radiotracers. A search on Scopus database using the keywords: ^{18}F, radiopharmaceuticals and pyrazoles resulted in 27 articles of our interest.

Products derived from *Cannabis sativa* are some of the oldest and widely used drugs in the world. These products are known as natural cannabinoids, but synthetic cannabinoids have been developed too. Cannabinoids have been used as analgesics for more than 100 years. [72] Additionally, they have been used as antiemetic agents, to prevent chemotherapy

induced nausea and vomiting, because they can bind to opiate receptors in the forebrain blocking the vomiting center in medulla. [73] In 1998, C. Williams and T. Kirkham have demonstrated that anandamide, an endogenous cannabinoid, provokes hyperphagia in satiated rats. [74] Cannabinoid-type compounds bind to cannabinoid receptors which can be divide in two groups – cannabinoid receptor type 1 (CB1), predominantly found in the brain, and cannabinoid receptor type 2 (CB2) mainly expressed in immune tissues. [75] Both are G-protein coupled receptors.

The first selective antagonist for CB1 receptors was [*N*-(piperidin-1-yl)-5-(4-chlorophenyl)-1-(2,4-dichlorophenyl)-4-methyl-1*H*-pyrazole-3-carboxamide] SR141716 (**14**), also known as rimonabant (Figure 14). [76] This compound was approved in Europe in 2006 to treat obesity by reducing the patients' appetite. Two years later, the EMA withdrawn rimonabant from sale due to evident secondary effects of this drug. Some studies demonstrated that SR141716 induced anxiety and depression, agitation, eating disorders, irritability, aggression and insomnia. Rimonabant was not approved in USA by FDA. [77] However, in the last years some analogs of SR141716 labelled with radionuclides have been developed for PET imaging. [^{18}F]SR144385 (**15**), [^{18}F]SR147963 (**16**), *N*-(piperidin-1-yl)-1-(2,4-dichlorophenyl)-5-{4-(5-fluoropentyl)phenyl}-4-methyl-1*H*-pyrazole-3-carboxamide (**17**), and AM5144 (**18**) are some examples of PET tracers labelled with ^{18}F (Figure 15). On the other hand, AM251 (**19**) and AM281 (**20**) are two examples of PET tracers labelled with ^{123}I (Figure 16). Except for compound **17**, the concentration of these radiopharmaceuticals in different brain sections after injection was concordant with the density of CB1 receptors in that sections (cerebellum>hippocampus>striatum>cerebral cortex>brainstem>thalamus). All these examples demonstrated a poor brain uptake expected for compounds with similar values of lipophilicity. However, new pyrazole-derived radioligands can be developed for PET imaging. Investigating the factors that affect brain uptake beyond lipophilicity will be necessary to a better comprehension of this process. Some studies highlighted that there may be a large species differences in brain penetration for a given pyrazole compound; For example, the brain uptake of AM251 (**19**) is very different comparing mices and monkeys. [75], [78], [79]

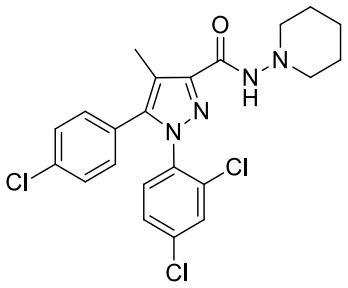

14

Figure 14: Structure of Rimonabant (SR141716)

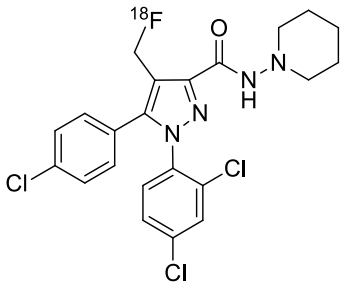

15

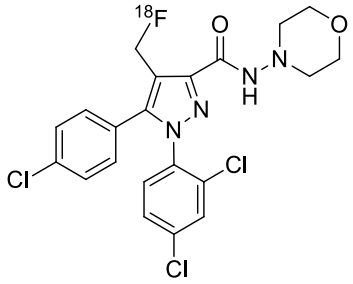

16

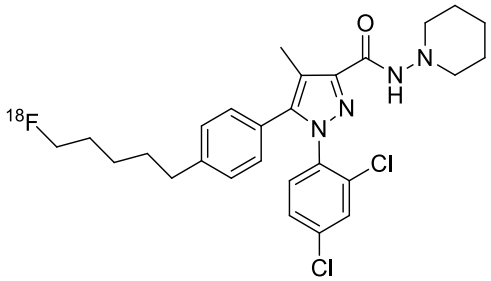

17

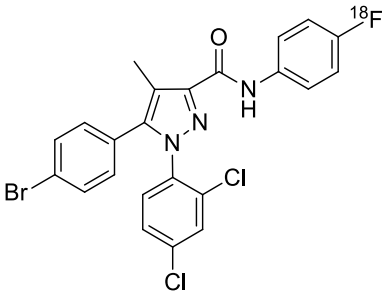

18

Figure 15: Pyrazole PET tracers labelled with ^{18}F

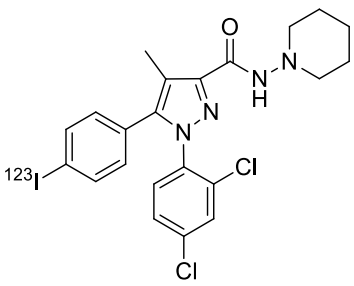

19

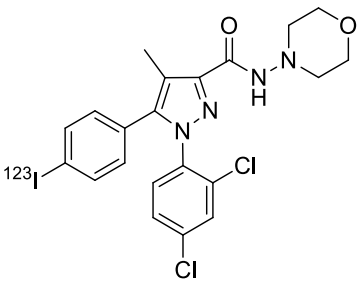

20

Figure 16: Pyrazole PET tracers labelled with ^{123}I

The translocator protein (TSPO), also known as peripheral benzodiazepine receptor, is an 18 kDa protein organized around five large transmembrane α-helices and located on the mitochondrial outer membrane. [39] This protein has a key role in the regulation of several cellular processes: steroid biosynthesis, cholesterol metabolism, apoptosis and

cellular metabolism. [80] TSPO is highly expressed in organs involved in steroid synthesis as adrenal glands, testis, ovaries and pituitary glands. [81] However, in CNS and liver TSPO expression is modest. In case of acute or neurodegenerative pathologies associated with microglia or astrocytes, levels of TSPO in brain are increased. [82] The expression of this protein is elevated in many cancers: colon, breast, glioma, prostate, colorectal, liver and ovary cancer relating TSPO with disease progression and survival. [39], [80], [81] These evidences increased the interest in TSPO and lead to the development of several ligands to evaluate the expression of this protein. Consequently, the development of these ligands leads to new PET tracers for detection of some diseases above mentioned. PK11195, an isoquinoline carboxamide synthesized by Inoue and co-workers in 1985, was the first nonbenzodiazepine ligand for TSPO and it was labelled with tritium. Some years later, Camsonne and co-workers labelled PK11195 with carbon-11 originating [^{11}C]PK11195 (Figure 17). [83] Although the short half-life of this radionuclide (20.4 min.), its low brain uptake, elevated level of non-specific binding and extensive binding to plasma proteins, [^{11}C]PK11195 (**21**) remains the most used PET tracer to detect TSPO. [84] Another important tracer for detection of TSPO is [^{11}C]DPA-713 (**22**) (Figure 17). The disadvantages associated with ^{11}C radionuclide have promoted the development of some PET ligands labelled with a longer half-life radionuclide like fluorine-18 (109.8 min.). [^{18}F]DPA-714 (**23**) is one of ^{18}F PET tracers for TSPO developed in the past twenty years (Figure 17). DPA-713 and DPA-714 are pyrazol[1,5-*a*]pyrimidine acetamides. PK11195 closely-related derivatives, PK13162, PK13168, DAA1106, PBR28, SSR180575, FEDAC and FEAC are some examples of other radioligands synthetized. [39] The pyrazolopyrimidine acetamide [^{18}F]DPA-714 (**23**) is a promising PET radiotracer for TSPO imaging (Figure17). Chauveau and co-workers compared [^{18}F]DPA-714 with [^{11}C]PK11195 and [^{11}C]DPA-713 using a rat model of acute neuroinflammation. AMPA was used to provoke neuroinflammation. The fluorine labelled tracer achieved a higher uptake and higher binding potential than the others radiotracers. [85] [^{18}F]DPA-714 is also used to monitor the TSPO levels after injection of some antibiotic like minocycline. This drug inhibits the activation of microglial cells. [86] Furthermore [^{18}F]DPA-714 was used on studies of rodent models of excitotoxicity, herpes encephalitis, astrocytic activation, excitotoxically-lesioned nonhumane primate brains, abdominal aortic aneurysm, rheumatoid arthritis and neuroinflammatory changes in brain after morphine exposure. [81], [82], [87 - 90] Nowadays some new derivatives of DPA-714

are being developed for use as TSPO PET tracers. [^{18}F]F-DPA (**24**), [^{18}F]GE-180 (**25**) (Figure 17) are two of the newest radioligands synthetized. [80], [83], [84], [91]

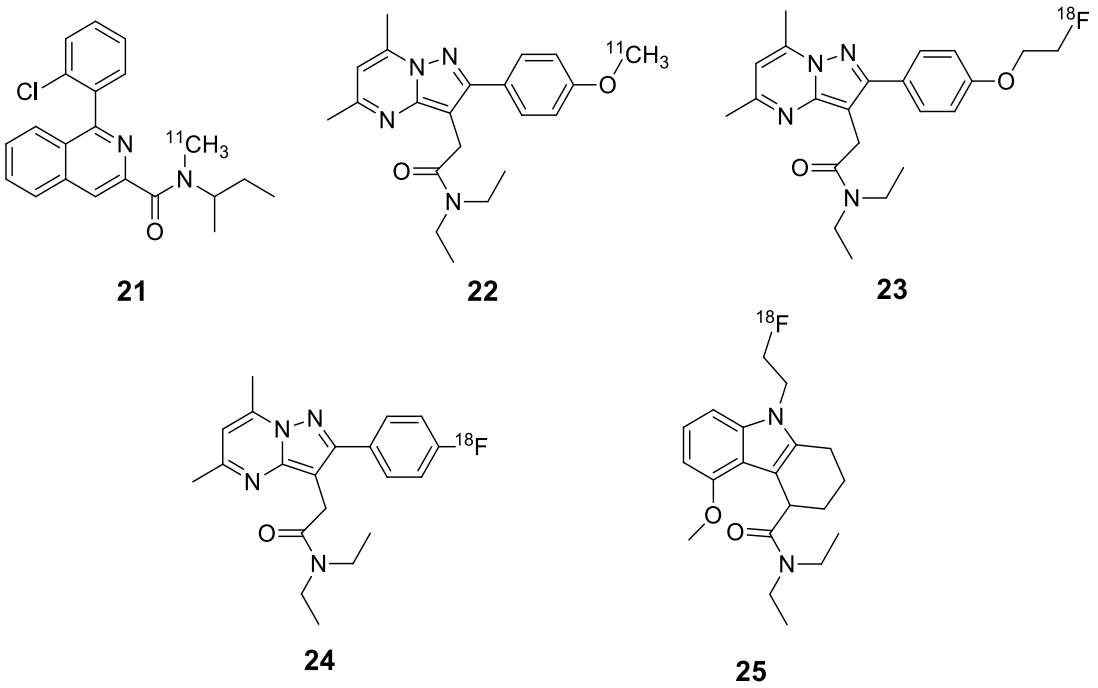

Figure 17: Radiotracers for TSPO PET imaging including pyrazole-derived compounds

Phosphodiester-10A (PDE10A) is an enzyme that hydrolyzes adenosine and/or guanosine 39,59-cyclic monophosphates (cAMP and cGMP, respectively). In the medium spiny neurons of the striatum PDE10A messenger RNA and the corresponding protein are highly abundant. PDE10A inhibitors are a potential target for diagnosis of schizophrenia, Huntington's disease, Parkinson's disease, obsessive-compulsive disorder and addiction. Tu and co-workers made a first attempt to visualize PDE10A using a ^{11}C-radiolabelled PDE10A inhibitor named papaverine. *In vitro*, ^{11}C-papaverine, showed selective PDE10A binding but *in vivo* failed because of rapid washout of the tracer. To overcome this problem, Celen and co-workers synthetized a specific and selective radioligand for PDE10A, a quinoline labeled with ^{18}F, the ^{18}F-JNJ41510417 (**26**) (Figure 18). S. Celen used rats and PDE10A knock-out mices to show that ^{18}F-JNJ41510417 binds specifically and reversibly to PDE10A in the striatum. [92] Three years later, Laere and co-workers showed that ^{18}F-JNJ41510417 have a promising kinetics and biodistribution. [93]

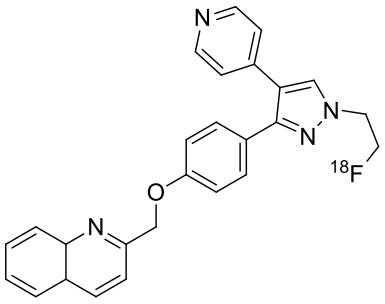

26

Figure 18: Structure of ^{18}F-JNJ41510417

Adenosine, an endogenous signaling substance, is a purine ribonucleoside composed of adenine (purine base) and ribose (sugar molecule). There are four types of adenosine receptors: A_1, A_{2A}, A_{2B} and A_3. In preclinical studies, A_{2A}R antagonists showed potential benefits in the treatment of some neurodegenerative diseases like AD. Khanapur and co-workers developed a pyrazolo[4,3-*e*]-1,2,4-triazolo[1,5-*c*]pyrimidine labelled with carbon-11, [^{11}C]SCH442416 (**27**) and its derivatives [^{18}F]Fluoroethyl and [^{18}F]Fluoropropyl ([^{18}F]FESCH (**28**) and [^{18}F]FPSCH (**29**), respectively) (Figure 19) and both radioligands showed a distribution in the rat brain, corresponding to the regional A_{2A}R densities. [94] In the last year, Shivashankar studied the full kinetics of [^{18}F]FESCH and [^{18}F]FPSCH in rat brains and concluded that [^{18}F]FESCH is the most suitable PET radioligand for quantifying A_{2A}R. However, before starting the clinical use of [^{18}F]FESCH its necessary to reevaluate the brain uptake in humans due to possible interspecies differences in tracer kinetics and metabolism. [95]

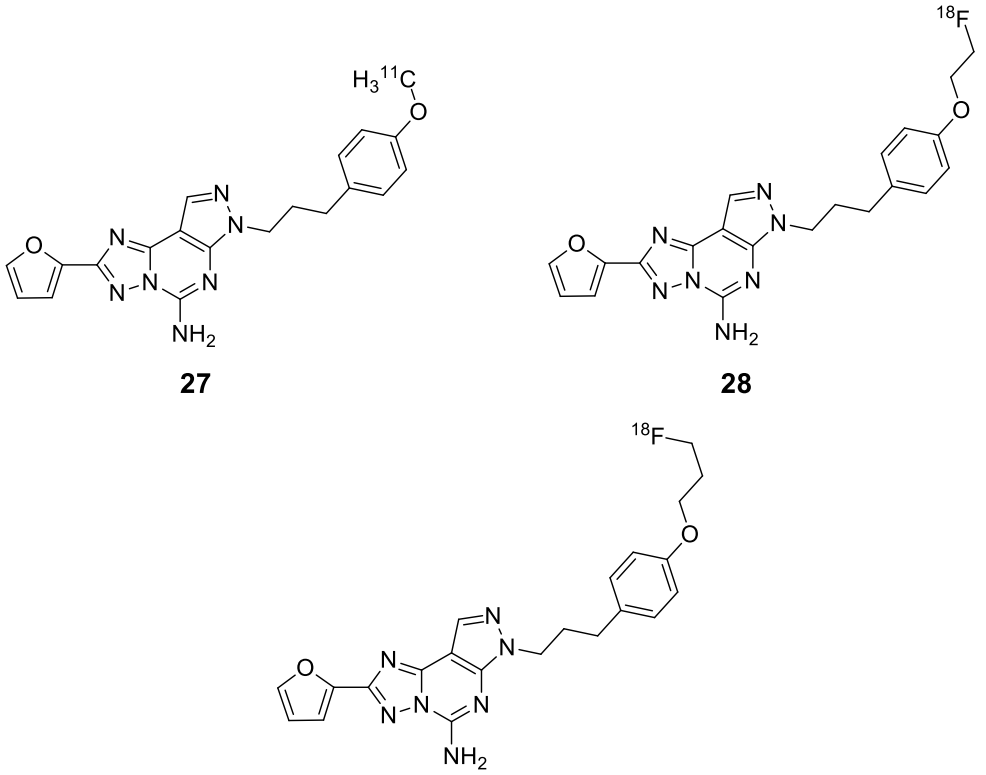

Figure 19: $A_{2A}R$ PET radioantagonists

In 2012, Xu and co-workers synthetized a ^{18}F-labelled pyrazolo[1,5-*a*]pyrimidine starting from 2,4-dinitrobenzamide or tosylated precursors showing that tosylated precursors were more suitable for the preparation of the ^{18}F-labelled pyrazolo[1,5-*a*] pyrimidine core than the 2,4-dinitrobenzamide precursor. [96] Chang and co-workers used a nitroimidazole radiolabeled with fluorine-18, [^{18}F]FAZA to evaluate the therapeutic response to treatment with BAY 87-2243, an inhibitor of mitochondrial complex I used to inhibit the growth of human lung cancer. [97] [^{18}F]BMS-754807, a potent and reversible small molecule inhibitor of the IGF-1R/IR kinases family, currently in phase II clinical trials, and fluorinated COX-2 inhibitor can be used as agents in PET imaging of inflammation and cancer. [98], [99] Finally, Prante and co-workers have demonstrated that pyrazolo[1,5-*a*]pyridine, an agonist of dopamine D_4 receptor, when radiolabelled with fluorine-18 can be used as radioligand with a specific binding in brain areas that are in agreement with the known D_4R distribution. [100]

In sum, AD is an intricate pathology responsible for the death of many people worldwide. To prevent the disease or to slow down its progression, the scientific community

is doing great efforts to find novel theranostics for AD treatment and diagnosis. Regarding the diagnosis, the potential of PET strongly depends on the availability of suitable PET radiotracers (probes). However, the development of new imaging probes is not trivial and radiochemistry is a major limiting factor for the field of PET. Hence, the research and development of new PET tracers is an issue of major importance within the scientific community.

Regarding the examples presented before, pyrazoles are interesting scaffolds for the development of ^{18}F-radiopharmaceuticals for diagnosis of several pathologies, including neuropathological ones. In addition, pyrazoles are known to possess interesting antioxidant activity, both as metal complexing agents and as radical scavengers. In this sense they have also great potential as drugs to treat oxidative stress, one of the main causes associated with AD.

Chapter 2 – Synthesis and structural characterization of target compounds

2.1 Nomenclature of the synthetized compounds

2.1.1 2-Acetylphenyl (*E*)-3-(4-fluorophenyl)prop-2-enoate

The 2-acetylphenyl (*E*)-3-(4-fluorophenyl)prop-2-enoate (**3**) is a compound with a prop-2-enoate as the main chain. The numbering started in the carbonyl carbon of the ester group. The C-3 of the main chain is linked with a phenyl group, that in turn has a fluorine atom at *para*-position. The other oxygen atom of ester group is linked with C-2' of a phenyl that has an acetyl group at C-1'. This compound is designated by (*E*) because the *trans* configuration of the double bond between C-2 and C-3.

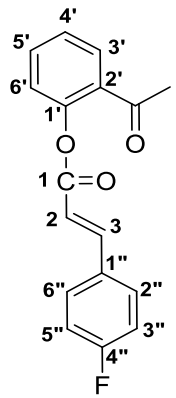

3

*Figure 20: Structure and numbering of 2-acetylphenyl (E)-3-(4-fluorophenyl)prop-2-enoate (**3**)*

2.1.2 (*E*)-5-(4-Fluorophenyl)-1-(2-hydroxyphenyl)pent-4-ene-1,3-dione

The compound **4** was named as a diketone with five carbons in the main chain, following the IUPAC recommendations. [101] Carbonyl groups are located at positions C-1 and C-3 and there is a double bond between carbons C-4 and C-5 (4-ene) with *trans* configuration, indicated as (*E*)-. At C-1 position there is a 2-hydroxyphenyl group attached, and the C-5 position is linked to a 4-fluorophenyl group. Often, in solution the enolic form of compound **4** is observed, as indicated in figure 21.

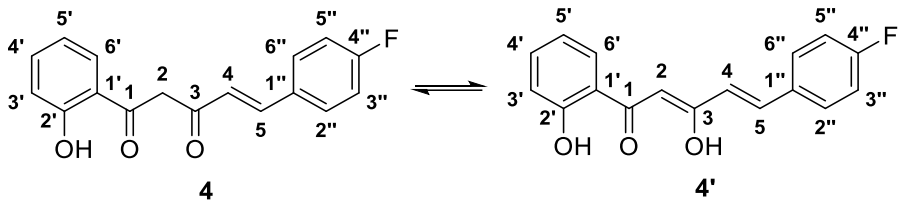

*Figure 21: Structure and numbering of (E)-5-(4-fluorophenyl)-1-(2-hydroxyphenyl)pent-4-ene-1,3-dione (**4**) and (2Z,4E)-5-(4-fluorophenyl)-3-hydroxy-1-(2-hydroxyphenyl)penta-2,4-dien-1-one (**4'**).*

2.1.3 (*E*)-3-styryl-4*H*-chromen-4-ones

Benzopyran ring results from the fusion of a benzene ring with a pyran ring. In chromones (4*H*-chromen-4-ones), the pyran ring has a keto group at C-4 position. The compounds **7** and **21** are chromones substituted at C-3 position with a 4-Rstyryl group (R = F or NO_2). The numbering of these compounds started in the oxygen atom of chromone ring which is the main chain. The designation (*E*)- in the compound's name indicates the *trans* configuration of C-α=C-β double bound.

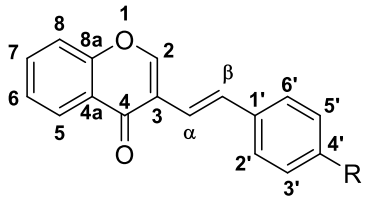

7a R = F
7b R = NO_2

*Figure 22: Structure and numbering of (E)-3-(4-fluorostyryl)-4H-chromen-4-one (**7a**) and (E)-3-(4-nitrostyryl)-4H-chromen-4-one (**7b**).*

2.1.4 5-(4-fluorophenyl)-3-(2-hydroxyphenyl)-4,5-dihydro-1*H*-pyrazole

The nomenclature adopted for the pyrazole-type compounds synthetized in this work does not follow the recommendations of IUPAC. Instead, pyrazole was always considered the main chain, having different substituent groups at C-3, C-4 or C-5 positions. The numbering of the pyrazole ring starts at the NH or at the substituted nitrogen atom, which is given the number 1 followed by the other nitrogen atom.

Pyrazole **9** is a reduced pyrazole (also known as pyrazoline) and therefore it is designated as 4,5-dihydro-1*H*-pyrazole (the numbers 4 and 5 indicated the "missing" double bond).

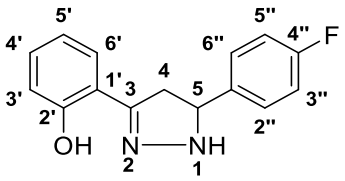

9

*Figure 23: Structure and numbering of 5-(4-fluorophenyl)-3-(2-hydroxyphenyl)-4,5-dihydro-1H-pyrazole (**9**).*

2.1.5 5(3)-(4-Fluorophenyl)-3(5)-(2-hydroxyphenyl)-1*H*-pyrazole

The name given to compound **10**, follows the same rules as aforementioned for all the pyrazole-type compounds synthetized in this work. However, non-substituted pyrazoles may exist as a mixture of tautomers **10** and **10'** due to prototropy. Therefore, as the numbering of the pyrazole core depends on the position of the hydrogen atom linked to the nitrogen, compound **5** is designated as 5-(4-fluorophenyl)-3-(2-hydroxyphenyl)-1*H*-pyrazole and its tautomer **5'** is named as 3-(4-fluorophenyl)-5-(2-hydroxyphenyl)-1*H*-pyrazole as indicated in figure 24.

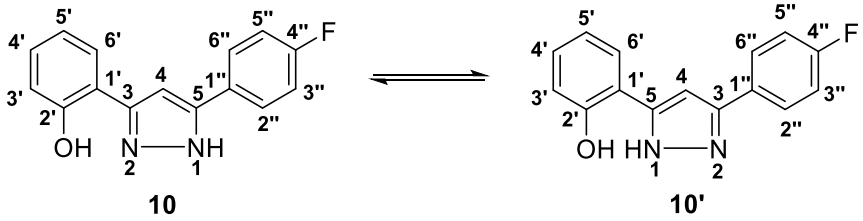

*Figure 24: Structure and numbering of 5(3)-(4-fluorophenyl)-3(5)-(2-hydroxyphenyl)-1H-pyrazole (**10**).*

2.1.6 (4-Fluorostyryl)-3(5)-(2-hydroxyphenyl)-1*H*-pyrazoles

Compounds **6** and **7** are pyrazoles that present a 2-hydroxyphenyl group at C-3(5)-position and a 4-fluorostyryl group at at C-3(5)-position (**11**) or C-4 position (**12**), as substituents. The nomenclature and numbering adopted for these compounds followed the rules aforementioned for pyrazole **5**. Both compounds have the designation (*E*)- due the *trans* configuration of the Cα=Cβ double bond. For the non-substituted derivatives, two tautomers may be formed as indicated in figure 25.

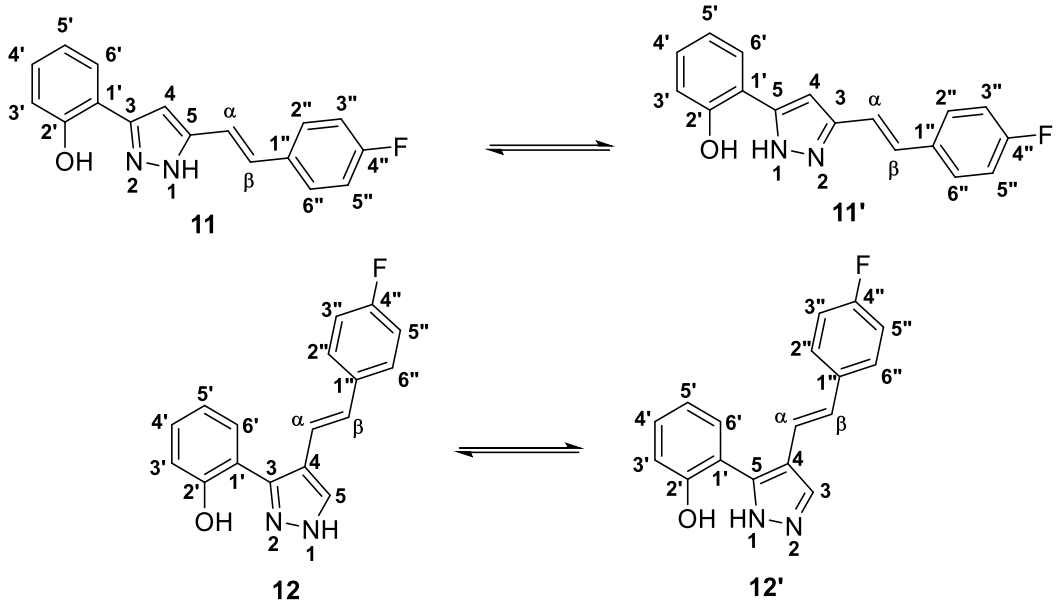

*Figure 25: Structure and numbering of 5(3)-(4-fluorostyryl)-3(5)-(2-hydroxyphenyl)-1H-pyrazole (**11**) and (E)-4-(4-fluorostyryl)-3(5)-(2-hydroxyphenyl)-1H-pyrazole (**12**) and the corresponding tautomers (**11'**) and (**12'**)*

2.1.7 *O*- and *N*-substituted 3(5)-(2-hydroxyphenyl)-1*H*-pyrazoles

Pyrazoles **13a**, **13b**, **14a, 14b**, **15a** and **15b** are similar to those aforementioned but present an alkyl chain of two or six carbons, having a terminal hydroxy group, linked to the nitrogen or oxygen atoms. Therefore, these compounds are named as 5-(4-fluorophenyl)-1-(6-hydroxyhexyl)-3-(2-hydroxyphenyl)-1*H*-pyrazole (**13a**) and 5(3)-(4-fluorophenyl)-3(5)-[2-(6-hydroxyhexyloxy)phenyl]-1*H*-pyrazole (**13b**), (*E*)-4-(4-fluorostyryl)-1-(2-hydroxyethyl)-3-(2-hydroxyphenyl)-1*H*-pyrazole (**14a**) and (*E*)-4-(4-fluorostyryl)-3(5)-[2-(2-hydroxyethoxy)phenyl]-1*H*-pyrazole (**14b**), (*E*)-4-(4-fluorostyryl)-1-(6-hydroxyhexyl)-3-(2-hydroxyphenyl)-1*H*-pyrazole (**15a**) and (*E*)-4-(4-fluorostyryl)-3(5)-[2-(6-hydroxyhexyloxy)phenyl]-1*H*-pyrazole (**15b**) (Figure 26).

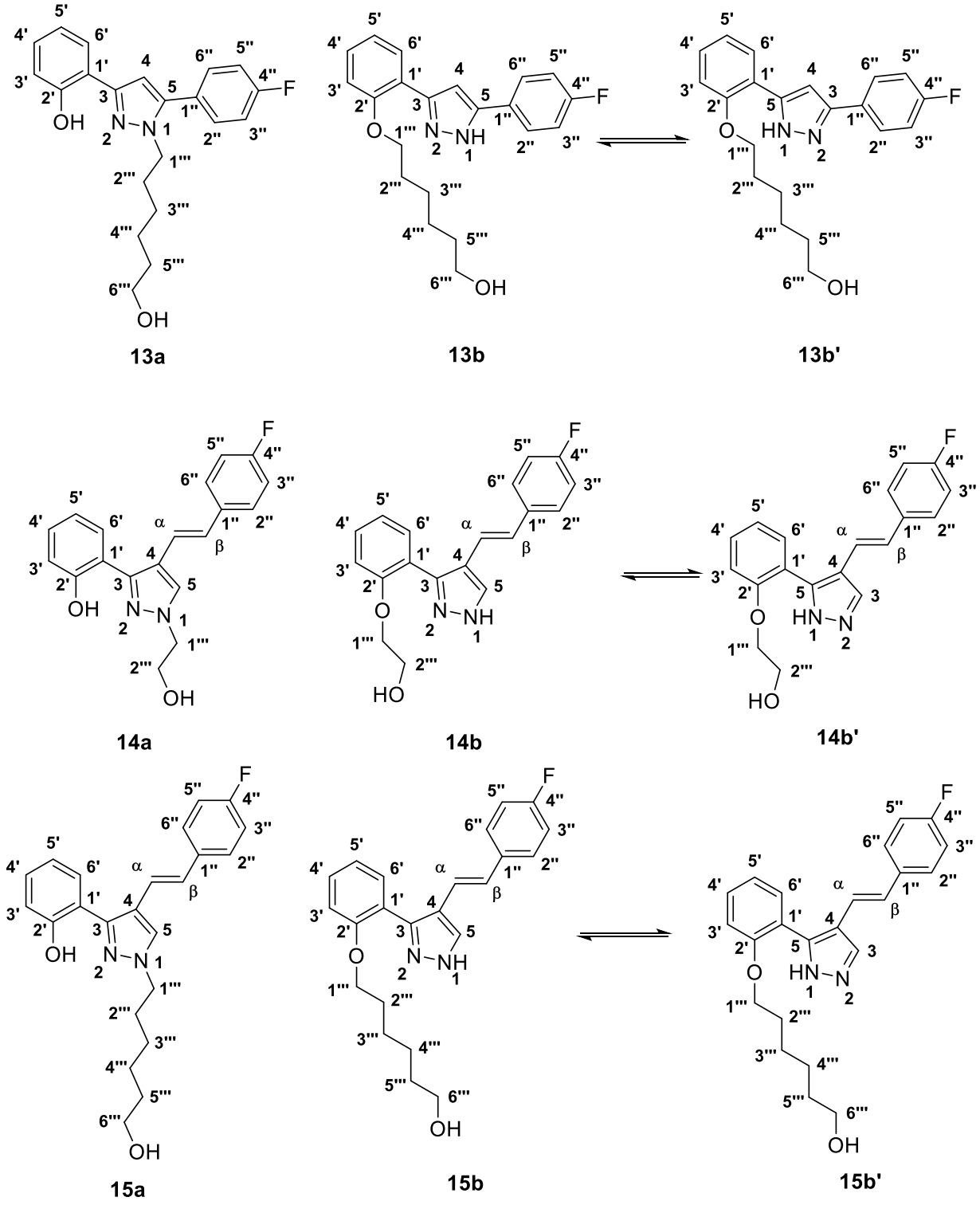

Figure 26: Structures and numbering of O- and N-substituted 3(5)-(2-hydroxyphenyl)-1H-pyrazoles

For compounds **18** and **19**, the alkyl chain contains a tosyl group or a fluorine at the end of the chain instead of a terminal hydroxy group. Accordingly, these compounds are named (*E*)-4-(4-fluorostyryl)-3-(2-hydroxyphenyl)-1-(6-tosylhexyl)-1*H*-pyrazole (**18**) and

(*E*)-1-(6-fluorohexyl)-4-(4-fluorostyryl)-3-(2-hydroxyphenyl)-1*H*-pyrazole (**19**) (Figure 27).

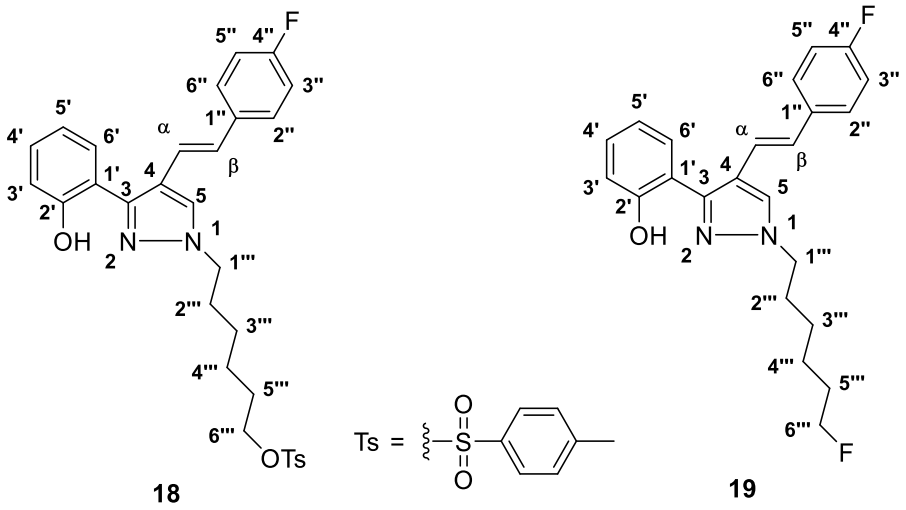

*Figure 27: Structures and numbering of (E)-4-(4-fluorostyryl)-3-(2-hydroxyphenyl)-1-(6-tosylhexyl)-1H-pyrazole (**18**) and (E)-1-(6-fluorohexyl)-4-(4-fluorostyryl)-3-(2-hydroxyphenyl)-1H-pyrazole (**19**)*

2.2 Synthesis

In this section, will be presented a brief description of the methods used to prepare the target compounds of this work. The fully detailed experimental protocols as well as the NMR data of compounds may be consulted in Chapter **5 –** Experimental Section.

This master's thesis was divided in two moments. The first is related to the first objective which was to synthetize three different types of fluorinated pyrazoles, as previously stated in the section Objectives of the work (Figure 1), to evaluate their radical scavenging activity against $ABTS^{+\bullet}$ and $NO^{\bullet}$ in order to assess their antioxidant capacity. Then, based on the results of the synthesis (particularly the yield) and radical scavenging assays, one or more compounds (those that provided the best results) will be chosen to develop a suitable pyrazole precursor to be labelled with fluorine-18. The strategy followed to prepare this precursor will be further discussed in this chapter. Labelling of the developed precursor with this radioisotope will be performed in a near future in collaboration with researchers at University of Coimbra, where the facilities to perform radiosynthesis are installed.

2.2.1 Synthesis of the starting compounds

2.2.1.1 Synthesis of 2-acetylphenyl (*E*)-3-(4-fluorophenyl)prop-2-enoate

The synthesis of 2-acetylphenyl-(*E*)-3-(4-fluorophenyl)prop-2-enoate (**3**) was achieved through the reaction of acetophenone (**1**) and 4-fluorocinnamic acid (**2**) using dicyclohexylcarbodiimide (DCC) and 4-pyrrolidinopyridine (4-PPy). This reaction is called "Steglich Esterification". The reaction was stirred under nitrogen, at room temperature, for 7 days (Scheme 1). With a recrystallization, using as solvents DCM and cyclohexane, it was possible to isolate the target compound in a very good yield (87%).

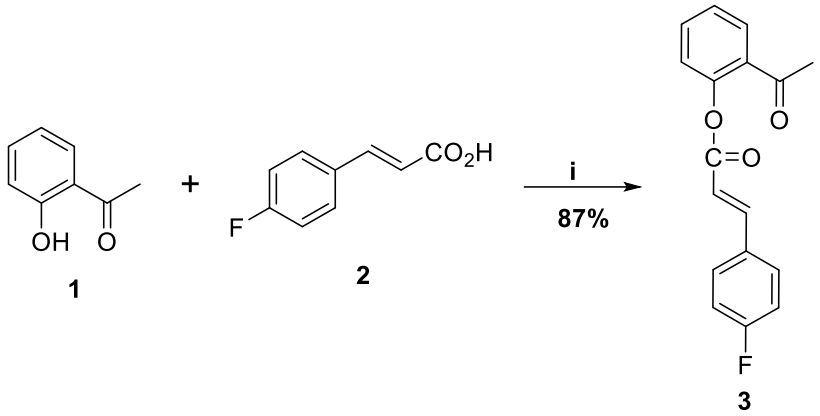

i) **2** (1.2 equiv.), 4-PPy (0.12 equiv.), DCC (1.2 equiv.), DCM, r.t, 7 days

*Scheme 1. Synthesis of 2-acetylphenyl-(E)-3-(4-fluorophenyl)prop-2-enoate (**3**)*

2.2.1.2 Synthesis of (*E*)-5-(4-fluorophenyl)-1-(2-hydroxyphenyl)pent-4-ene-1,3-dione

The diketone **4** [(*E*)-5-(4-fluorophenyl)-1-(2-hydroxyphenyl)pent-4-ene-1,3-dione] was synthetized by Baker-Venkataraman rearrangement of the ester **3** under strong alkaline conditions (Scheme 2). The ester was dissolved in DMSO and KOH (5.0 equiv) was added. The reaction was stirred under nitrogen atmosphere for 1 hour. After that period, the reaction mixture was poured over ice and water and acidified. The precipitate formed was dissolved in DCM and washed with water. The organic solvent was evaporated to dryness and the resulting solid was recrystallized in ethanol, affording the expected diketone with a good yield (57%).

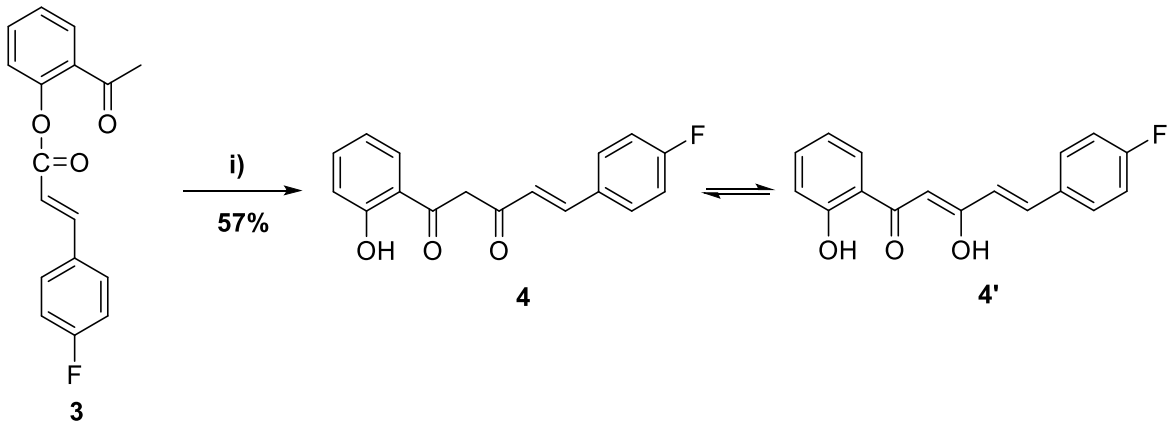

i) KOH (5 equiv.), DMSO, r.t, 1h

*Scheme 2. Synthesis of (E)-5-(4-fluorophenyl)-1-(2-hydroxyphenyl)pent-4-ene-1,3-dione (**4**).*

2.2.1.3 Synthesis of (*E*)-3-styryl-4*H*-chromen-4-ones

The synthesis of (*E*)-3-styryl-4*H*-chromen-4-ones **7a** and **7b** was performed by Knoevenagel condensation of chromone-3-carboxaldehyde (**5**) with the appropriate 4-arylacetic acid (**6a** or **6b**) in pyridine and in the presence of a strong base (*t*-BuOK) followed by decarboxylation, following a method already reported in the literature (Scheme 3). [102] The reaction was stirred and heated at reflux for 24 hours. After that period, the reaction mixture was poured over ice and water and acidified. The precipitate formed was dissolved in chloroform and the organic layer was washed with water. After purification by column chromatography, using DCM as eluent, and crystallization with ethanol, the expected (*E*)-3-(4-fluorostyryl)-4*H*-chromen-4-one (**7a**) and (*E*)-3-(4-nitrostyryl)-4*H*-chromen-4-one (**7b**)[103] were isolated in 44% and 80% yields, respectively.

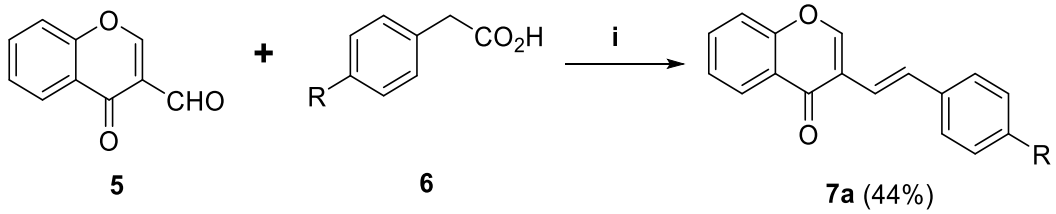

a) R = F, b) R = NO_2

i) **6** (5 equiv.), *t*-BuOK (1.5 eq.), pyridine, reflux, 24h

*Scheme 3. Synthesis of (E)-3-styryl-4H-chromen-4-ones (**7a**) and (**7b**).*

2.2.2 Synthesis and transformation of pyrazoles

2.2.2.1 Synthesis of 5(3)-(4-fluorophenyl)-3(5)-(2-hydroxyphenyl)-1*H*-pyrazole

The 5-(4-fluorophenyl)-3-(2-hydroxyphenyl)-4,5-dihydro-1*H*-pyrazole (**9**) was synthetized from the reaction of (*E*)-3-(4-fluorophenyl)-1-(2-hydroxyphenyl)prop-2-en-1-one (**8**) with hydrazine hydrate (55%) in refluxing methanol for 3 hours. After that period, the reaction was cooled down to 6ºC and the pyrazoline **9** was isolated with 75% yield. The 5(3)-(4-fluorophenyl)-3(5)-(2-hydroxyphenyl)-1*H*-pyrazole (**10**) was obtained by dehydrogenation (oxidation) of pyrazoline **9** with chloranil in toluene at reflux for 23 h (Scheme 4). After purification of the reaction mixture, by TLC using DCM as eluent, the expected pyrazole (**10**) was isolated with 52% yield.

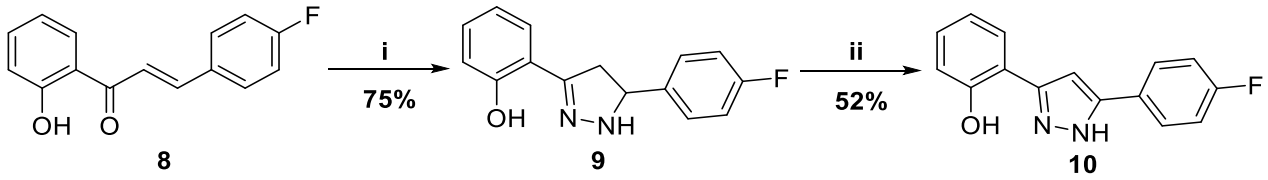

i) $H_2NNH_2.H_2O$ (8 equiv.), CH_3OH, reflux, 3h
ii) Chloranil (3 equiv.), toluene, reflux, 23h

*Scheme 4. Synthesis of 5(3)-(4-fluorophenyl)-3(5)-(2-hydroxyphenyl)-1H-pyrazole (**10**)*

2.2.2.2 Synthesis of (4-fluorostyryl)-3(5)-(2-hydroxyphenyl)-1*H*-pyrazoles

The 5(3)-(4-fluorostyryl)-3(5)-(2-hydroxyphenyl)-1*H*-pyrazole (**11**) was synthetized from the reaction of (*E*)-5-(4-fluorophenyl)-1-(2-hydroxyphenyl)pent-4-ene-1,3-dione (**4**) with hydrazine hydrate (55%) in methanol at room temperature for 2 hours, following a procedure already reported in literature (Scheme 5). [104] After purification of the reaction mixture by TLC using DCM as eluent, and crystallization with DCM and cyclohexane, the expected pyrazole (**11**) was isolated with low yield (26%).

On the other hand, the 4-(4-fluorostyryl)-3(5)-(2-hydroxyphenyl)-1*H*-pyrazole (**12**) was synthetized from the reaction of (*E*)-3-(4-fluorostyryl)-4*H*-chromen-4-one (**7**) with hydrazine hydrate (55%) in methanol at room temperature for 2 hours (Scheme 5). [105] The expected pyrazole (**12**) was isolated with a good yield (85%) after purification of the reaction

mixture by TLC using DCM:acetone (9:1) as eluent and crystallization with DCM and cyclohexane.

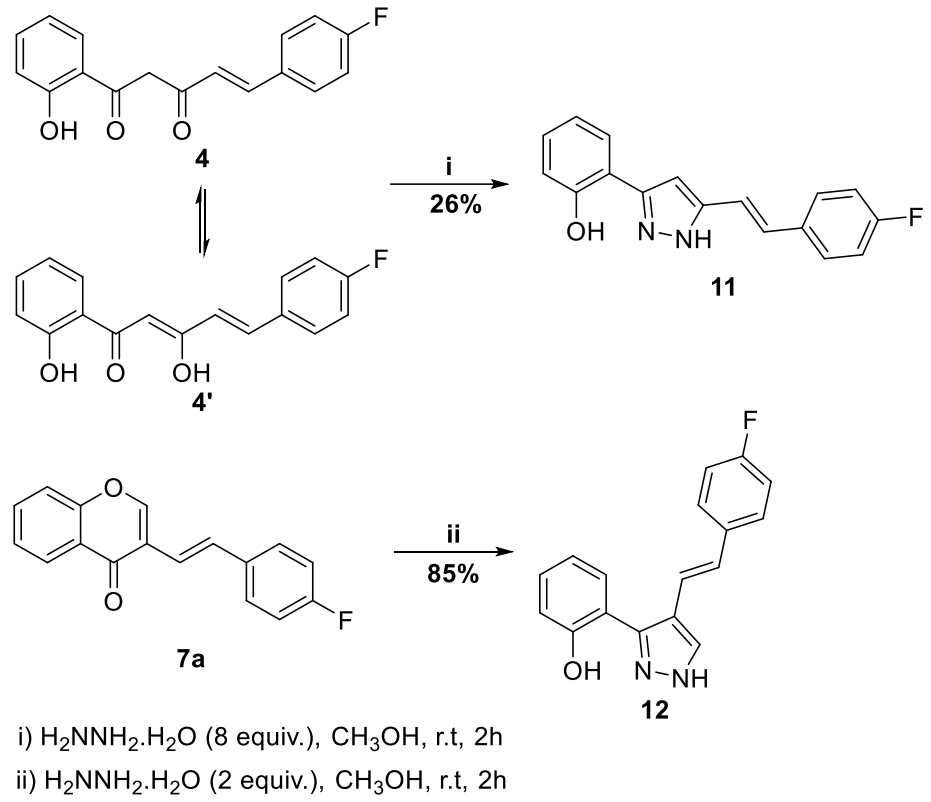

*Scheme 5. Synthesis of 5(3)-(4-fluorostyryl)-3(5)-(2-hydroxyphenyl)-1H-pyrazole (**11**) and 4-(4-fluorostyryl)-3(5)-(2-hydroxyphenyl)-1H-pyrazole (**12**)*

Analyzing the aforementioned results regarding the methods and yields of the synthesis of pyrazoles **10**, **11** and **12**, it is evident that pyrazole **12** is obtained from commercially available starting materials in a more straightforward way (two-step synthesis) and better yield (85%) than pyrazoles **10** and **11** (three-step synthesis)[1]. The yield of the synthesis of pyrazole **10** was moderate (52%) while a low yield was obtained for compound **11** (26%). Moreover, the ability of pyrazoles **10**, **11** and **12** to scavenge the $ABTS^{+\bullet}$ and $NO^{\bullet}$ was determined by chemical assays to evaluate the antioxidant potential of these compounds. In these assays, the results and discussion of which will be presented later in Chapter 3, pyrazole **12** revealed the higher free radical scavenging activity of both radicals. Therefore, compounds **11** and **12** were chosen as the templates for the development of a suitable precursor for the preparation of the ^{18}F-labelled pyrazoles to be used as a PET probe.

[1] Only two steps are presented for the synthesis of pyrazole **10** (Scheme 4) because we started from chalcone **8** which was already available in the laboratory, otherwise, this compound would have to be synthetized.

2.2.3 Synthesis of a pyrazole precursor for ^{18}F-fluorination via nucleophilic aliphatic substitution reaction

As previously mentioned, in Chapter 1, labelling of radiopharmaceuticals with fluorine-18 for use in PET is particularly attractive because of the longer half-life of fluorine-18 that permits more 'complex' chemical syntheses, the transportation of the radiotracer and its use in different place from the site of production. Thus, this radioisotope has been used for the labelling of numerous relatively simple or even more complex bioactive chemical compounds. Two strategies can be followed for the radiolabelling: i) Nucleophilic aliphatic substitution reactions (S_N2 type) or ii) Nucleophilic aromatic substitution reactions (S_NAr), both involving [^{18}F]fluoride.

In this work, we started by exploring the first strategy- the simple S_N2 type displacement of a suitable leaving group- a sulfonate ester (tosyl group)- which required the preparation of the tosylated precursor of the [^{18}F]pyrazole, starting from the previously synthetized 5(3)-(4-fluorophenyl)-3(5)-(2-hydroxyphenyl)-1*H*-pyrazole (**10**) and 4-(4-fluorostyryl)-3(5)-(2-hydroxyphenyl)-1*H*-pyrazole (**12**) as represented in Scheme 6. The strategy proposed involves the alkylation of the starting pyrazole **10** or **12** with an alkyl chain of two or six carbons having a terminal hydroxy group, followed by tosylation of the hydroxy group, and in the last step, the S_N2 type displacement of the tosyl group by fluorine. This last reaction was not yet attempted with the fluorine-18, but with fluorine-19 as a proof-of-concept.

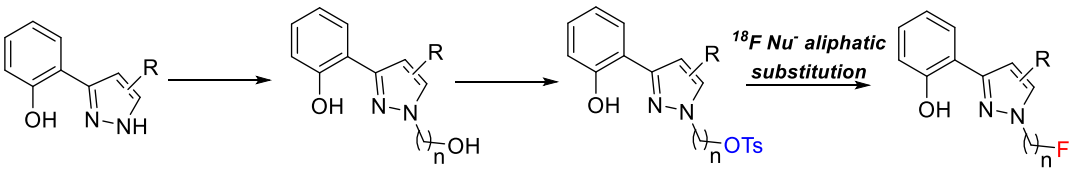

R = 4-(4-fluorostyryl)
R = 5-(4-fluorophenyl)

n = 2 or 6

Scheme 6: Strategy proposed for the synthesis of a [^{18}F]pyrazole-derived radioligand by nucleophilic aliphatic substitution reaction.

2.2.3.1 Alkylation of 5(3)-(4-fluorophenyl)-3(5)-(2-hydroxyphenyl) -1*H*-pyrazole and 4-(4-fluorostyryl)-3(5)-(2-hydroxyphenyl)-1*H*-pyrazole

All alkylation reactions were performed in acetone, in the presence of potassium carbonate (3.0 equiv) as base and the appropriate alkylating agent (1.2-1.5 equiv) (Schemes 7 and 8). Alkylation of 5(3)-(4-fluorophenyl)-3(5)-(2-hydroxyphenyl)-1*H*-pyrazole (**10**) was carried out with 6-bromohexanol (Scheme 7). The alkylation of 4-(4-fluorostyryl)-3(5)-(2-hydroxyphenyl)-1*H*-pyrazole (**12**) was carried out with two different alkylating agents, 2-bromoethanol and 6-bromohexanol (Scheme 8), to introduce alkyl chains of different size, since a different size can provide different properties to the obtained compounds for instance regarding lipophilicity or binding affinity. [2]

The reaction with 2-bromoethanol required a long time (more than 4 days) because of the boiling point of 2-bromoethanol which is the same of acetone (56ºC) and therefore the reaction was heated at a temperature lower than reflux temperature. For all alkylations, after purification of the reaction mixture by TLC using ethyl acetate:hexane (3:2) as eluent, *N*- and *O*-alkylated pyrazoles were isolated. Since the 2'-OH proton is involved in a hydrogen bond with N2 of pyrazole ring, the *O*-alkylated pyrazole was the minor product of these reactions.

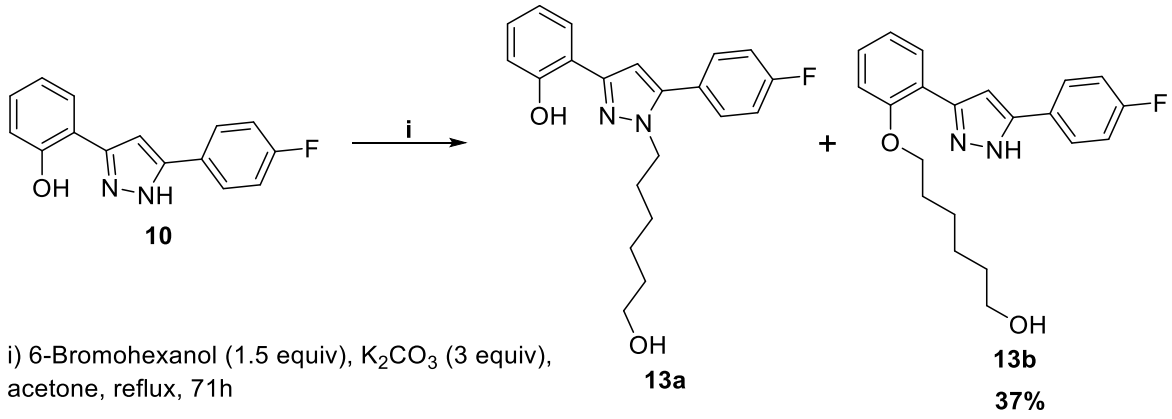

*Scheme 7: Alkylation of 5(3)-(4-fluorophenyl)-3(5)-(2-hydroxyphenyl)-1H-pyrazole (**10**).*

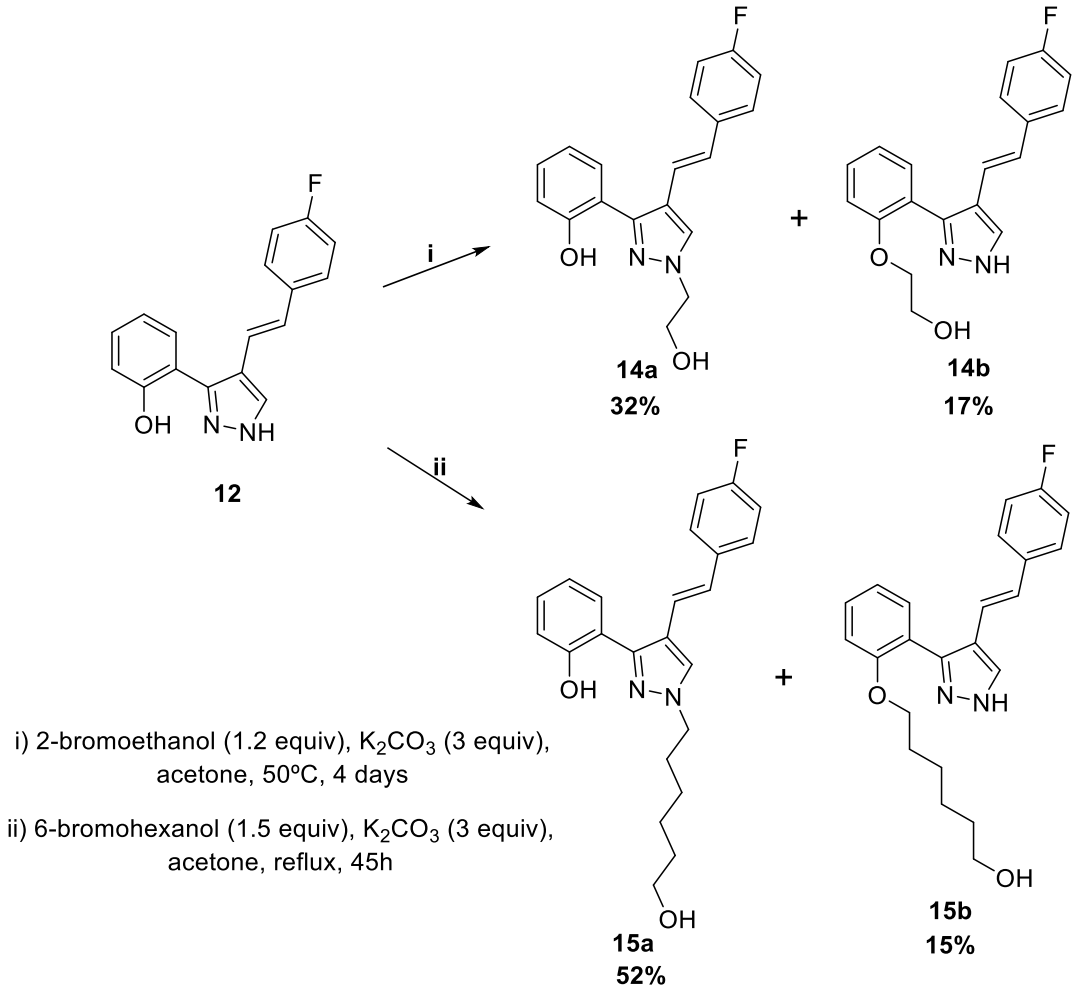

*Scheme 8: Alkylation of 4-(4-fluorostyryl)-3(5)-(2-hydroxyphenyl)-1H-pyrazole (**12**).*

2.2.3.2 Tosylation of (*E*)-4-(4-fluorostyryl)-1-(2-/6-hydroxyalkyl)-3-(2-hydroxyphenyl)-1*H*-pyrazoles and (*E*)-4-(4-fluorostyryl)-3(5)-[2-(2-hydroxyethyl)phenyl]-1*H*-pyrazole

The synthesis of the tosylated precursors of the [^{18}F]pyrazole was performed starting from (*E*)-4-(4-fluorostyryl)-1-(2-hydroxyethyl)-3-(2-hydroxyphenyl)-1*H*-pyrazole (**14a**), (*E*)-4-(4-fluorostyryl)-3(5)-[2-(2-hydroxyethyl)phenyl]-1*H*-pyrazole (**14b**) and (*E*)-4-(4-fluorostyryl)-1-(6-hydroxyhexyl)-3-(2-hydroxyphenyl)-1*H*-pyrazole (**15a**) and which were available in higher amounts. These alkylated pyrazoles were reacted with *p*-toluenesulfonyl chloride (tosyl chloride, *p*-TsCl) and triethylamine (TEA) in DCM as solvent, at room temperature for 24h. After that period, the reaction mixture was poured over ice and water and acidified. The precipitate formed was dissolved in DCM. After purification by TLC,

using ethyl acetate:hexane (3:2) as eluent the expected compounds were isolated in low to moderate yields (16-43%) (Scheme 9).

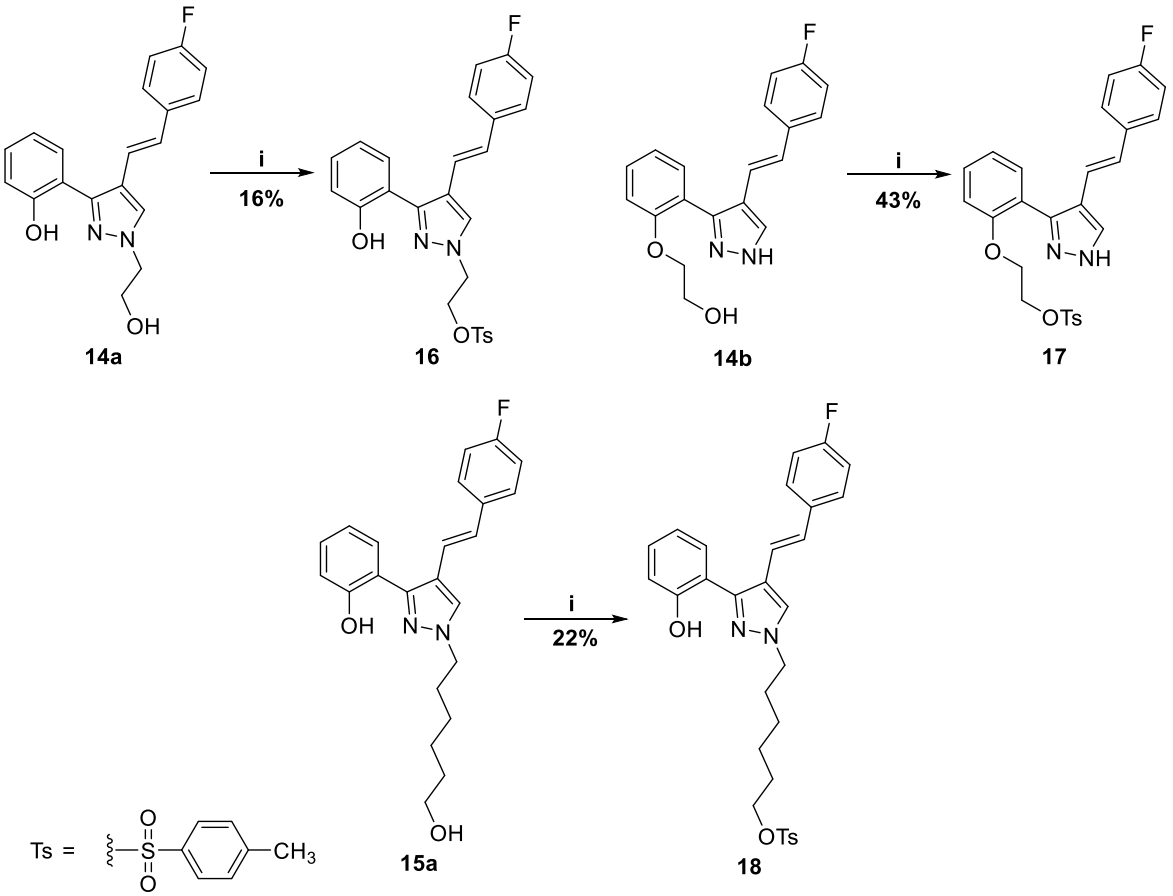

i) *p*-TsCl (1.2 equiv.), TEA (2.0 equiv.), DCM, r.t, 24h

*Scheme 9: Tosylation of alkylated pyrazoles **14a, 14b** and **15a**.*

2.2.3.3 Synthesis of [^{19}F]-(*E*)-4-(4-fluorostyryl)-1-(6-fluorohexyl)-3-(2-hydroxyphenyl)-1*H*-pyrazole

The relatively short physical half-lives of the positron emitting nuclides, such as ^{18}F require that the synthesis time for a PET imaging probe is kept as short as possible. Ideally, the synthesis and purification period should not exceed 2 to 3 times the physical half-life of the radionuclide in use, and strategies for the radiolabeling should aim to introduce the label in the synthetic sequence as late as possible. Multistep syntheses may be employed for complex molecules that require labeling via prosthetic groups or have sensitive functional groups that need to be protected and deprotected after the radiolabeling. Usually a large excess of unlabeled precursor typically about 103- to 104-fold of the radioactive reagent is employed during the radiosynthesis to help drive the radiolabeling reaction to completion.

This very high stoichiometric ratio results in pseudo-first-order reaction kinetics, which leads to an increased reaction rate and a rapid turnover of the radiolabeling entity. Practical reaction times vary and range from 1 to 30 min depending on the physical half-life of the radioisotope in use. Reaction volumes are typically 0.2–1 mL, and reaction temperatures also vary from room temperature to 190 °C.

An attempt was made to test the introduction of ^{19}F into the structure of compound **18** by nucleophilic aliphatic substitution of the tosyl group, as a proof-of-concept, thus simulating the reaction that will be performed for the introduction of ^{18}F radionuclide. In this attempt, we used tetra-*N*-butylammonium fluoride (TBAF) as source of ^{19}F and dry THF as solvent (Scheme 10). The reaction was stirred at reflux for 30 minutes. After that period, the reaction mixture was extracted with DCM. After purification by TLC, using DCM as eluent the target compound (**19**) was isolated. Since the reaction was performed with a small amount of the tosylated pyrazole (**18**) it was difficult to calculate the reaction yield. However, the reaction was complete (no starting material was observed in the TLC) and the appearance of a new peak in the ^{19}F-NMR spectrum and disappearance of signals corresponding to the resonance of the protons of the tosyl group in ^{1}H-NMR of compound (**19**) confirm the S_N2 type displacement of the tosyl group by fluorine and consequent formation of compound (**19**).

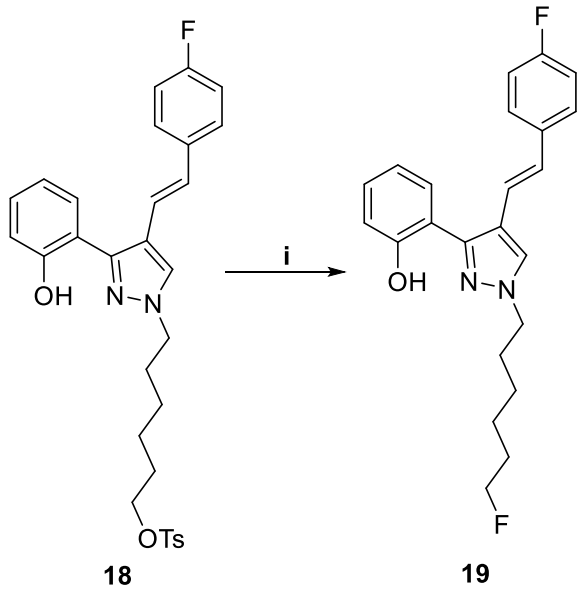

18 **19**

i) TBAF (2.0 equiv.), THF, reflux, 30 min.

*Scheme 10: Synthesis of (E)-1-(6-fluorohexyl)-4-(4-fluorostyryl)-3-(2-hydroxyphenyl)-1H-pyrazole (**19**).*

All PET radiopharmaceuticals whether for human or animal use should show a high level of radiochemical purity (typically>95%). Therefore, for the radiolabeled compound analog the purification should be achieved by high pressure liquid chromatography (HPLC). In some cases, the use of disposable cartridges is sufficient enough to achieve highly purified radiolabeled compounds.

Besides aliphatic nucleophilic substitutions, the fluorine-18 atom can be introduced into a chemical structure via aromatic nucleophilic substitution reactions. The strategy proposed, in this work, for the synthesis of a suitable pyrazole precursor for labelling via aromatic nucleophilic substitution reactions is described in the next section.

2.2.4 Synthesis of a pyrazole precursor for ^{18}F-fluorination via nucleophilic aromatic substitution reaction

Nucleophilic aromatic substitution reactions are facilitated when the aromatic ring is activated by the presence of at least one electron-withdrawing group (for instance, a nitro group) positioned *ortho*- or *para*- to the leaving group, that will be replaced by fluorine-18. However, when this group is not present in the chemical structure or in the case of electron-rich structures, the preparation of aromatic precursors featuring a substituent with exceptional property as a leaving group is required for labelling.

Once evaluated the antioxidant capacity of the synthesized pyrazoles **10**, **11** and **12**, and having found that some of them have significant radical scavenging activity, we proposed the method presented in Scheme 11 to obtain analogous pyrazoles labelled with fluorine-18. To achieve this goal, it was planned to introduce a sydnone group, which is a stable group that can be easily replaced by fluorine, in the aromatic ring of the pyrazole. Starting from a (nitro)pyrazole, the method is initiated with the reduction of the nitro group to an amine group, and transformation of the aniline into a sydnone following a two-step procedure (Scheme 11).

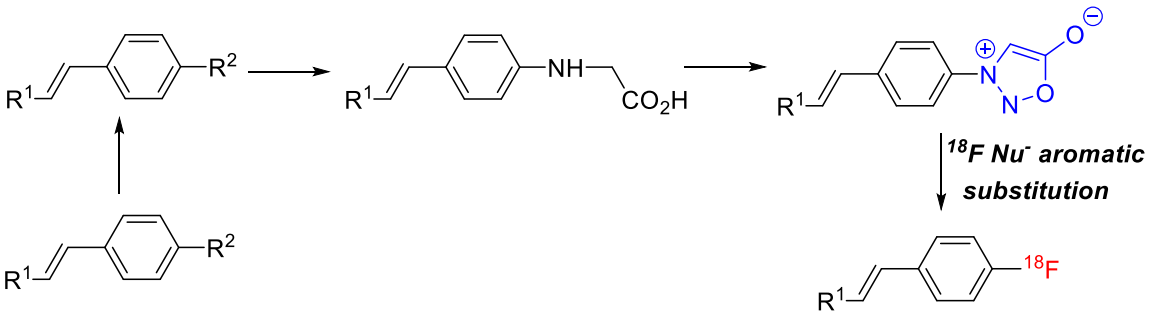

R^1 = (2-hydroxyphenyl)pyrazole
R^2 = NO_2, NH_2

Scheme 11: Strategy proposed for the synthesis of a [^{18}F]pyrazole-derived radioligand by nucleophilic aromatic substitution reaction.

2.2.4.1 Synthesis of (*E*)-3(5)-(2-hydroxyphenyl)-4-(4-nitrostyryl)-1*H*-pyrazole

The (*E*)-3(5)-(2-hydroxyphenyl)-4-(4-nitrostyryl)-1*H*-pyrazole **21** was synthetized from the reaction of (*E*)-3-(4-nitrostyryl)-4*H*-chromen-4-one **7b** with hydrazine hydrate (55%) in methanol at room temperature for 3 hours (Scheme 12). The expected pyrazole **21** was isolated in good yield (60%) after crystallization with methanol.[104]

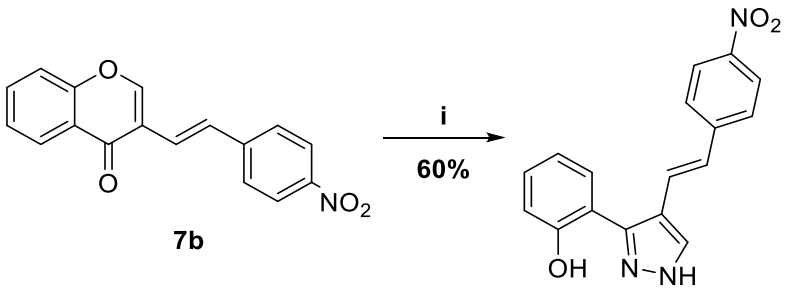

i) $H_2NNH_2.H_2O$ (2 equiv.), CH_3OH, r.t, 3h

*Scheme 12: Synthesis of (E)-3(5)-(2-hydroxyphenyl)-4-(4-nitrostyryl)-1H-pyrazole (**21**).*

2.2.4.2 Synthesis of (*E*)-4-(4-aminostyryl)-3(5)-(2-hydroxyphenyl)-1*H*-pyrazoles

The reduction of the nitro group of (*E*)-3(5)-(2-hydroxyphenyl)-4-(4-nitrostyryl)-1*H*-pyrazoles **21a,b** (pyrazole **21b** was already available in the laboratory) to the amino group was performed by reaction with tin in HCl, using chloroform as solvent, at room temperature for 2 hours (Scheme 13). After this period, the reaction mixture was filtered using celite and neutralized using $NaHCO_3$. After purification by TLC, using

chloroform:methanol (9.5:0.5) for **22a** and DCM:acetone (9:1) for **22b** as eluent, the expected pyrazoles were isolated in very low (**22a**,10%) to good (**22b**, 65%) yields. Although the full structural characterization of compound **22b** was not obtained, the comparison of the ^{1}H NMR spectra of both compounds **21b** and **22b** confirmed the reduction of the nitro group. In the ^{1}H NMR spectrum of compound **22b** it was observed a shift of the two doublets corresponding to the resonance of the protons H-2",6" and H-3",5", of the *para*-substituted aryl ring, to lower chemical shifts when compared to the chemicals shifts of these protons in compound **21b**. The shielding of these protons is due to the strong electron-donating effect of the amino group, particularly on the protons at the *ortho*-position.

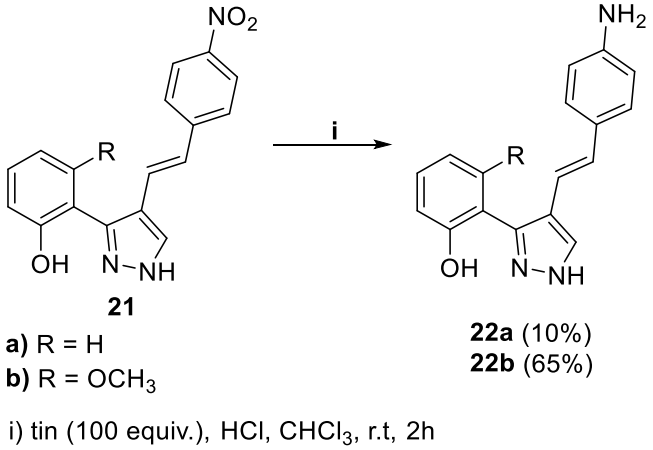

*Scheme 13: Synthesis of (E)-4-(4-aminostyryl)-3(5)-(2-hydroxyphenyl)-1H-pyrazoles (**22a,b**)*

2.2.4.3 Synthesis of glycine derivatives of pyrazoles

To introduce the glycine group in the pyrazole structure, three different methods were attempted. In the first attempt, the (*E*)-3(5)-(2-hydroxy-6-methoxyphenyl)-4-(4-aminostyryl)- 1*H*-pyrazole (**22b**) which was obtained in higher amount in the previous step, as described in section 2.2.4.2, was reacted with sodium acetate, glacial acetic acid, sodium cyanoborohydride and glyoxylic acid monohydrate in methanol for 4 hours with stirring at room temperature (Scheme 14). After this period, the reaction mixture was washed with brine and extracted with ethyl acetate. After purification by TLC using DCM:acetone (9:1) as eluent, the expected pyrazole **23** was isolated with 12% yield. The small amount of compound obtained did not allow to proceed to the next step which would be the synthesis of the sydnone. Therefore, the synthesis of the glycine derivative of 5-(4-fluorophenyl)-3-(2-hydroxyphenyl)-1*H*-pyrazole (**10**) was attempted through the reaction of this pyrazole with glycine and sodium bicarbonate using water as solvent. The reaction was heated at

reflux with stirring for 40 hours (Scheme 14). After that period, the reaction mixture was poured over ice and water and acidified. The precipitate formed was dissolved in ethyl acetate and the organic layer was washed with water. After purification by TLC using ethyl acetate:hexane (3:2) as eluent the expected pyrazole **24** wasn't isolated. Finally, it was attempted the reaction of (*E*)-3-(4-aminostyryl)-1-phenyl-5-(2-hydroxyphenyl)-1*H*-pyrazole (**25**) with chloroacetic acid and water as solvent. The reaction was heated at reflux with stirring for 24 hours (Scheme 14). After that period, the reaction mixture was poured over ice and water and neutralized with NaOH. Then, the aqueous layer was extracted using ethyl acetate and the resulting organic layer was evaporated at dryness. After NMR and mass spectrometry it was not possible to confirm the presence of expected pyrazole **26**.

Since the glycine-derivative of any of the pyrazoles **10** and **25** was not obtained it was not possible to proceed to next step which would be the synthesis of the sydnone. In the near future, higher amounts of the glycine derivative of pyrazole **10** will be prepared in order to perform the synthesis of the corresponding sydnone to prepare the suitable precursor for ^{18}F-radioflurination via nucleophilic aromatic substitution.

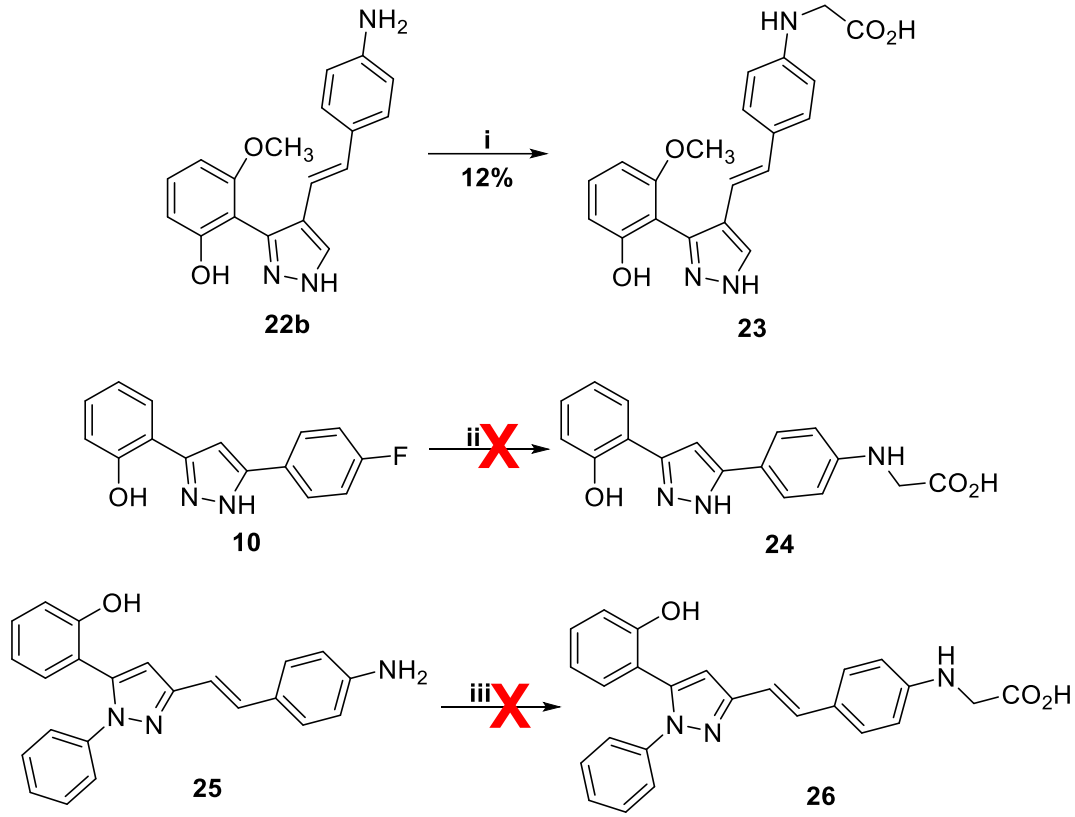

i) $C_2H_3NaO_2$ (2.0 equiv.), glacial CH_3COOH (4.0 equiv.), $NaBH_3CN$ (1.05 equiv.), $C_2H_4O_4$ (1.5 equiv.), CH_3OH, r.t, 4h
ii) glycine (1.1 equiv.), $NaHCO_3$ (1.5 equiv.), H_2O, reflux, 40h
iii) $ClCH_2CO_2H$ (2.0 equiv.), H_2O, reflux, 24h

*Scheme 14: Strategies followed for the synthesis of glycine derivatives of pyrazoles **22b**, **10** and **25**.*

2.3 Structural characterization of the synthetized compounds

In this section, will be presented and discussed the structural characterization of the new and most relevant synthetized compounds, namely pyrazoles **10**, **11**, **12** and the alkylated derivatives of pyrazole **12**. All these new compounds were characterized by mono- (^1H and ^{13}C) and two-dimensional (HSQC and HMBC) NMR techniques, and whenever possible by mass spectrometry (ESI^+) and high-resolution mass spectrometry. These techniques allowed to unequivocally confirm the structure of synthesized compounds.

2.3.1 Characterization of 5(3)-(4-fluorophenyl)-3(5)-(2-hydroxyphenyl)-1*H*-pyrazole (10)

The structure and numbering of 5(3)-(4-fluorophenyl)-3(5)-(2-hydroxyphenyl)-1*H*-pyrazole (**10**) was presented in figure 24, section 2.1.5. In the aromatic region of the spectrum of compound **10** (Figure 28), the most deshielded protons are H-2'' and H-6'' which appear as a doublet of doublets at $\delta = 7.88$ ppm due the coupling of these protons with H-3'' and H-5'' and with fluorine atom at a longer distance. At $\delta = 7.72$ ppm appears a doublet of doublets corresponding to the resonance of H-6'. This proton is more deshielded than H-3', H-4' and H-5' due to the effect of the pyrazole ring and because it is in *meta*-position relatively to the 2'-OH group. The multiplicity of this signal is justified by the coupling of H-6' with H-5' and with H-4'at a longer distance. The resonance of protons H-3'',5'', H-4 and H-4' appear as a multiplet at $\delta = 7.13 - 7.38$ ppm. Due to the overlap of signals in this region, it was impossible to identify the multiplicity of each signal. Theoretically, protons H-3'',5'' should appear as a triplet, due to the coupling with fluorine atom and H-2'',6'', H-4 should appear as a singlet and H-4' which may couple with H-3', H-5' and H-6'at a longer distance was expected to be a doublet of doublets of doublets. Lastly, the resonances of H-3' and H-5' were observed as a multiplet at $\delta = 6.89 - 6.99$ ppm. These signals should appear as a doublet of doublets (H-3') and double of doublets of doublets (H-5'), respectively. They are also more protected that the remaining protons because they are in *ortho*- and *para*-positions, relatively to the 2'-OH group.

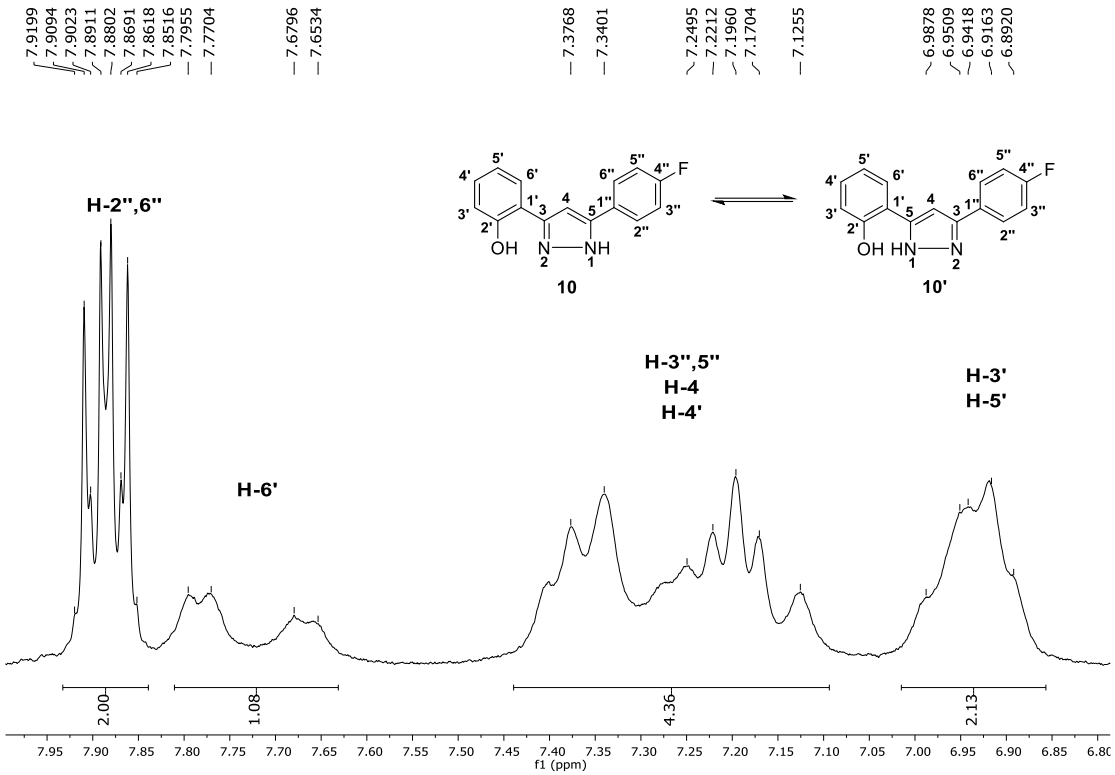

*Figure 28: Expansion of the aromatic region of the ^1H NMR spectrum of mixture of tautomers 5(3)-(4-fluorophenyl)-3(5)-(2-hydroxyphenyl)-1H-pyrazole (**10**) (300.13 Hz, $CDCl_3$)*

Also typical of pyrazole **10** are the four singlets at high frequency ($\delta \geq 10.0$ ppm) which indicate a mixture of tautomers (**10** and **10'**). The resonances of the OH proton of each tautomer appear as singlets at $\delta = 13.64$ ppm and $\delta = 12.90$ ppm and those of NH protons appear also as singlets at $\delta = 10.86$ ppm and $\delta = 10.24$ ppm (Figure 29).

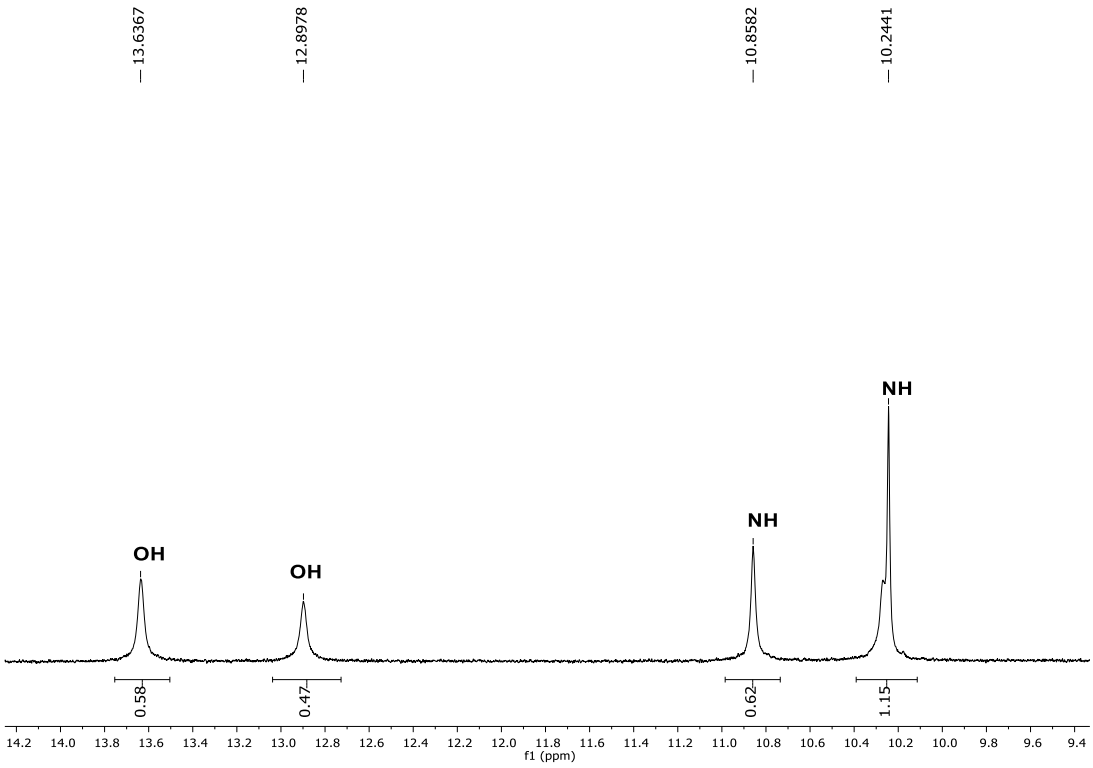

*Figure 29: Expansion of the ^{1}H NMR spectrum of 5(3)-(4-fluorophenyl)-3(5)-(2-hydroxyphenyl)-1H-pyrazole (**10**) (300.13 Hz, $CDCl_3$)*

2.3.2 Characterization of 5(3)-(4-fluorostyryl)-3(5)-(2-hydroxyphenyl)-1*H*-pyrazole (11) and (*E*)-4-(4-fluorostyryl)-3(5)-(2-hydroxyphenyl)-1*H*-pyrazole (12)

The structure and numbering of 5(3)-(4-fluorostyryl)-3(5)-(2-hydroxyphenyl)-1*H*-pyrazole (**11**) and (*E*)-4-(4-fluorostyryl)-3(5)-(2-hydroxyphenyl)-1*H*-pyrazole (**12**) whose structural characterization will be discussed in this section are presented in figures 26 and 27.

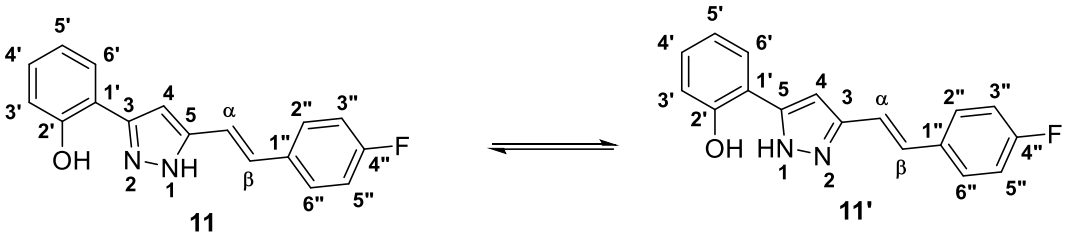

*Figure 26: Structure and numbering of 5(3)-(4-fluorostyryl)-3(5)-(2-hydroxyphenyl)-1*H*-pyrazole (**11**) and the corresponding tautomer (**11'**)*

The most characteristic signals in the ^{1}H NMR spectra of pyrazole **11 (**Figure 26**)** are: i) the broad singlet at $\delta = 6.79$ ppm, due to the resonance of the proton of the pyrazole

ring H-4, and a broad singlet at $\delta = 10.55$ ppm that corresponds to the resonance of two protons of the N*H* and 2'-O*H*. Also typical of the structure of analogues of pyrazole **11** are the signals due to the resonance of protons H-α and H-β, however for pyrazole **11** these protons appear at $\delta = 7.03$-7.09 ppm as a multiplet, together with the resonance of protons H-3',5'. The presence of a triplet at $\delta = 6.94$ ppm, due to the resonance of H-3",5", and a doublet of doublets at $\delta = 7.44$ ppm, due to the resonance of H-2",6", confirm the substitution at the *para*-position of the phenyl ring with fluorine, since the multiplicity of these signals is due to the coupling of these protons with each other and with fluorine.

Pyrazole **12** (Figure 27) can be distinguished from its isomer, pyrazole **11**, based on the following signals:

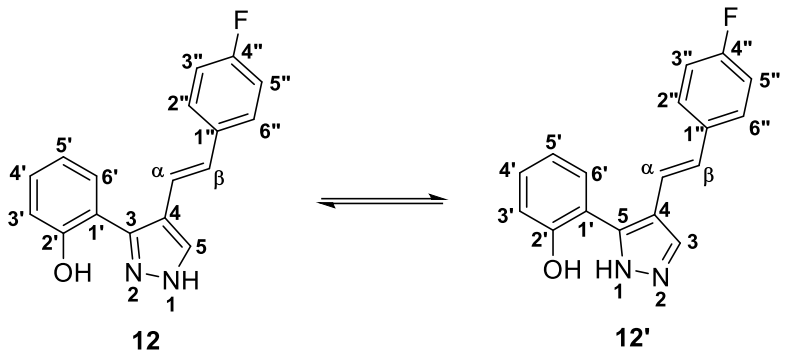

*Figure 27: Structure and numbering of 5(3)-(4-fluorostyryl)-3(5)-(2-hydroxyphenyl)-1*H*-pyrazole (**11**) and (*E*)-4-(4-fluorostyryl)-3(5)-(2-hydroxyphenyl)-1*H*-pyrazole (**12**) and the corresponding tautomers (**11'**) and (**12'**)*

i) the presence of a singlet due to the proton of the pyrazole ring (H-5) at a higher chemical shift, $\delta = 7.83$ ppm (Figure 28). The high frequency value for H-5 is due the fact that it is a proton of a carbon that is linked to N-1 of the pyrazole; ii) the doublets at $\delta = 6.85$ ppm and $\delta = 7.06$ ppm corresponding to the resonance of H-β and H-α, respectively. The H-α appears at highest values due the resonance effect of pyrazole ring. These doublets have a large coupling constant, J = 16.9 Hz, due the *trans* configuration of the double bond. The remaining protons appear as expected; A double triplet was observed at $\delta = 6.96$ ppm due the resonance of H-5' and the multiplicity of this signal suggests that H-5' is coupling with H-4' and H-6' with the same coupling constant J = 7.4 Hz although they are chemically different protons, and H-5' also couples with H-3' at a long distance ($^4J_{H5'\text{-}H3'} = 1.3$ Hz). H-3' and H-5' appear at lower chemical shifts due the presence of the electron-donating hydroxy group at C-2' that causes the shielding of *ortho*- and *para*-positions. The signal corresponding to H-4' appears as a doublet of doublets of doublets at $\delta = 7.31$ ppm due the

coupling of H-4' with H-3' ($^3J_{H4'-H3'}$ = 8.6 Hz), H-5' ($^3J_{H4'-H5'}$ = 7.4 Hz) and H-6' ($^4J_{H4'-H6'}$ = 1.7 Hz). The most deshielded proton of this aromatic ring is H-6'. This signal appears as a doublet of doublets at δ = 7.60 ppm. The coupling of H-6' with H-5' ($^3J_{H6'-H5'}$ = 7.4 Hz) and H-4' ($^4J_{H6'-H4'}$ = 1.7 Hz) justifies the multiplicity of the signal. The resonance of protons H-2'',6'' and H-3'',5'' suffer the effect of *para*-substitution with fluorine atom that activates the aromatic ring shielding *orto*- positions and deshielding *meta*- positions relative to its position. This fact justifies the appearance of the signal corresponding to the resonance of H-2'',6'' at higher chemical shift, δ = 7.44 ppm, when compared to the resonance of H-3'',5'' that appears at δ = 7.05 ppm. These two signals appear as a triplet for H-3'',5'' and as a doublet of doublets for H-2'',6''due to the coupling of each other and with fluorine atom (Figure 28). The presence of the fluorine atom at *para*-position is also confirmed by the signal (m, 4'-F) observed at δ = -138.7 ppm in the ^{19}F NMR spectrum.

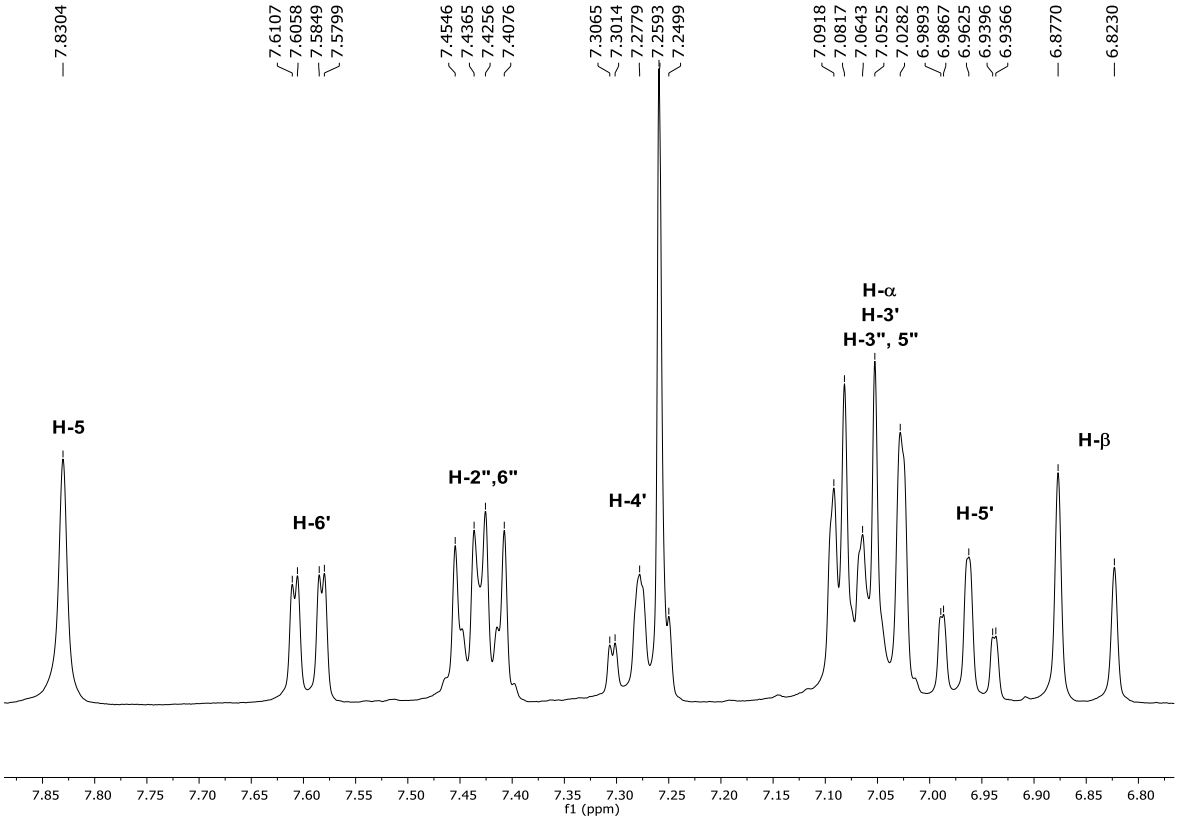

*Figure 28: Expansion of the aromatic region of the ^{1}H NMR spectrum of (E)-4-(4-fluorostyryl)-3(5)-(2-hydroxyphenyl)-1H-pyrazole (**12**) (300.13 Hz, $CDCl_3$)*

The identification of the carbons in the ^{13}C NMR spectrum of pyrazole **12** (Figure 29), was based on the analysis of the heteronuclear single quantum correlation (HSQC) spectrum (Figure 30), that allowed the assignment of the following protonated carbons: C-3'',5'' (δ = 115.7 ppm), C-3' (δ = 117.0 ppm), C-α (δ = 118.6 ppm), C-5' (δ = 119.6

ppm), C-5 (δ = 127.7 ppm), C-2'',6'' (δ = 127.9 ppm), C-6' (δ = 128.6 ppm), C-β (δ = 128.8 ppm) and C-4' (δ = 129.6 ppm).

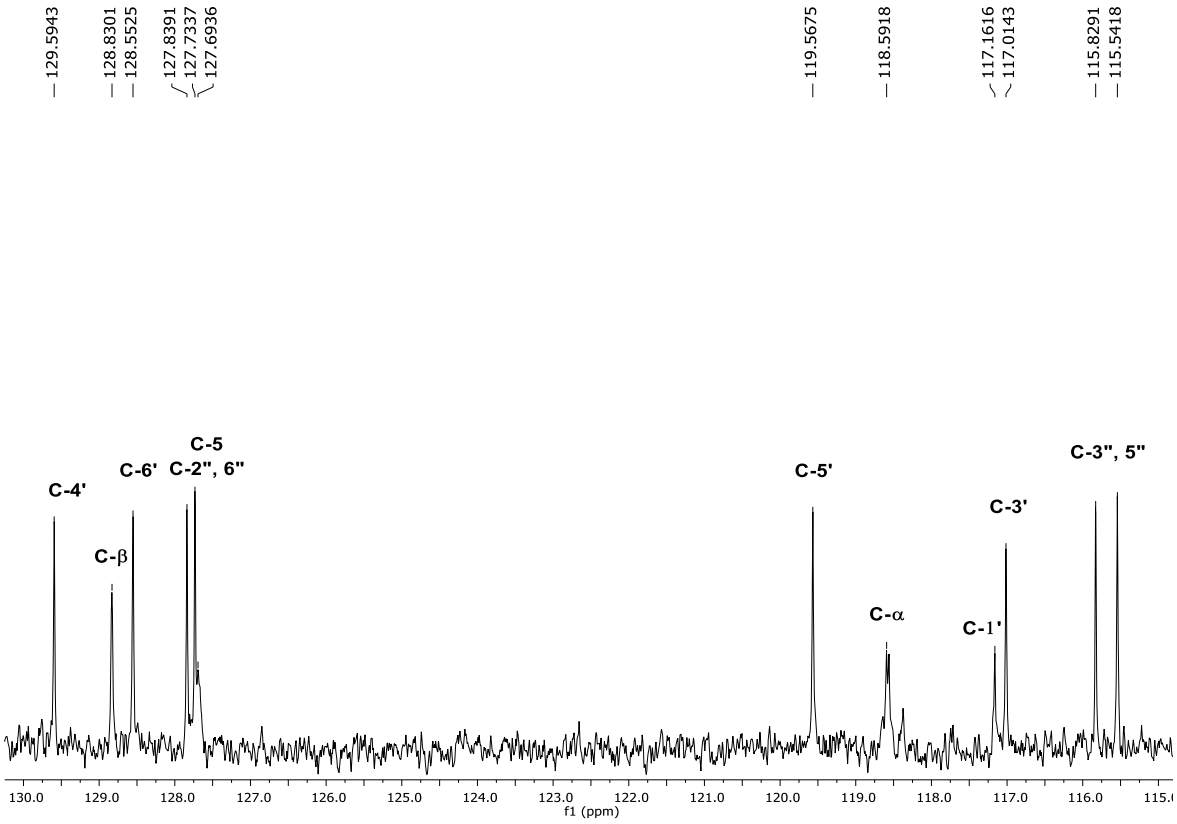

*Figure 29: Expansion of the aromatic region of the ^{13}C NMR spectrum of (E)-4-(4-fluorostyryl)-3(5)-(2-hydroxyphenyl)-1H-pyrazole (**12**) (75.47 Hz, $CDCl_3$)*

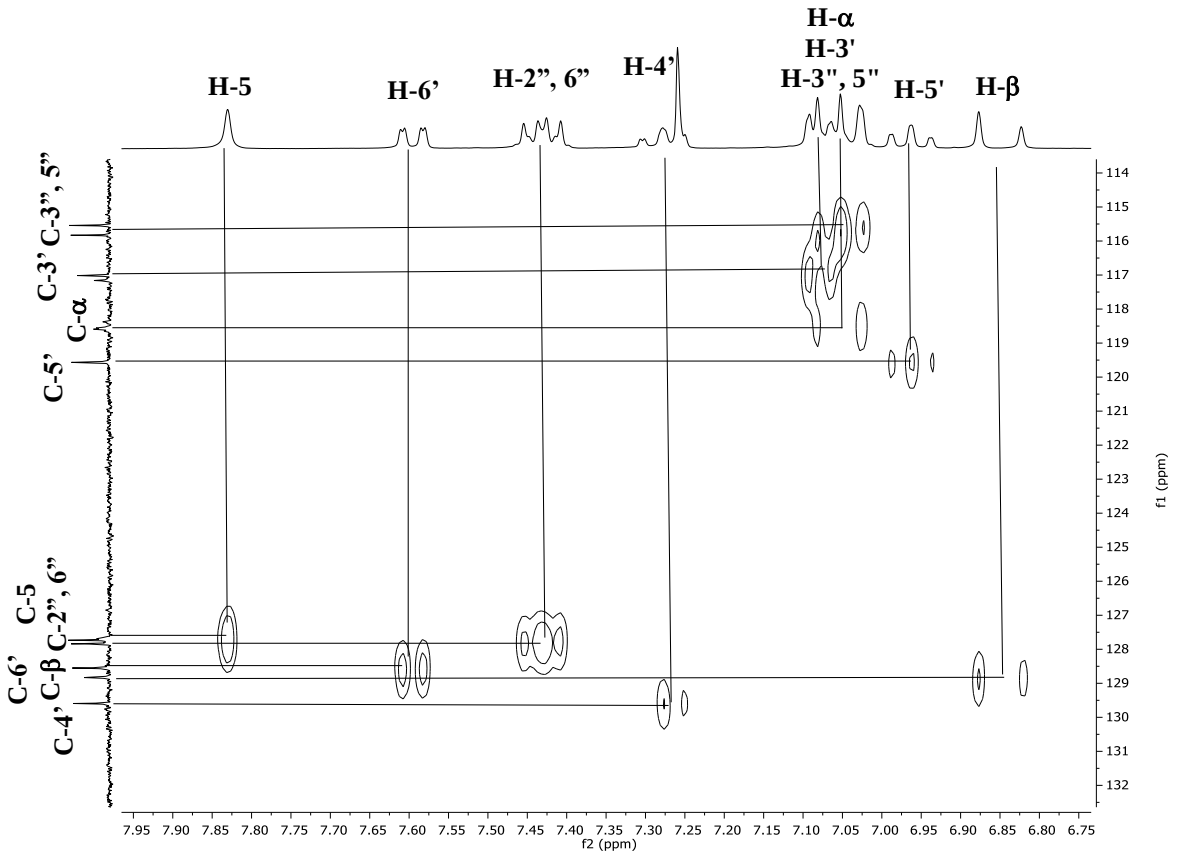

*Figure 30: Expansion of the HSQC spectrum of (E)-4-(4-fluorostyryl)-3(5)-(2-hydroxyphenyl)-1H-pyrazole (**12**)*

In addition, the assignment of the non-protonated carbons, C-1' (δ =117.2 ppm), C-4 (δ = 119.6 ppm), C-1" (δ =133.5 ppm) (Figure 31) and C-3 (δ =147.5 ppm), C-2' (δ =155.6 ppm) and C-4" (δ =162.3 ppm) (Figure 32), was possible based on the analysis of the heteronuclear multiple bond correlation (HMBC) spectrum.

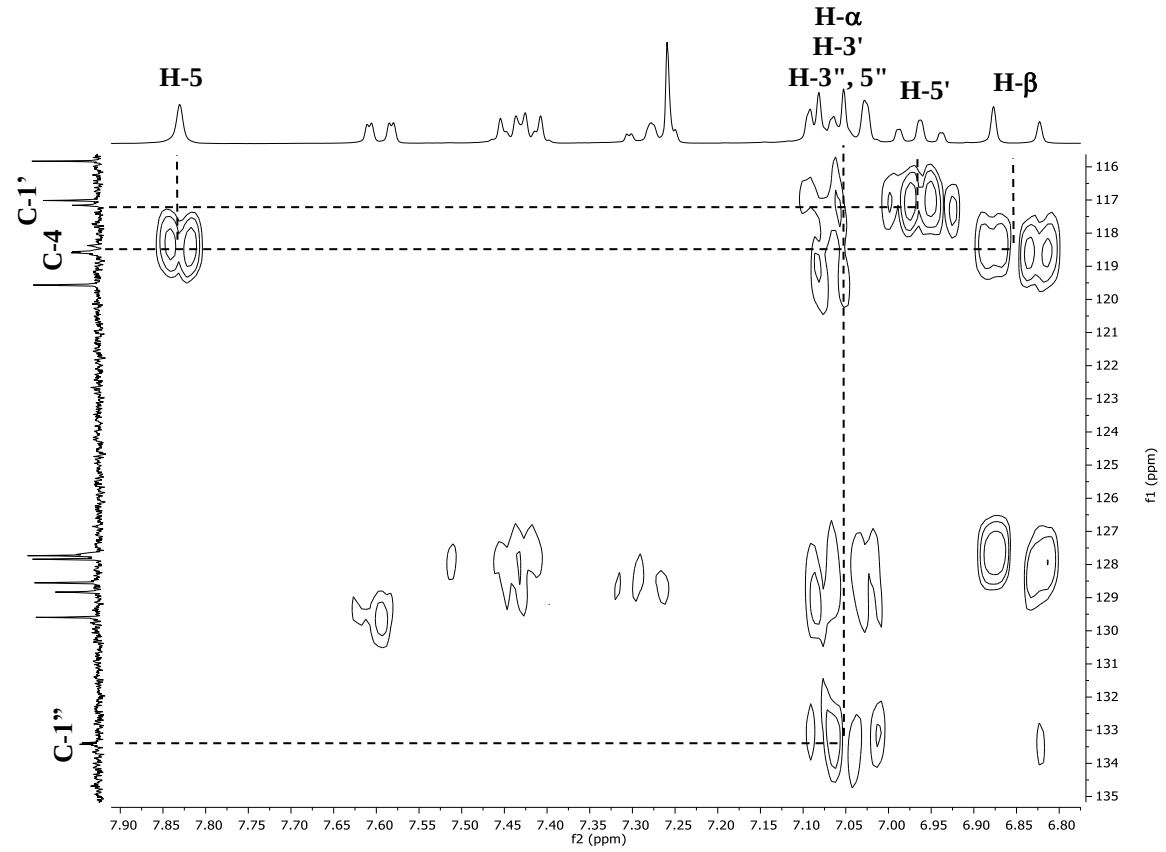

*Figure 31: Expansion of the HMBC spectrum of (E)-4-(4-fluorostyryl)-3(5)-(2-hydroxyphenyl)-1H-pyrazole (**12**)*

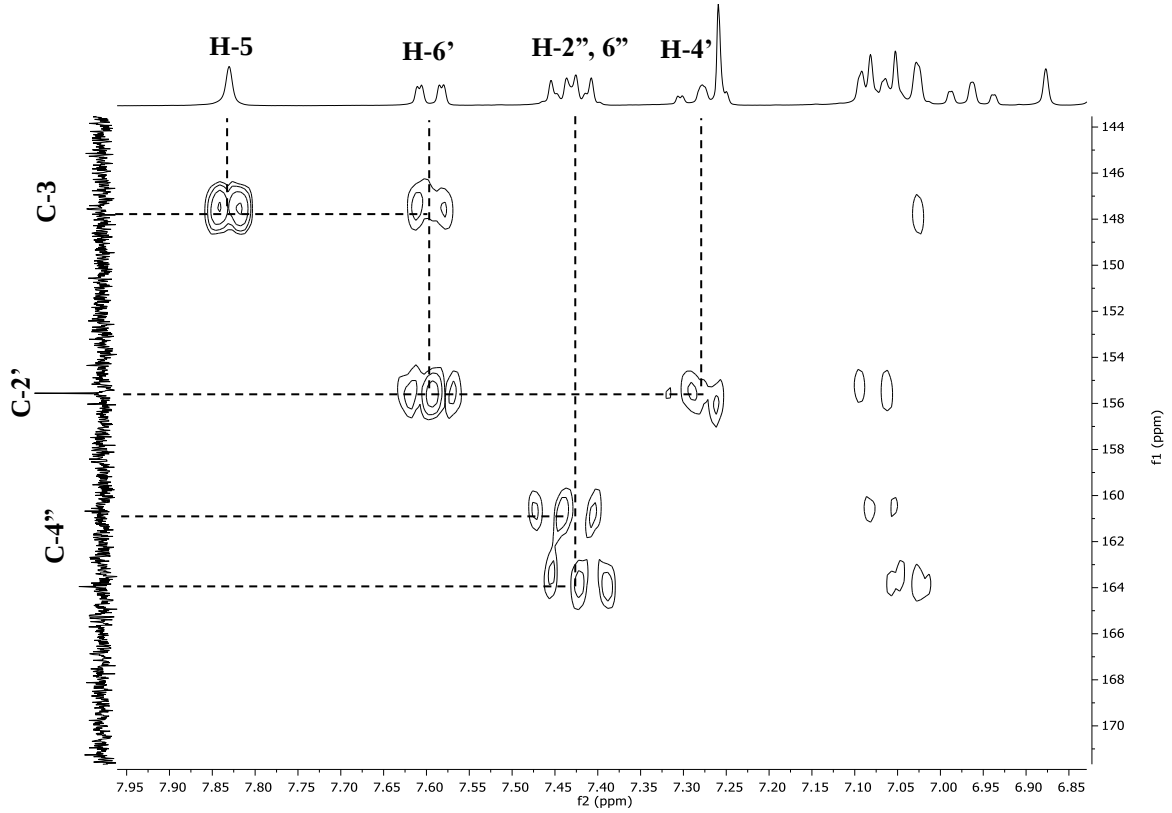

*Figure 32: Expansion of the HMBC spectrum of (E)-4-(4-fluorostyryl)-3(5)-(2-hydroxyphenyl)-1H-pyrazole (**12**)*

2.3.3 Characterization of alkylated pyrazoles (14a, 15a and 15b)

Among the alkylated pyrazoles, the NMR data of which are presented in the experimental section, pyrazoles **14a** and **15a** were chosen as models for the discussion of the main features found in the NMR spectra of these compounds. The structure and numbering of compound **14a** is presented in Figure 33.

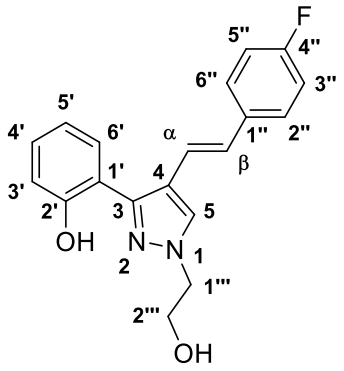

14a

*Figure 33: Structure and numbering of (E)-4-(4-fluorostyryl)-1-(2-hydroxyethyl)-3-(2-hydroxyphenyl)-1H-pyrazole (**14a**).*

The main characteristic signals of the alkylated pyrazoles appear in the aliphatic region of the spectrum and are due to the introduction of the alkyl chain. In the case of compound (**14a**) two triplets appear in aliphatic region at δ = 4.05 ppm (2'''-CH_2) and δ = 4.30 ppm (1'''-CH_2) (Figure 34). The other protons of the compound's structure appear in the expected chemical shifts, based on the comparison with the spectrum of the parent compound, pyrazole **12**. Note that the signal due to the resonance of H-4' appears superimposed with the signal of the chloroform (Figure 34).

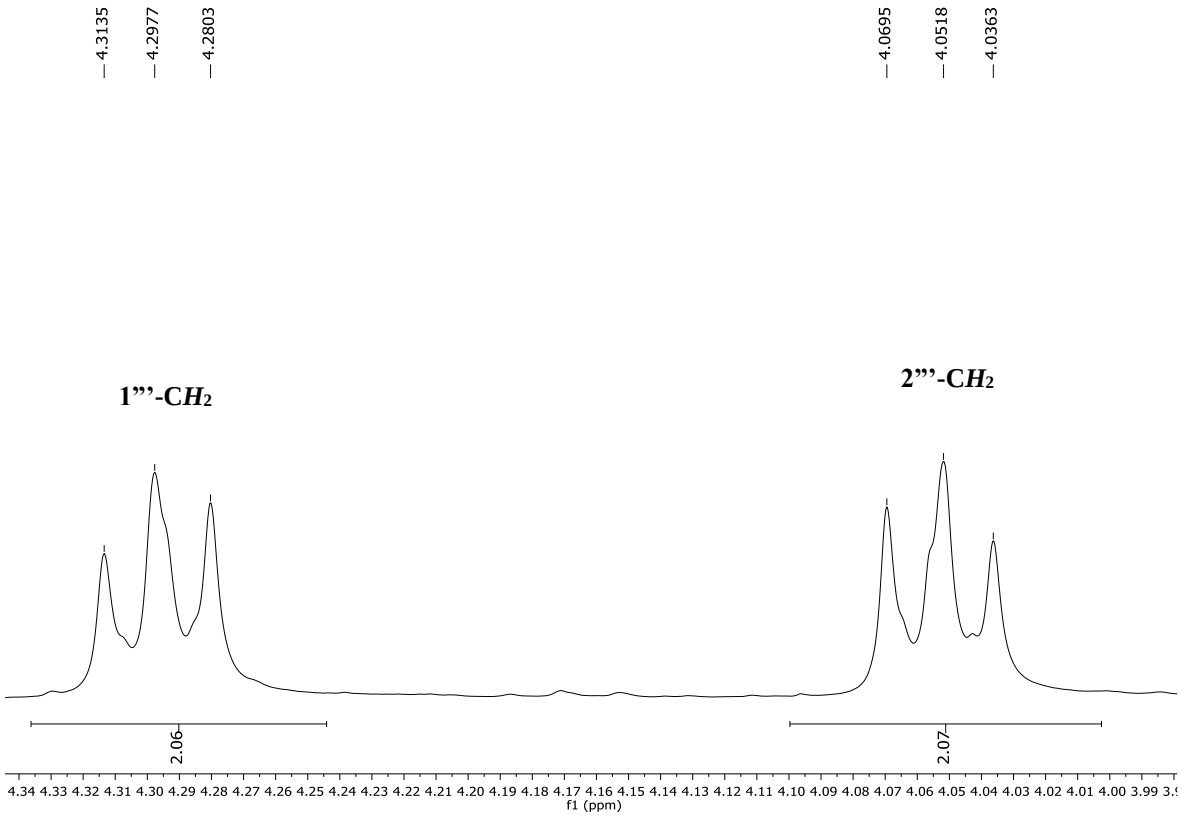

*Figure 34: Expansion of the aliphatic region of the ^{1}H NMR spectrum of (E)-4-(4-fluorostyryl)-1-(2-hydroxyethyl)-3-(2-hydroxyphenyl)-1H-pyrazole (**14a**) (300.13 Hz, $CDCl_3$)*

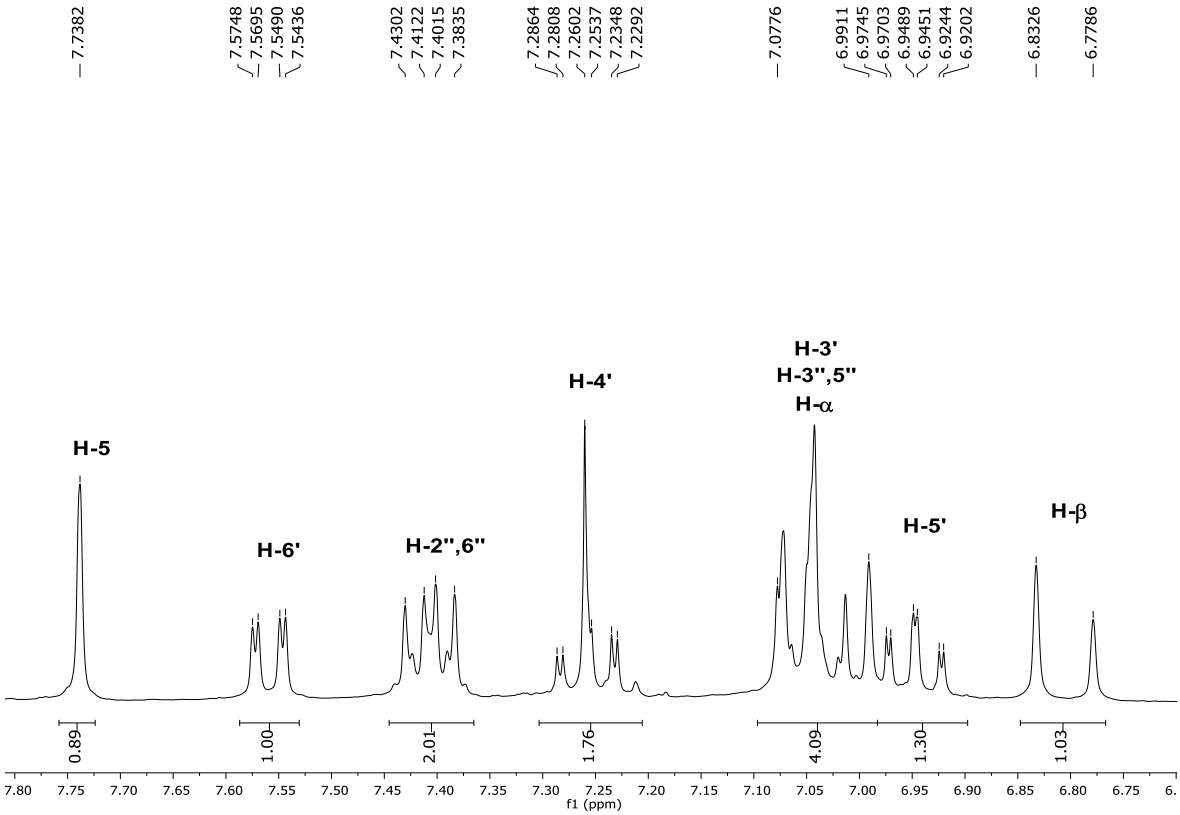

*Figure 35: Expansion of the aromatic region of the ^{1}H NMR spectrum of (E)-4-(4-fluorostyryl)-1-(2-hydroxyethyl)-3-(2-hydroxyphenyl)-1H-pyrazole (**14a**) (300.13 Hz, $CDCl_3$)*

The identification of the carbons of compound **14a** (Figure 36) was based on the analysis of the HSQC spectrum that allowed to assign C-3'',5'' (δ = 115.8 ppm), C-3' (δ = 117.0 ppm), C-α (δ = 118.6 ppm), C-5' (δ = 119.6 ppm), C-2'',6'' (δ = 127.9 ppm), C-6' (δ = 128.6 ppm), C-β (δ = 128.6 ppm), C-5 (δ = 129.5 ppm), and C-4' (δ = 129.6 ppm) and based on the proton assignments (Figure 37).

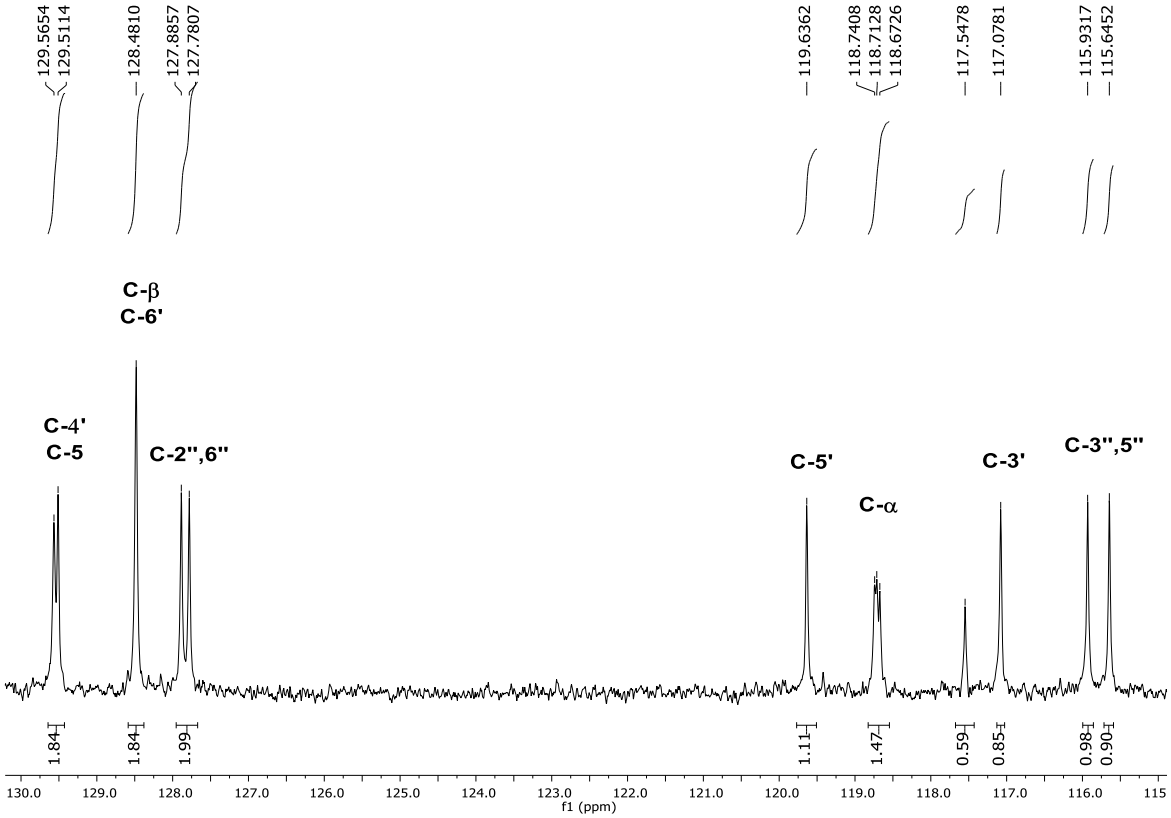

*Figure 36: Expansion of the aromatic region of the ^{13}C NMR spectrum of (E)-4-(4-fluorostyryl)-1-(2-hydroxyethyl)-3-(2-hydroxyphenyl)-1H-pyrazole (**14a**) (75.47 Hz, $CDCl_3$)*

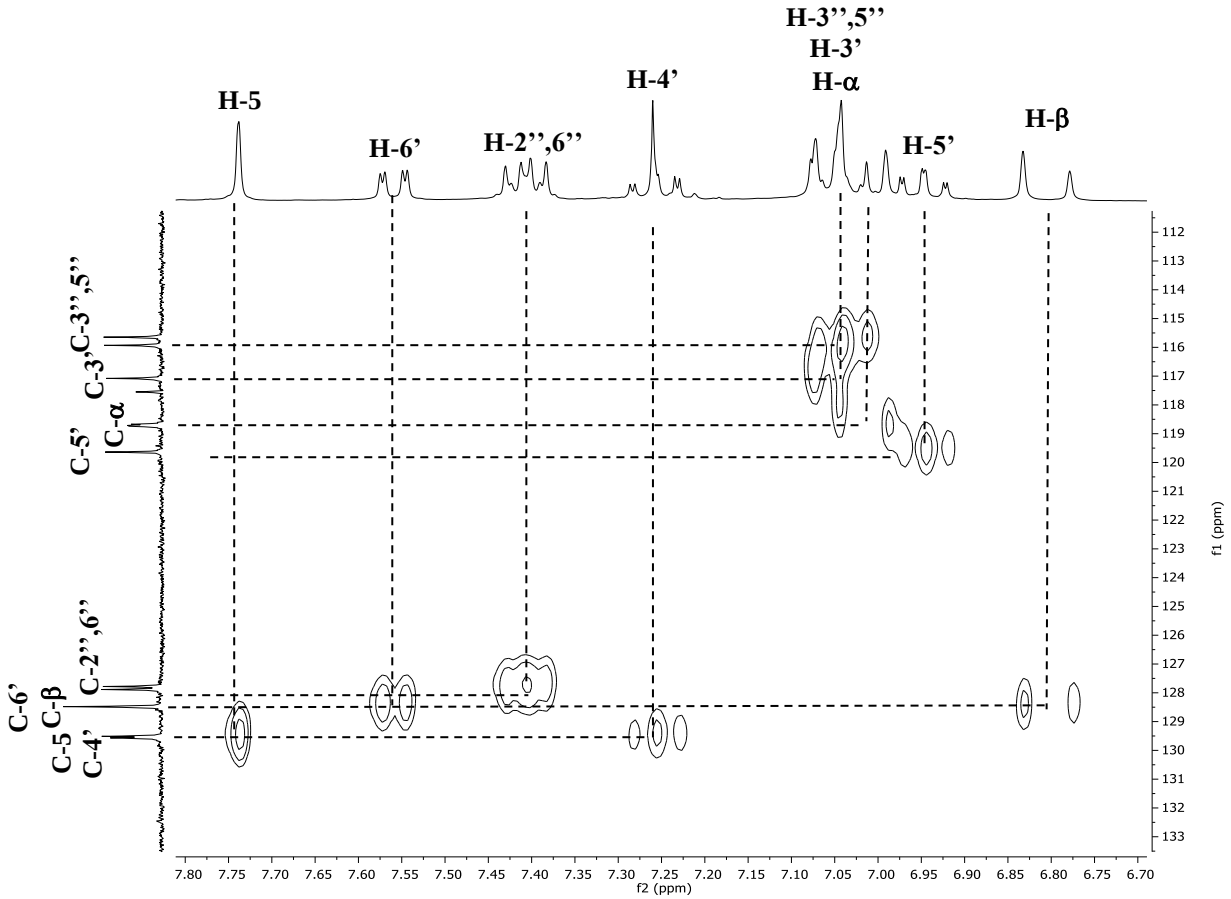

*Figure 37: Expansion of the HSQC spectrum of (E)-4-(4-fluorostyryl)-1-(2-hydroxyethyl)-3-(2-hydroxyphenyl)-1H-pyrazole (**14a**)*

Based on the correlations observed in the HMBC spectrum of **14a** (Figure 38) it was possible to identify the non-protonated carbons. For example, the following correlations H-5', H-3' → C-1', and H-5, H-6', H-α → C-3 allowed the assignment of carbons C-1' at δ = 117.6 ppm and C-3 at δ = 148.2 ppm, respectively. C-2' is linked to a hydroxy group and therefore is a deshielded carbon which has correlation ^{3}J with H-6'and H-4' and ^{2}J with H-3'. So, it was possible to unequivocally identify C-2' at δ = 155.6 ppm. C-1'' has correlation with H-3'',5'' and H-α at ^{3}J and with H-β at ^{2}J, being assigned at δ = 133.6 ppm. Finally, C-4" has correlation with H-2", 6" and H-3", 5" and appears as doublet due the coupling with fluorine atom at δ = 162.4 ppm.

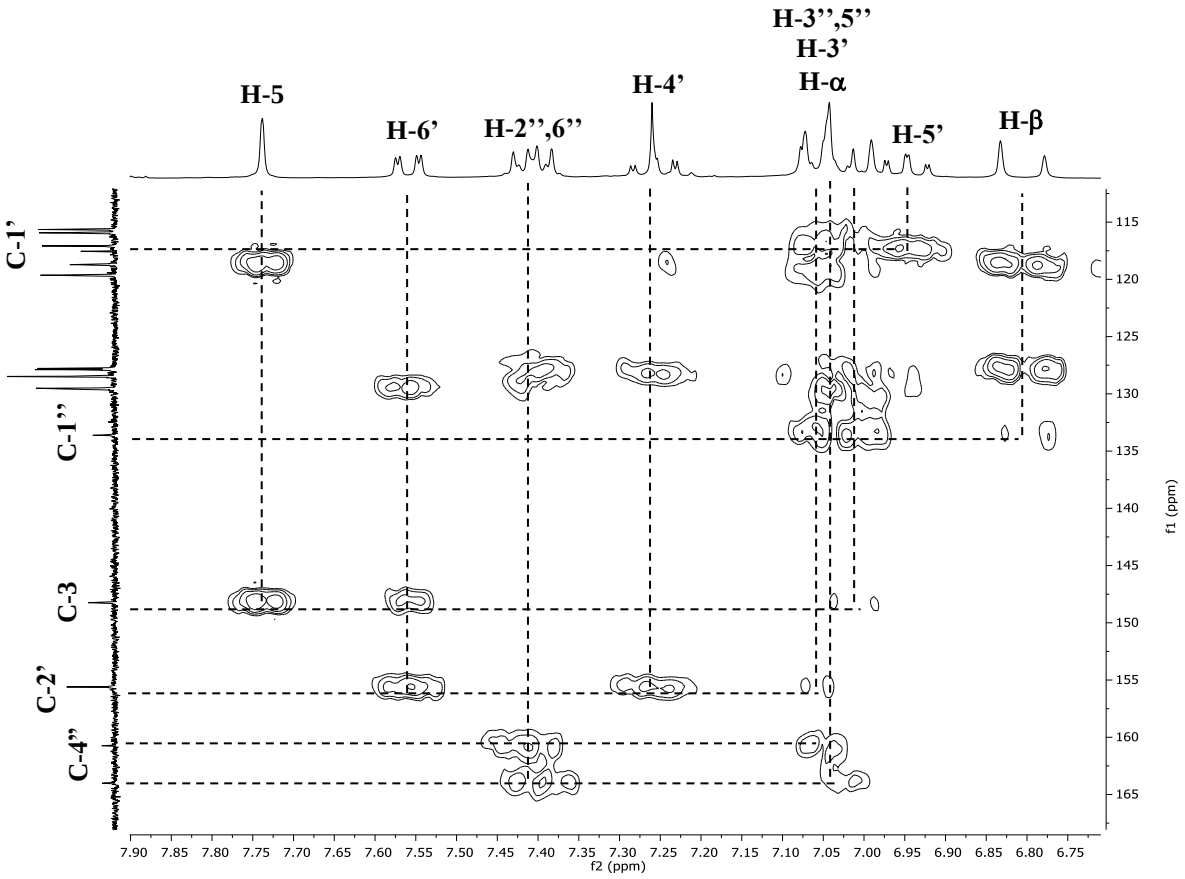

*Figure 38: Expansion of the HMBC spectrum of (E)-4-(4-fluorostyryl)-1-(2-hydroxyethyl)-3-(2-hydroxyphenyl)-1H-pyrazole (**14a**)*

The assignment of the aliphatic carbons of pyrazole **14a**, due to the presence of the alkyl chain, was made based on the correlation of H-1''' at ^{3}J with C-5 of pyrazole ring. In Figure 39 it was possible to observe the correlation of the carbon C-5, that appears in the aromatic region, with the triplet at δ = 4.30 ppm, which was assigned to 1'''-CH_2. Subsequently, the resonance of 2'''-CH_2 was assigned at δ = 4.05 ppm. Taking into consideration these data and based on the analysis of HMBC spectrum, the aliphatic carbons were unequivocally identified, C-1' at δ = 54.6 ppm and C-2' at δ = 61.5 ppm (Figure 40).

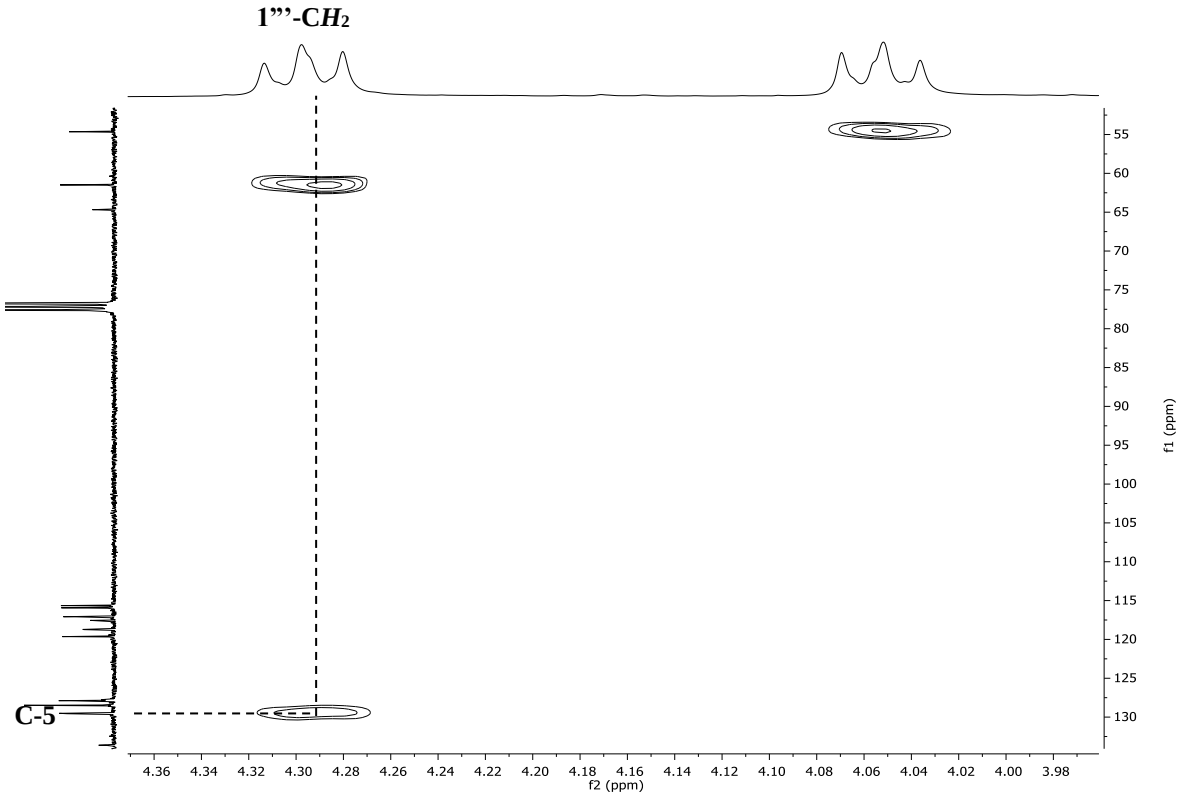

*Figure 39: Expansion of the HMBC spectrum of (E)-4-(4-fluorostyryl)-1-(2-hydroxyethyl)-3-(2-hydroxyphenyl)-1H-pyrazole (**14a**)*

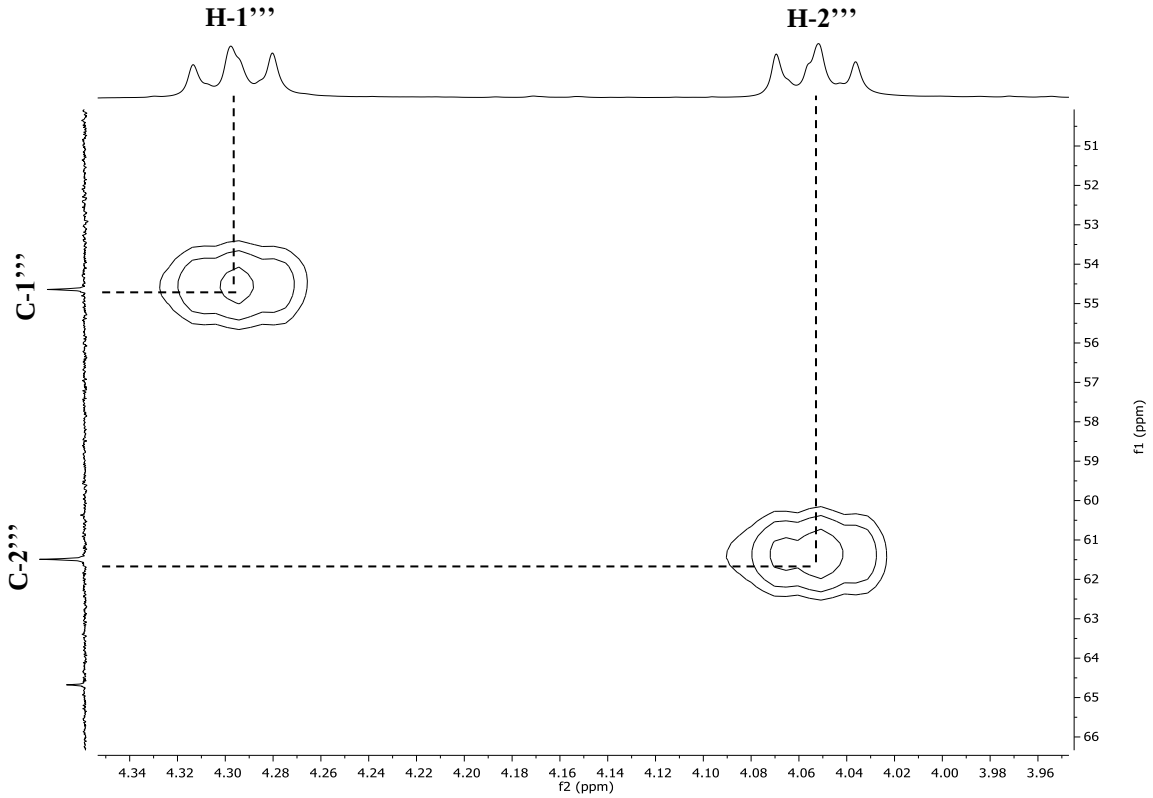

*Figure 40: Expansion of the HSQC spectrum of (E)-4-(4-fluorostyryl)-1-(2-hydroxyethyl)-3-(2-hydroxyphenyl)-1H-pyrazole (**14a**)*

The (*E*)-4-(4-fluorostyryl)-1-(6-hydroxyhexyl)-3-(2-hydroxyphenyl)-1*H*-pyrazole **(15a)** (Figure 41) can be distinguished from the parent compound, pyrazole **12**, and from pyrazole **14a**, by the presence of a high number of signals in the aliphatic region of the ^{1}H and ^{13}C NMR spectra due to the resonance of the protons and carbons of the 1-hydroxyhexyl chain, respectively. Figure 42 presents the aliphatic region of ^{1}H NMR spectra of pyrazole **15a**.

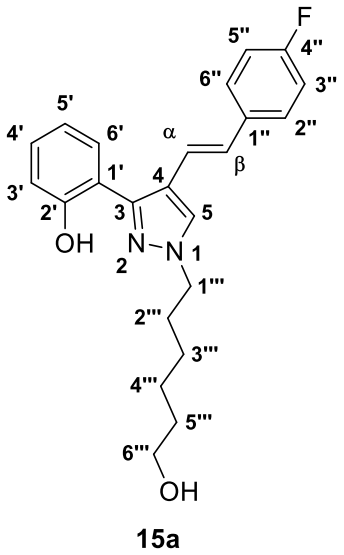

15a

*Figure 41: Structure and numbering of (E)-4-(4-fluorostyryl)-1-(6-hydroxyhexyl)-3-(2-hydroxyphenyl)-1H-pyrazole (**15a**)*

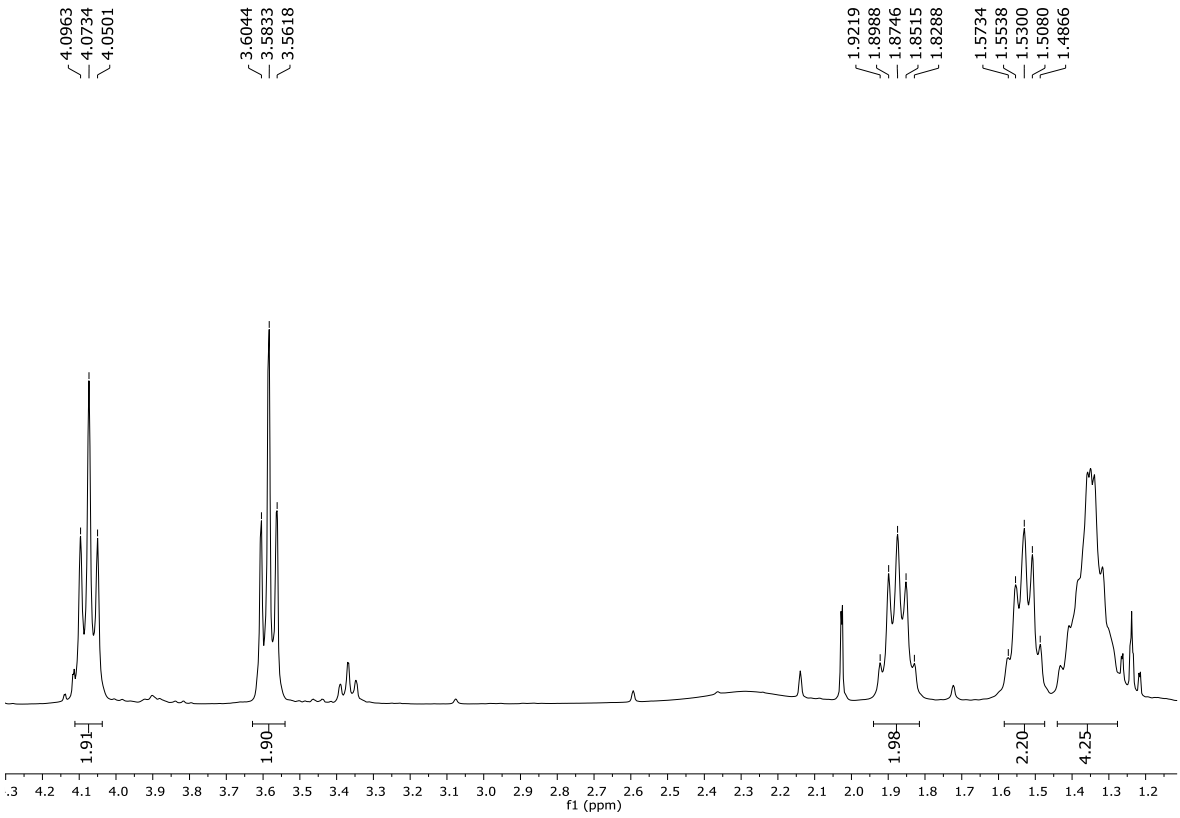

*Figure 42: Expansion of the aliphatic region of the ^1H NMR spectrum of (E)-4-(4-fluorostyryl)-1-(6-hydroxyhexyl)-3-(2-hydroxyphenyl)-1H-pyrazole (**15a**) (300.13 Hz, $CDCl_3$)*

In figure 43 it is possible to compare the aliphatic region of the ^1H NMR spectra of compounds **14a** (below) and compound **15a** (above) and confirm the existence of the 1-hydroxyethyl chain in compound **14a** and 1-hydroxyhexyl chain in compound **15a.** For compound **14a**, the signals appear at higher chemical shifts due the proximity of the -CH_2 protons to nitrogen and oxygen atoms.

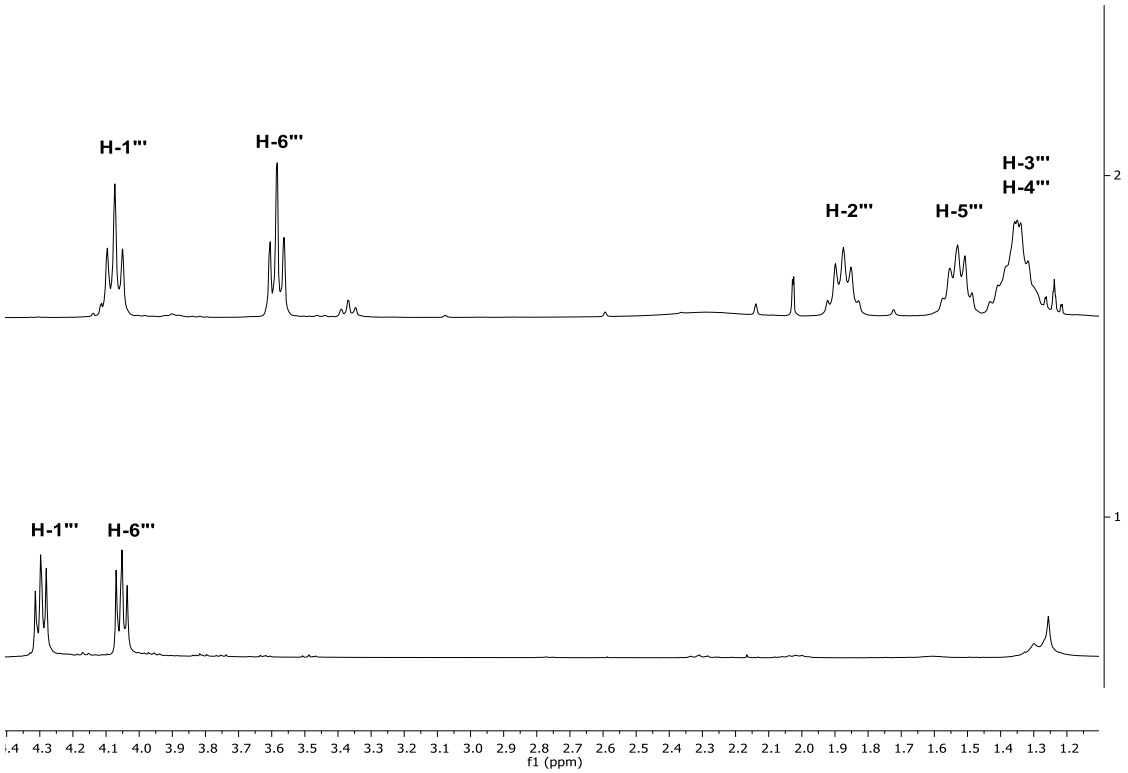

*Figure 43: Expansion of the aliphatic region of the ^{1}H NMR spectrum of (E)-4-(4-fluorostyryl)-1-(6-hydroxyhexyl)-3-(2-hydroxyphenyl)-1H-pyrazole (**15a**) and (E)-4-(4-fluorostyryl)-1-(2-hydroxyethyl)-3-(2-hydroxyphenyl)-1H-pyrazole (**14a**) (300.13 Hz, $CDCl_3$)*

Confirmation of the alkyl chain position, that is, whether it is attached to the oxygen or to the nitrogen atom, was based on the analysis of the HMBC spectra. In the case of *O*-alkylated derivatives, such as the (*E*)-4-(4-fluorostyryl)-3(5)-[2-(6-hydroxyhexyloxy)phenyl]-1*H*-pyrazole (**15b**) (Figure 44), there is a strong correlation between the protons 1'''-CH_2 and the C-2'. Based on this observation it was possible to unequivocally distinguish *O*-alkylated from *N*-alkylated pyrazoles.

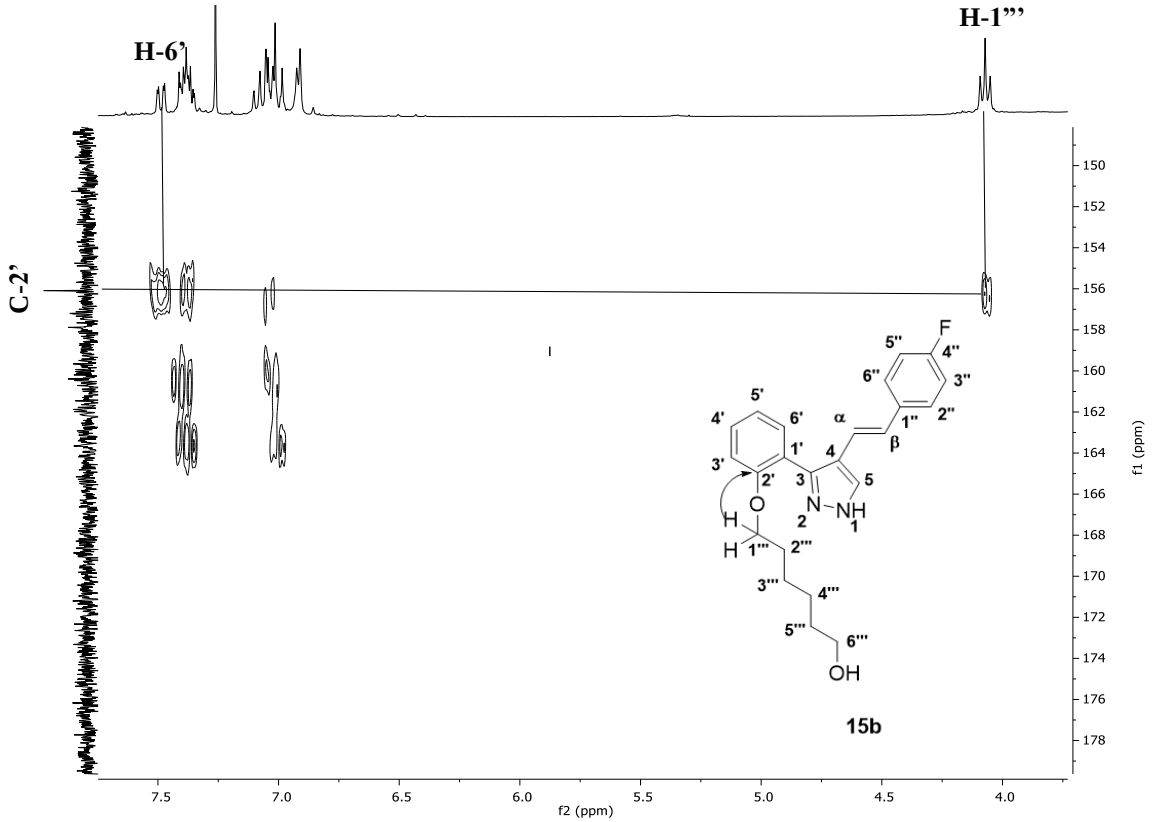

*Figure 44: Expansion of HMBC spectrum of (E)-4-(4-fluorostyryl)-3(5)-[2-(6-hydroxyhexyloxy)phenyl]-1H-pyrazole (**15b**)*

2.3.4 Characterization of tosylated pyrazoles

The structure and numbering of (*E*)-4-(4-fluorostyryl)-3-(2-hydroxyphenyl)-1-(2-tosylethyl)-1*H*-pyrazole (**16**) whose structural characterization will be discussed in this section is presented in figure 45.

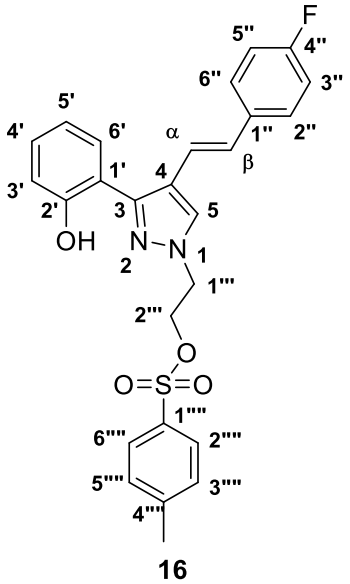

*Figure 45: Structure and numbering of (E)-4-(4-fluorostyryl)-3-(2-hydroxyphenyl)-1-(2-tosylethyl)-1H-pyrazole (**16**)*

The most characteristic signals in the ^{1}H NMR spectrum of compound **16** are: i) the singlet at δ_H= 2.20 ppm corresponding to the resonance of the protons of the methyl of the tosyl group; ii) the resonance of protons H-2"", 6"" and H-3"", 5"" observed as doublets at the aromatic region (δ = 7.60 ppm and δ = 7.15 ppm, respectively); iii) the singlet at δ = 4.40 ppm, due the resonance of protons 1'''-CH_2 and 2'''-CH_2. Although these protons have different chemical environments, the corresponding signals overlapped due to the effect of the tosyl group and appear as a singlet. The comparison between the aliphatic regions of the ^{1}H NMR spectra of compounds **14a** (above) and **16** (below) is presented in figure 46 and confirms the existence of the two characteristic signals at δ = 2.20 ppm and δ = 4.40 ppm above mentioned. In the aromatic region of the ^{1}H NMR spectrum of pyrazole **16**, can be observed the signals corresponding to resonance of the aromatic protons of the tosyl ring (Figure 47).

The comparison of the ^{13}C NMR spectra of pyrazoles **12**, **14a** and **16** allowed the identification of the signals due to the resonance of the carbons of the tosyl group, namely CH_3 (δ = 21.4 ppm), C-2"",6"" (δ = 127.7 ppm), C-3"",5"" (δ = 129.9 ppm), C-1"" (δ = 131.7) and C-4"" (δ =145.4 ppm).

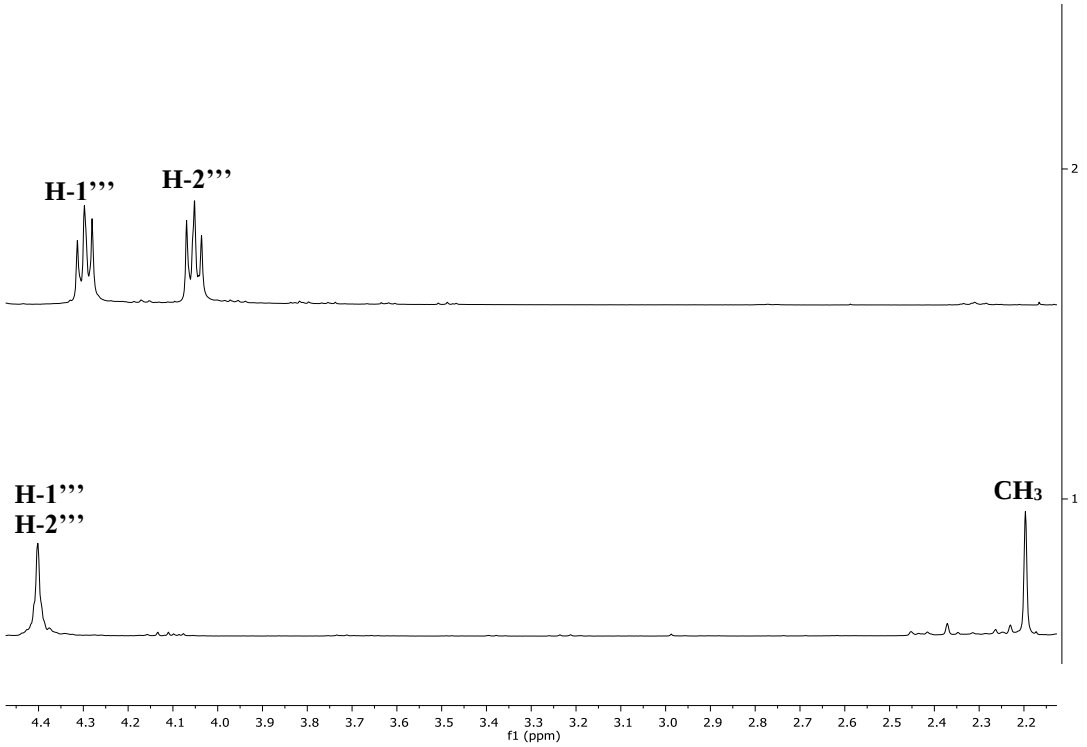

*Figure 46: Expansion of the aliphatic region of the ^{1}H NMR spectrum of (E)-4-(4-fluorostyryl)-1-(2-hydroxyethyl)-3-(2-hydroxyphenyl)-1H-pyrazole (**14a**) and (E)-4-(4-fluorostyryl)-3-(2-hydroxyphenyl)-1-(2-tosylethyl)-1H-pyrazole (**16**) (300.13 Hz, $CDCl_3$)*

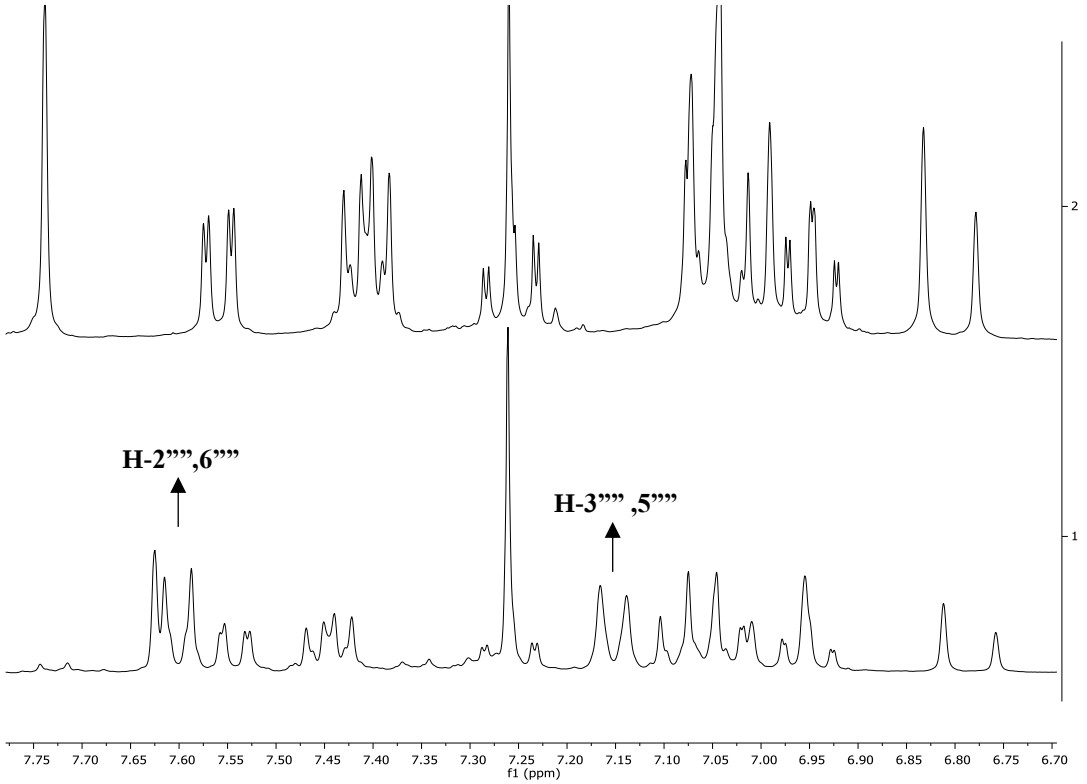

*Figure 47: Expansion of the aromatic region of the ^{1}H NMR spectrum of (E)-4-(4-fluorostyryl)-1-(2-hydroxyethyl)-3-(2-hydroxyphenyl)-1H-pyrazole (**14a**) and (E)-4-(4-fluorostyryl)-3-(2-hydroxyphenyl)-1-(2-tosylethyl)-1H-pyrazole (**16**) (300.13 Hz, $CDCl_3$)*

2.3.5 Characterization of [^{19}F]-(*E*)-4-(4-fluorostyryl)-1-(6-fluorohexyl)-3-(2-hydroxyphenyl)-1*H*-pyrazole (19)

The main difference between compound **19** and its precursor, compound (**18**), is the appearance of a new signal at δ = -215.1 ppm in the ^{19}F NMR spectrum. Based on this signal we can unequivocally confirm that the alkyl chain has a fluorine atom at C-6''' position (Figure 48). Moreover, this result confirms that the substitution of the tosyl group by fluorine was achieved with success. In the ^{1}H NMR spectrum of compound **19** it was also observed the disappearance of the signals typical of the tosyl group (Figure 49).

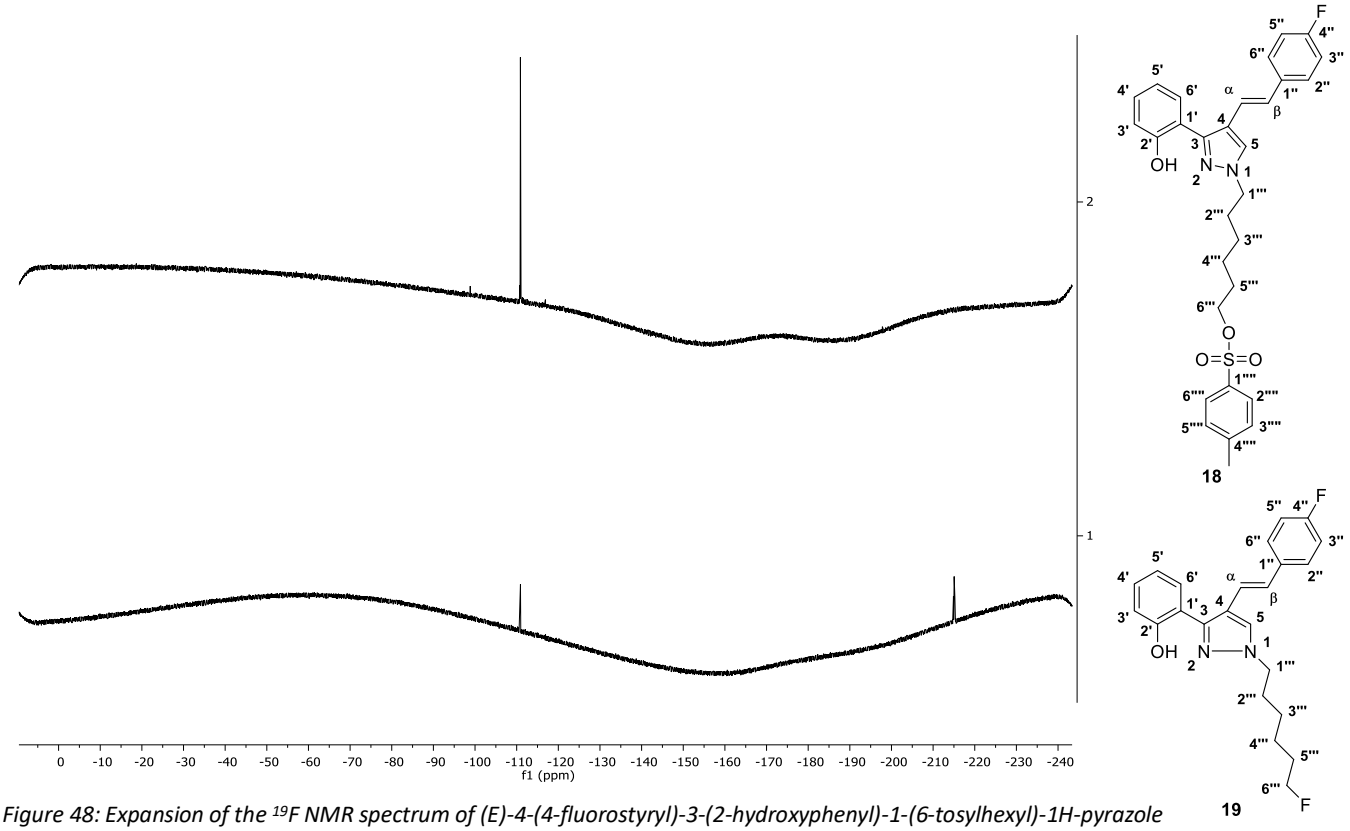

*Figure 48: Expansion of the ^{19}F NMR spectrum of (E)-4-(4-fluorostyryl)-3-(2-hydroxyphenyl)-1-(6-tosylhexyl)-1H-pyrazole (**18**) and [^{19}F]-(E)-4-(4-fluorostyryl)-1-(6-fluorohexyl)-3-(2-hydroxyphenyl)-1H-pyrazole (**19**) (300.13 Hz, $CDCl_3$)*

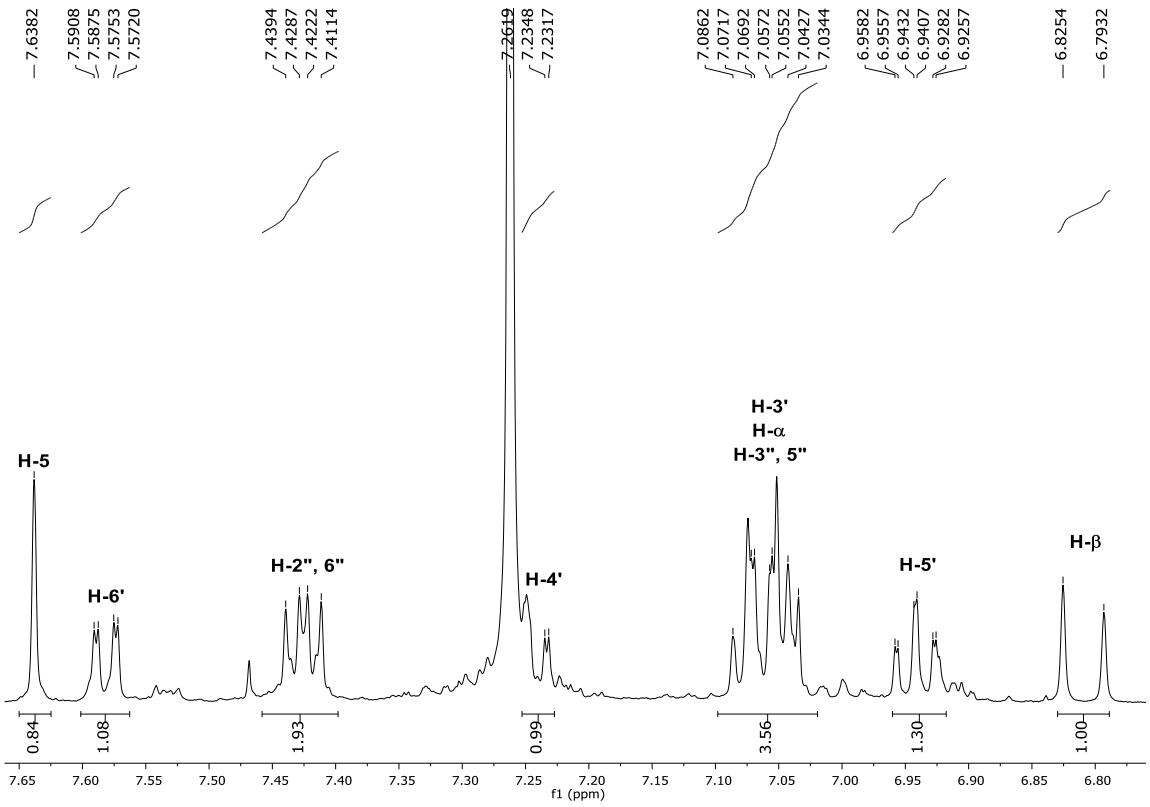

*Figure 49: Expansion of the aromatic region of the ^1H NMR spectrum of [^{19}F]-(E)-4-(4-fluorostyryl)-1-(6-fluorohexyl)-3-(2-hydroxyphenyl)-1H-pyrazole (**19**) (300.13 Hz, $CDCl_3$).*

Chapter 3 – Antioxidant activity of target compounds

3.1 Antioxidant capacity

The oxidative stress is known to be involved in the pathogenesis and progression of several diseases such as AD. Therefore, antioxidant therapy could positively contribute to slow the progression of several diseases which justifies the increased interest in the search of compounds with the capacity to scavenge free radicals and act as antioxidant and neuroprotective agents. The assessment of the antioxidant activity of the compounds that were developed for use as PET probes aims at searching for compounds that combine both functions, diagnosis and therapy, known as theranostics.

Pyrazoles are considered privileged structures in medicinal chemistry. Several biological activities are attributed to these compounds, including neuroprotective and antioxidant activities. [64,65,68] In this work the antioxidant capacity of pyrazoles **10-12, 13a, 13b, 14a, 14b, 15a and 15b** (Figure 46) was assessed by determining their ability to scavenge $ABTS^{+\bullet}$ and $NO^{\bullet}$ in comparison with ascorbic acid used as reference.

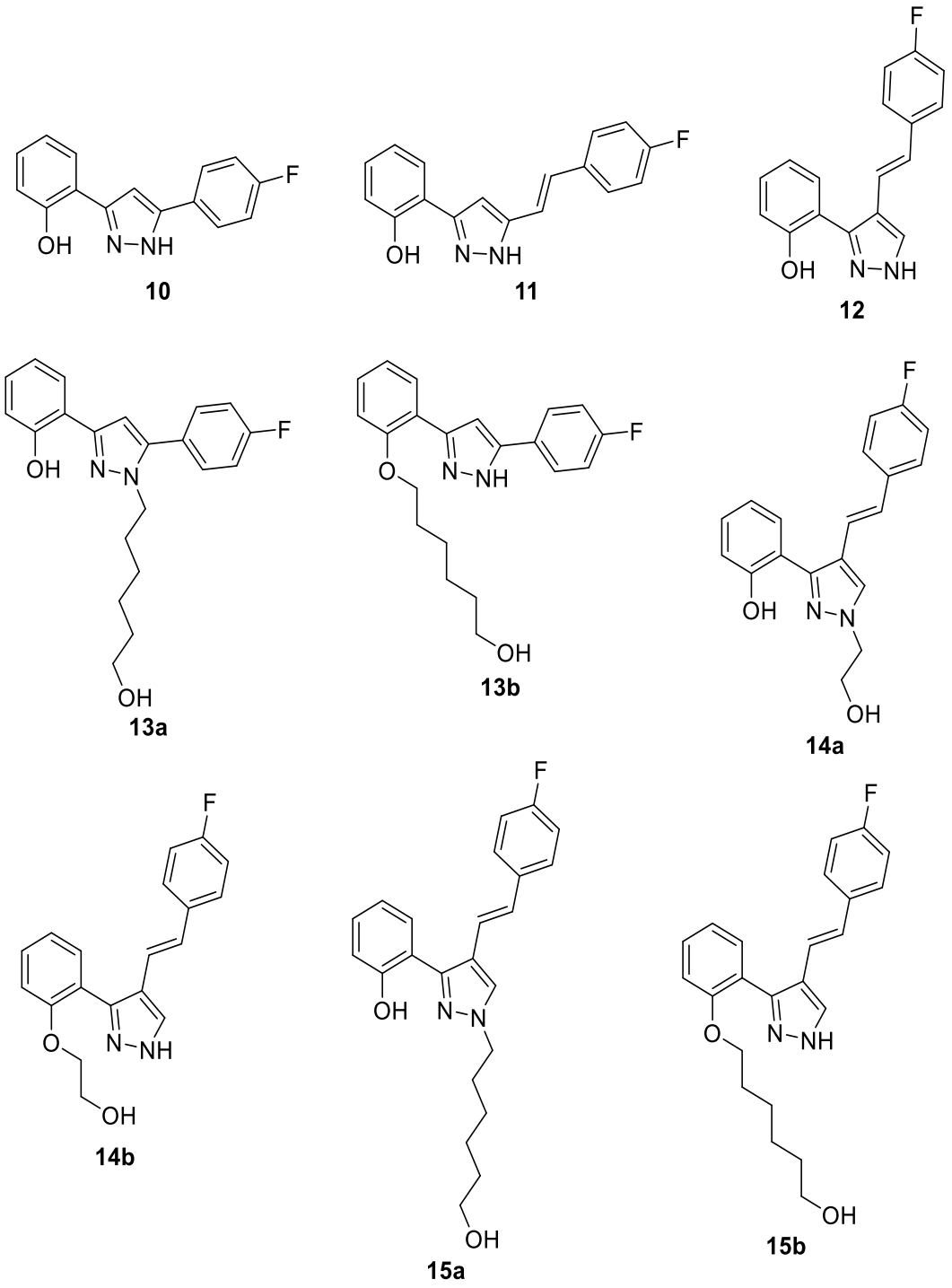

*Figure 46: Structures of tested compounds **10-12**, **13a,b**, **14a,b** and **15a,b**.*

3.1.1 $ABTS^{+\bullet}$ and $NO^{\bullet}$ scavenging assays

ABTS [2,2'-azino-bis(3-ethylbenzothiazoline-6-sulphonic acid)] assay is a widely used method to evaluate the radical scavenging capacity of compounds/extracts. The free radical scavenging activity of pyrazole-type compounds synthetized in this work was

determined by $ABTS^{+\bullet}$ radical cation decolorization assay, which is a spectrophotometric technique based on quenching of stable colored radicals ($ABTS^{\bullet+}$). The first step of ABTS assay was the generation of $ABTS^{+\bullet}$ from a reaction of ABTS-NH_4 aqueous solution (7 mM) with 2.45 mM potassium persulfate (final concentration). To allow the completion of radical generation it was necessary to store the solution in the dark at room temperature for 12-16h. To ensure the linearity of the method, the stock solution was diluted with water so that its absorbance was adjusted to 0.70±0.02 at 734 nm. To determine the scavenging activity, stock solutions with concentrations of 1.0 mM of compounds **10-12**, 2-4 mM for **13a, 13b, 14a, 14b and 15a** and 0.4 mM for **15b** were prepared using DMSO as solvent. Detailed experimental procedure for this assay as well as the method for determination of the IC_{50} (in μM) were presented in section 5.3.1. The solution of $ABTS^{+\bullet}$ has an intense blue-green colour. Throughout the test, the colour was fading due to the capacity of the pyrazole to scavenge the radical through a proton donation as shown in Figure 47. [106]

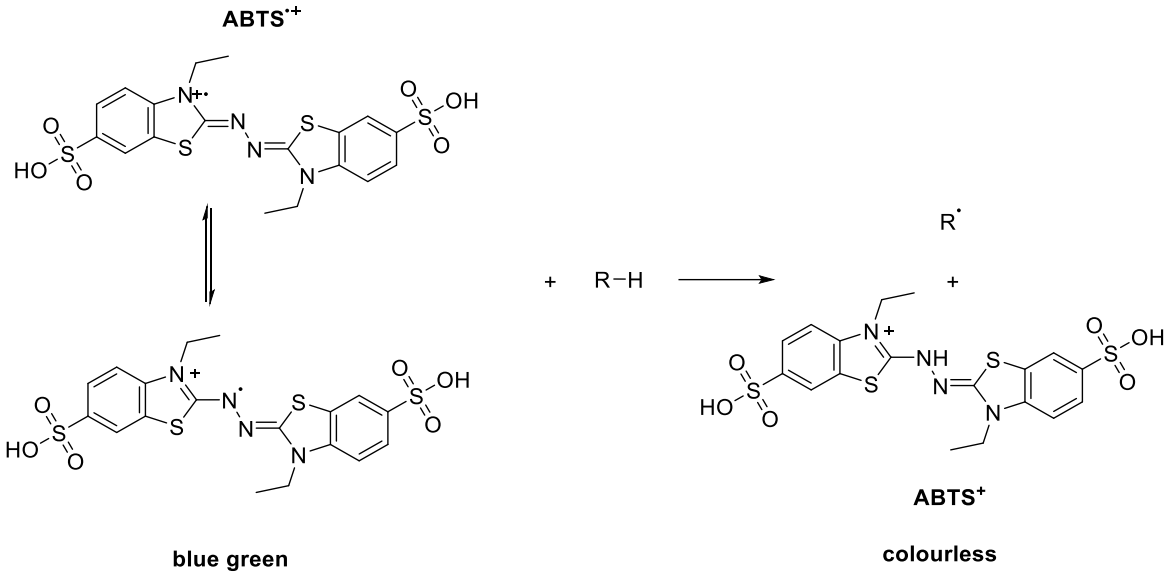

Figure 47. Principle of $ABTS^{+\bullet}$ radical scavenging assay (734 nm)

The nitric oxide ($NO^{\bullet}$) assay was the other method used to assess the antioxidant potential of the synthetized compounds. Scavenging activity of $NO^{\bullet}$ was estimated by the Griess Ilosvay reaction. In this method, sodium nitroprusside (SNP) decomposes at physiological pH spontaneously generates five cyanide anion and one nitric oxide radical. [107] Then the nitric oxide radical reacts with oxygen and produces nitrite ions. These nitrite ions react with sulphanilamide forming 4-sulfamoylbenzenediazonium that then reacts with *N*-(1-naphthyl)ethylenediamine affording a compound known as Anzo product (Figure 48).

The Anzo product has a pink color being possible to determine the amount of nitrite ions generated by measuring the absorbance at 562 nm. In the presence of nitric oxide scavengers, they compete with the oxygen, culminating in a lower production of nitrite ions and subsequently the formation of the Anzo product, reducing the color tonality. To determine the scavenging activity, stock solutions with concentrations of 0.8-2.0 mM of compound **10-12** and 1-5 mM for **13a, 13b, 14a, 14b, 15a and 15b** were prepared using DMSO as solvent. Detailed experimental procedure for this assay is presented in section 5.3.2.

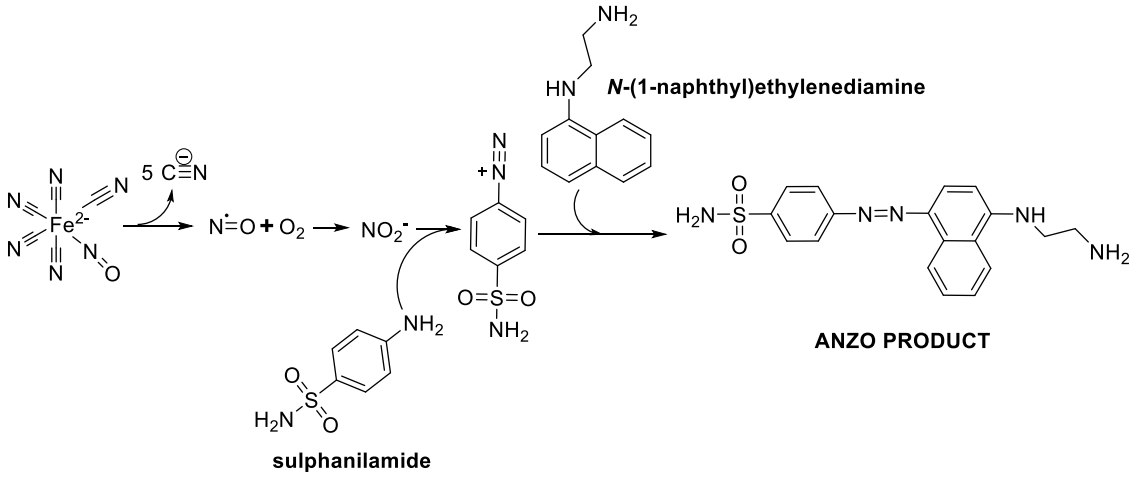

Figure 48: Principle of NO• radical scavenging assay (562 nm)

3.1.2 Results and discussion

The results found have shown that pyrazoles **10** and **11** (Figure 50) have a similar capacity to scavenge the $ABTS^{+\bullet}$ radical (IC_{50} = 19.33 ± 2.01 μM and 19.67 ± 0.68 μM) to that of the standard ascorbic acid (IC_{50} = 20.51 ± 3.50 μM) and pyrazole **12** (IC_{50} = 17.61 ± 0.96 μM) was slightly more active than ascorbic acid (Table 1). The 4-(4-fluorostyryl)-3(5)-(2-hydroxyphenyl)-1*H*-pyrazole (**12**) demonstrated a better capacity to scavenge the $ABTS^{+\bullet}$ than pyrazoles **10** and **11** and the standard (increase of 12% and 16% respectively) (Figure 50).

Regarding the NO• scavenging activity, the pyrazole **12** (IC_{50} = 40.35 ± 9.99 μM) was 4 times more active than ascorbic acid (IC_{50} = 174.58 ± 13.57 μM). On the other hand, the pyrazoles **10** (IC_{50} = 201.02 ± 19.73 μM) and **11** (IC_{50} = 297.21 ± 122.26 μM) showed a worse capacity to scavenge NO• (Table 1).

The differences found regarding the NO• scavenging capacity of 5(3)-(4-fluorostyryl)-3(5)-(2-hydroxyphenyl)-1*H*-pyrazole **11** and 4-(4-fluorostyryl)-3(5)-(2-

hydroxyphenyl)-1*H*-pyrazole (**12**), demonstrated that the position of 4-fluorostyryl group seems to be a determining factor for this activity.

Based on these results, the 4-(4-fluorostyryl)-3(5)-(2-hydroxyphenyl)-1*H*-pyrazole (**12**) was selected as the scaffold to prepare the ^{18}F-labelled radioligand for PET imaging.

*Table 1: Results of free radicals ($ABTS^{+\bullet}$) and ($NO^{\bullet}$) scavenging activity of pyrazoles **10, 11** and **12**.*

Compounds	**ABTS assay**	**NO assay**
	IC_{50} (µM ± SD)	**IC_{50} (µM ± SD)**
10	19.33 ± 2.01	297.21 ± 122.26
11	19.67 ± 0.68	201.02 ± 19.73
12	17.61 ± 0.96	40.35 ± 9.99
Ascorbic Acid	20.51 ± 3.50	174.58 ± 13.57

The antioxidant capacity of alkylated pyrazoles **13a, 13b, 14a, 14b, 15a and 15b** (Figure 49) was also evaluated. The methods and reference used were the same as aforementioned for pyrazoles **10-12**.

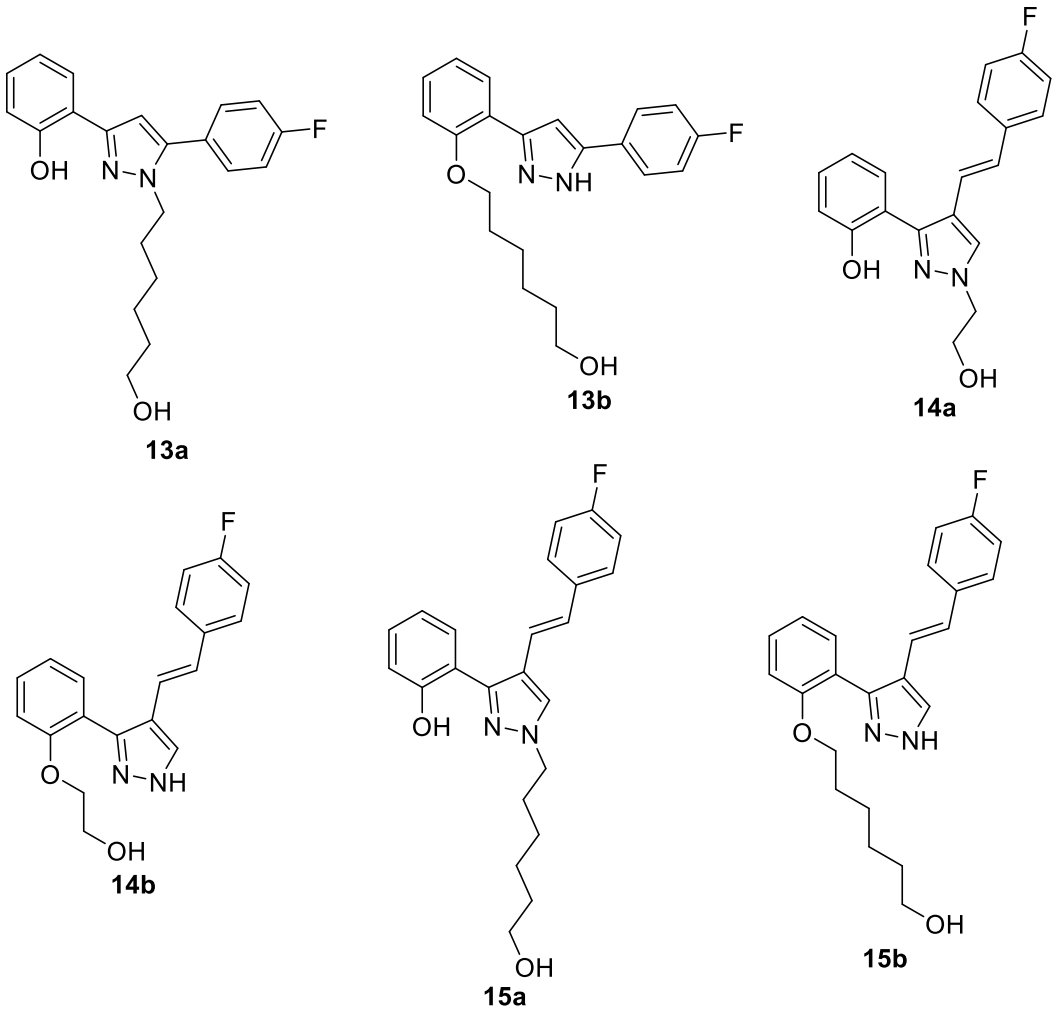

*Figure 49: Structures of tested compounds **13a,b**, **14a,b** and **15a,b**.*

As showed in table 2, the *O*-alkylated pyrazoles **13b**, **14b** and **15b** did not demonstrate scavenging capacity of either $ABTS^{+\bullet}$ or $NO^{\bullet}$ (stock solution of 5 mM was the highest concentration used). In ABTS assay (Figure 50), the 4-(4-fluorostyryl)-1*H*-pyrazoles **14a** and **15a** (IC_{50} = 16.68 ± 0.35 μM and 20.05 ± 0.08 μM respectively) demonstrated a higher capacity to scavenge $ABTS^{+\bullet}$ radical when compared to ascorbic acid (IC_{50} = 20.51 ± 3.50 μM) and with the other pyrazole derivative **13a** (IC_{50} = 38.74 ± 0.59 μM).

In NO assay (Figure 51), the *N*-alkylated pyrazoles **14a** and **15a** (IC_{50} = 37.96 ± 2.82 and 65.30 ± 3.34 μM, respectively) demonstrated a much higher capacity to scavenge the $NO^{\bullet}$ radical when compared to ascorbic acid (IC_{50} = 174.58 ± 13.57 μM). Even pyrazole **13a** presented $NO^{\bullet}$ radical scavenging activity superior to that of ascorbic acid although it was less active than pyrazoles **14a** and **15a**.

*Table 2: Results of free radicals ($ABTS^{+\bullet}$) and ($NO^{\bullet}$) scavenging activity of pyrazoles **13a,b, 14a,b** and **15a,b**.*

Compound	ABTS assay IC_{50} (µM ± SD)	NO assay IC_{50} (µM ± SD)
13a	38.74 ± 0.59	139.60 ± 4.49
13b	----------	----------
14a	16.68 ± 0.35	37.96 ± 2.82
14b	----------	----------
15a	20.05 ± 0.08	65.30 ± 3.34
15b	----------	----------
Ascorbic Acid	20.51 ± 3.50	174.58 ± 13.57

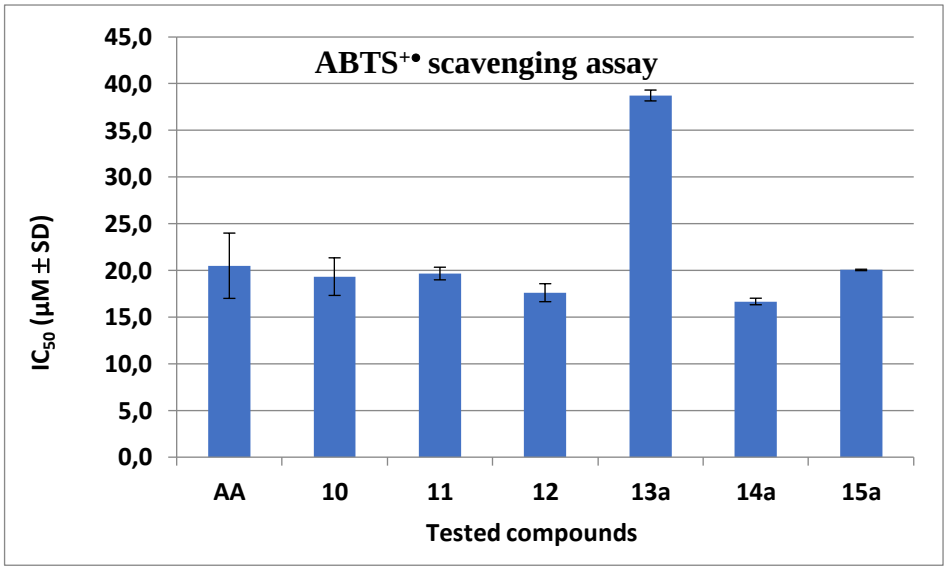

*Figure 50: IC50 values obtained in the $ABTS^{+\bullet}$ scavenging assay for compounds **10-12, 13a, 14a, 15a** and **ascorbic acid.***

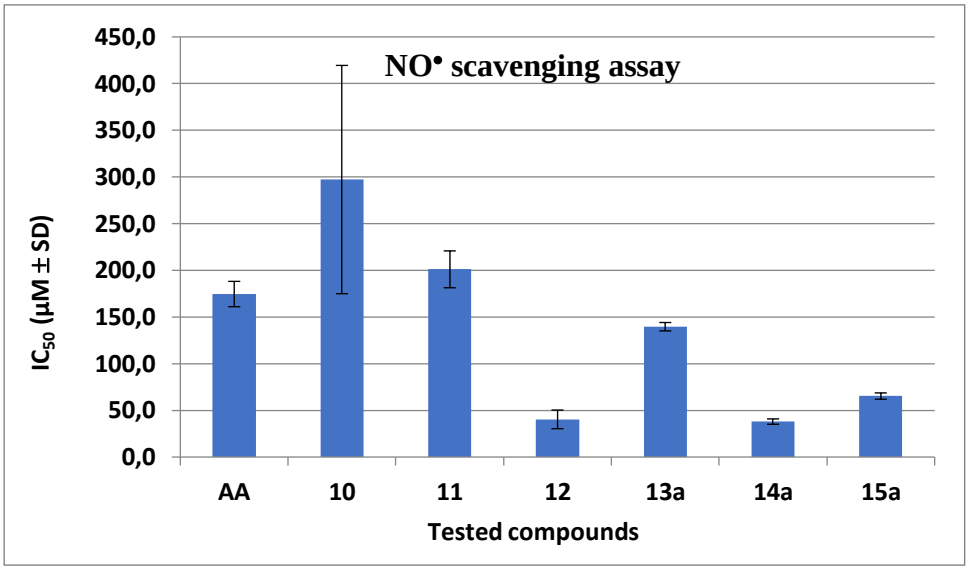

*Figure 51: IC_{50} values obtained in the NO• scavenging assay for compounds **10-12, 13a, 14a, 15a** and **ascorbic acid**.*

Based on the above-mentioned results some structure-activity relationships were found. The results obtained suggested that the scavenging activity of pyrazoles **10-12**, **13a**, **13b, 14a, 14b, 15a** and **15b** arises from the hydroxy group of 2-hydroxyphenyl ring because *O*-alkylated pyrazoles **13b**, **14b** and **15b** do not demonstrate scavenging capacity of either $ABTS^{+\bullet}$ or NO• radicals. On the other hand, *N*-alkylated pyrazoles demonstrated scavenging capacity, thus showing that it is not relevant if the pyrazole ring has a free NH group or if this position is substituted. Moreover, the insertion of the 4-fluorostyryl group at C4 or C5(3)-position contributes to increase the activity compared to the 4-fluorophenyl group at C5(3)-position. Comparing the activity of (*E*)-4-(4-fluorostyryl)-1-(2-hydroxyethyl)-3-(2-hydroxyphenyl)-1*H*-pyrazole (**14a**) and (*E*)-4-(4-fluorostyryl)-1-(6-hydroxyhexyl)-3-(2-hydroxyphenyl)-1*H*-pyrazole (**15a**) it was observed that a shorter alkyl chain (two carbons) contributes more positively to the increase of activity than a longer alkyl chain (six carbons), since pyrazoles **14a** have a better $ABTS^{+\bullet}$ and NO• radicals scavenging activity when compared to compound **15a** (1.25 and 1.71 times, respectively). This effect could be due to the proximity between the terminal hydroxy group of the alkyl chain of the pyrazole ring, thus facilitating the radical stabilization. However, further studies are needed to better understand the effect of the length of the alkyl chain.

Chapter 4 – Conclusions and future perspectives

4.1 Conclusions

In this work three types of pyrazoles, the 5(3)-(4-fluorophenyl)-3(5)-(2-hydroxyphenyl)-1*H*-pyrazole (**10**), the 5(3)-(4-fluorostyryl)-3(5)-(2-hydroxyphenyl)-1*H*-pyrazole (**11**) and the 4-(4-fluorostyryl)-3(5)-(2-hydroxyphenyl)-1*H*-pyrazole (**12**), were synthetized and their radical scavenging activity against $ABTS^{+\bullet}$ and $NO^{\bullet}$ was evaluated in comparison with ascorbic acid. In this *in chimico* assays, the 4-(4-fluorostyryl)-3(5)-(2-hydroxyphenyl)-1*H*-pyrazole (**12**) was found to be more active than pyrazoles **10** and **11** and therefore it was chosen as the scaffold to synthetize the pyrazole precursor for ^{18}F-radiofluorination via aliphatic nucleofilic substitution reaction (S_N2-type displacement of the tosyl group). Moreover, pyrazole **12** was obtained in a very good yield (85%) compared to the yields of pyrazoles **10** and **11** (52% and 26%, respectively).

Starting from pyrazole **12**, *N*- and *O*- alkylated pyrazoles (**14a**,**15a** and **14b,15b,** respectively) were synthetized by alkylation with 2-bromoethanol and 6-bromohexanol. These compounds were also tested to assess their radical scavenging activity against $ABTS^{+\bullet}$ and $NO^{\bullet}$ radicals. The results obtained suggested that the antioxidant activity of the synthetized pyrazoles arises from the hydroxy group of the 2'-hydroxyphenyl moiety since the *O*-alkylated pyrazoles did not show significant antioxidant activity. Among the *N*-alkylated pyrazoles, those presenting the shorter alkyl chain were the most active compounds, suggesting that the size of the alkyl chain has some effect of this activity.

After the alkylation, the alkyl chain terminal hydroxy group was converted in a tosyl group via tosylation reaction. Finally, the ^{19}F-fluorination reaction was carried out, as a proof-of-concept, thus simulating the reaction that will be performed for the introduction of ^{18}F radionuclide. Tetra-*N*-butylammonium fluoride (TBAF) was used as source of ^{19}F and the reaction occurred in dry THF as solvent for 30 minutes.

Attempts were made to synthetize a pyrazole precursor for ^{18}F-radiofluorination via aromatic nucleophilic substitution. This strategy was more challenging since it required the preparation of a sydnone-type derivative of the pyrazole via a three-step strategy starting from a pyrazole having a nitro group. The first step, which involved the reduction of the nitro group to an amine was achieved with success, however further studies are needed to overcome some problems related to the conversion of the amine into a glycine and preparation of the sydnone.

4.2 Future perspectives

In this work, ^{19}F-fluorination was performed for (*E*)-4-(4-fluorostyryl)-3-(2-hydroxyphenyl)-1-(6-tosylhexyl)-1*H*-pyrazole (**18**), as a proof- of-concept, because this pyrazole was obtained in higher amounts. However, since it was found that a shorter alkyl chain seems to contribute more positively to the antioxidant activity, ^{19}F-fluorination of (*E*)-4-(4-fluorostyryl)-3-(2-hydroxyphenyl)-1-(2-tosylethyl)-1*H*-pyrazole (**16**) will be carried out in the future. Besides, ^{18}F-radiofluorination will be performed, in the near future, in collaboration with researchers at University of Coimbra where the equipment for radiosynthesis is installed.

Assessing the usefulness of a PET imaging probe for diagnosis of human diseases is a multidisciplinary work that requires the expertise of several scientists including radiochemists, pharmacologists, and clinicians who should work in close collaboration. Moreover, for the PET imaging probe to be useful for *in vivo* applications, several prerequisites have to be fulfilled. Some of these prerequisites are:

- High selectivity/affinity for the "receptor" (protein aggregates)
- High specific radioactivity
- Metabolism and position of label of the imaging probe
- Blood-brain barrier (BBB) permeability

Once synthetized the tosylated-pyrazoles and tested the nucleophilic aliphatic substitution, that allows the introduction of fluorine-19, the future work aims at the evaluation of the affinity and selectivity of the ^{19}F-pyrazole derivatives, especially of ^{19}F-4-styrylpyrazoles, for protein aggregates and evaluation of their blood-brain barrier penetration ability. Two main reasons of failure of CNS PET imaging probes are the high nonspecific binding *in vivo* and the inability of the compounds to cross the blood-brain barrier (BBB). In assessing whether a radiopharmaceutical may undergo a lipid-mediated transport across the BBB, two important factors need to be taken into consideration: (a) the extent of hydrogen bond formation of the drug with water and (b) the molecular weight of the drug or radiopharmaceutical. Hydrogen bond formation should be minimal and the total number of hydrogen bonds a drug forms with water should be less than eight to ten.[108] The molecular weight, which is a measure for molecule volume, should be below the 400–600 Da threshold. Our compounds have few positions or groups to form hydrogen bonds with water. Moreover,

among the synthetized compounds the highest molecular weight is 534.65 g/mol (compound **18**) and so the molecular weight of our compounds is in the reference range shown above. In the future, computational methods will be used to predict the BBB ability. Another way to evaluate this parameter will be the determination of the octanol/water partition coefficient, P (log P values between 2 and 3.5 are generally considered optimal). The evaluation of these parameters could allow the design of new pyrazole derivatives with improved properties for use as theranostics for AD diagnosis and treatment.

Chapter 5 – Experimental section

5.1 General

Reagents and solvents were purchased as reagent-grade and used without further purification unless otherwise stated. Preparative TLC was carried out with silica gel (60 DGF254) plates. Melting points were determined with a Büchi melting point B-540 apparatus and are uncorrected. NMR spectra were recorded with 300 or 500 MHz [300.13 MHz (^{1}H), 75.47 MHz (^{13}C), or 500.16 MHz (^{1}H), 125.77 MHz (^{13}C)] Bruker Avance III NMR spectrometers with tetramethylsilane as the internal reference. Deuterated solvent used was specified for each compound. Chemical shifts (δ) are quoted relative to TMS. Unequivocal ^{13}C assignments were made on the basis of 2D *g*HSQC (^{1}H/^{13}C) and *g*HMBC (delays for one-bond and long-range JC/H couplings were optimised for 145 and 7 Hz, respectively) experiments. Positive-ion ESI mass spectra and high-resolution mass spectra [ESI(+)-HRMS] were performed using a Q Exactive Orbitrap mass spectrometer (Thermo Fischer Scientific, Bremen, Germany) controlled by THERMO Xcalibur 4.1. The capillary voltage of the electrospray ionization (ESI) was set to 3000 V. The capillary temperature was 250 ºC. The sheath gas flow rate (nitrogen) was set to 5 (arbitrary unit as provided by the software settings).

5.2 Synthesis

5.2.1 Synthesis of 2-acetylphenyl (*E*)-3-(4-fluorophenyl)prop-2-enoate (3)

To 2'-hydroxyacetophenone (**1**) (1.0 mL, 8.30 mmol) were added 50 mL of DCM. Then 1.2 equiv. of 4-fluorocinnamic acid (**2**) (1.660 g, 9.99 mmol) and diciclohexylcarbodiimide (DCC) (2.060 g, 9.99 mmol) and 0.12 equiv. of 4-pyrrolidinopyridine (PPy) (0.148 g, 1.00 mmol) were added to that solution. The reaction was stirred under nitrogen at room temperature for 7 days. The solid formed in the reaction was filtered and washed with DCM, and the solvent of the filtrate was evaporated to dryness. The solid obtained was recrystallized from DCM and cyclohexane.

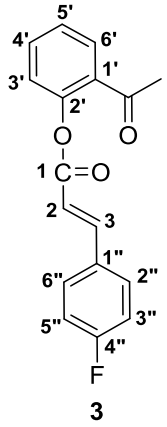

3

2-Acetylphenyl (*E*)-3-(4-fluorophenyl)prop-2-enoate (**3**), 87% yield, 2.09 g (beige solid), m.p. 82.7 – 83.0 ºC. ^{1}H NMR (300.13 MHz, $CDCl_3$): δ = 2.57 (s, 3H, C*H*$_3$), 6.60 (d, 1H, *J* 16.0 Hz, H-2), 7.12 (t, 2H, *J* 8.6 Hz, H-3",5"), 7.19 (dd, 1H, *J* 1.1, 8.1 Hz, H-3'), 7.35 (dt, 1H, *J* 1.1, 7.7 Hz, H-5'), 7.54-7.62 (m, 3H, H-4', 2", 6"), 7.84 (dd, 1H, *J* 1.7, 7.7 Hz, H-6'), 7.85 (d, 1H, *J* 16.0 Hz, H-3) ppm.

^{13}C NMR (75.47 MHz, $CDCl_3$): δ = 29.7 (*C*H$_3$), 116.2 (d, 2C, *J* 21.7 Hz, C-3",5") , 116.6 (C-2) , 123.8 (C-3'), 126.1 (C-5'), 130.0 (C-1''), 130.2 (C-6'), 130.3 (d, 2C, *J* 8.7 Hz, C-2",6"), 131.3 (C-1'), 133.4 (C-4'), 146.0 (C-3), 149.1 (C-2'), 162.6 (C-4''), 165.2 (C-1), 197.8 (C=O, ketone) ppm. MS (ESI$^+$) m/z (%): 307.1 (100) $[M+H]^+$.

5.2.2 Synthesis of (*E*)-5-(4-fluorophenyl)-1-(2-hydroxyphenyl)pent-2,4-ene-3-hydroxy-1-one (4')

To a solution of 2-acetylphenyl (*E*)-3-(4-fluorophenyl)prop-2-enoate **(1)** (1.00 g, 3.52 mmol) in DMSO (22 mL) were added 5 equiv. of KOH (0.987 g, 17.6 mmol). The reaction was stirred under nitrogen at room temperature for 1 hour. Then, the reaction mixture was poured over ice and water and acidified at pH ≈ 3 with an HCl solution. The resulting solid was filtered, dissolved in DCM and washed with water. The combined organic layer was dried with anhydrous sodium sulfate and the solvent was evaporated to dryness. The obtained solid was crystalized with ethanol.

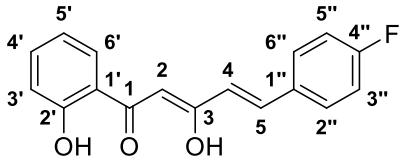

4'

(*E*)-5-(4-Fluorophenyl)-1-(2-hydroxyphenyl)pent-2,4-ene-3-hydroxy-1-one (**4'**), 57% yield, 564.9 mg (light yellow solid), m.p. 213 – 215 ºC. ^{1}H NMR (300.13 MHz, $CDCl_3$): δ = 6.31 (s, 1H, H-2), 6.51 (d, 1H, *J* 15.8 Hz, H-4), 6.90 (ddd, 1H, *J* 1.2, 7.1, 8.1 Hz, H-5'), 6.99 (d, 1H, *J* 8.4 Hz, H-3'), 7.10 (t, 2H, *J* 8.7 Hz, H-3'',5''), 7.46 (ddd, 1H, *J* 1.5, 7.1, 8.4 Hz, H-4'), 7.55 (dd, 2H, *J* 5.4, 8.7 Hz, H-2'',6''), 7.62 (d, 1H, *J* 15.8 Hz, H-5), 7.70 (dd, 1H, *J* 1.5, 8.1 Hz, H-6'), 12.2 (s, 1H, 2'-O*H*), 14.6 (s, 1H, 3-*OH*) ppm. ^{13}C NMR (75.47 MHz, $CDCl_3$): δ = 97.0 (C-2), 116.1 (d, 2C, *J* 22.0 Hz, C-3",5"), 118.8 (C-3'), 119.0 (C-1'), 119.1 (C-5'), 121.9 (C-4), 128.5 (C-6'), 129.8 (d, 2C, *J* 8.5 Hz, C-2",6"), 131.3 (C-1''), 135.9 (C-4'), 138.5 (C-5), 162.6 (C-2'), 163.8 (d, 1C, *J*

251.4 Hz, C-4”), 174.2 (C-3), 196.0 (C-1) ppm. ^{19}F NMR (300.13 MHz, $CDCl_3$): δ = -132.8 to -132.7 (m, 4’’-F) ppm. MS (ESI^+) m/z (%): 285.1 (17) $[M+H]^+$, 323.1 (13) $[M+K]^+$.

5.2.3 Synthesis of (*E*)-3-(4-fluorostyryl)-4*H*-chromen-4-one (7a)

To a solution of 4-oxo-4*H*-chromene-3-carbaldehyde (0.500 g, 2.87 mmol) in dry pyridine (112 mL) were added 1.5 equiv. of potassium *tert*-butoxide (0.483 g, 4.31 mmol) and 5 equiv. of 4-fluorophenylacetic acid (2.212 g, 14.35 mmol). The reaction was stirred and heated at reflux for 24 hours. Then, the reaction mixture was poured over water and ice and was acidified to pH 3-4. The resulting solid was filtered, dissolved in DCM and washed with water. The solvent was evaporated to dryness and the solid residue was dissolved in a small amount of DCM and it was purified by column chromatography using DCM as solvent. Then, solid residue obtained after purification was crystallized with ethanol.

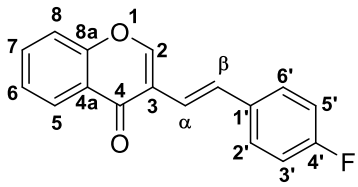

7a

(*E*)-3-(4-Fluorostyryl)-4*H*-chromen-4-one (**7a**), 50% yield, 0.386 g (white solid), m.p. 138 - 140 ºC. ^{1}H NMR (300.13 MHz, $CDCl_3$): δ = 6.89 (d, 1H, *J* 16.4 Hz, H-α), 7.05 (t, 2H, *J* 8.7 Hz, H-3’,5’), 7.40-7.52 (m, 4H, H-2’,6’,6,8), 7.62 (d, 1H, *J* 16.4 Hz, H-β), 7.68 (ddd, 1H, *J* 1.6, 7.1, 8.7 Hz, H-7), 8.11 (s, 1H, H-2), 8.30 (dd, 1H, *J* 1.6, 8.0 Hz, H-5) ppm. ^{13}C NMR (75.47 MHz, $CDCl_3$): δ = 115.6 (d, 2C, *J* 21.7 Hz, C-3’,5’), 118.1 (C-8), 118.8 (C-α), 121.7 (C-3), 124.1-124.8 (C-4a), 125.3 (C-6), 126.3 (C-5), 128.1 (d, 2C, *J* 8.1 Hz, C-2’,6’), 130.6 (C-β), 133.6 (C-7,1’), 153.1 (C-2), 155.8 (C-8a), 162.7 (d, 1C, *J* 220.4 Hz, C-4’), 176.6 (C-4) ppm. ^{19}F NMR (300.13 MHz, $CDCl_3$): δ = -137.0 to -136.9 (m, 4’-F) ppm. MS (ESI^+) m/z (%): 267.1 (100) $[M+H]^+$, 289.1 (60) $[M+Na]^+$.

5.2.4 Synthesis of (*E*)-3-(4-nitrostyryl)-4*H*-chromen-4-one (7b)

To a solution of 4-oxo-4*H*-chromene-3-carbaldehyde (0.500 g, 2.87 mmol) in dry pyridine (50 mL) were added 1.5 equiv of potassium tert-butoxide (0.483 g, 4.31 mmol) and 5 equiv. of 4-nitrophenylacetic acid (2.600 g, 14.35 mmol). The reaction was stirred and heated at reflux for 24 hours. Then, the reaction mixture was poured over water and ice and was acidified to pH 3-4. The resulting solid was filtered, dissolved in DCM and washed with water. The solvent was evaporated to dryness and the solid residue was dissolved in a small

amount of DCM and it was purified by column chromatography using DCM as solvent. Then, the solid residue obtained after purification was crystallized with ethanol.

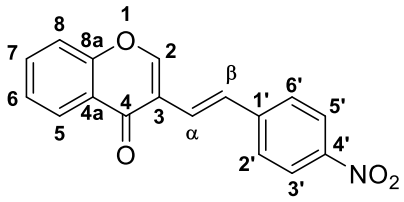

(*E*)-3-(4-nitrostyryl)-4*H*-chromen-4-one (**7b**), 80% yield, 673 mg (yellow solid).

The NMR data of this compound are already reported in the literature. [103]

5.2.5 Synthesis of 5-(4-fluorophenyl)-3-(2-hydroxyphenyl)-4,5-dihydro-1*H*-pyrazole (9)

To a solution of (*E*)-3-(4-fluorophenyl)-1-(2-hydroxyphenyl)prop-2-en-1-one (416.6 mg, 1.72 mmol) in methanol (50 mL) were added 8.0 equiv of hydrazine hydrate (55%) (668 µL, 13.76 mmol). The reaction was stirred and heated at reflux for 3 hours. After that period, the reaction was cooled down to 6 ºC overnight, to allow the crystallization of the reaction product, and afterward the pyrazoline was isolated by filtration.

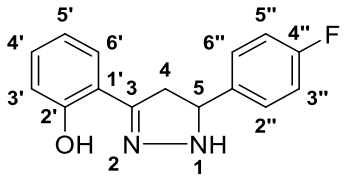

9

5-(4-Fluorophenyl)-3-(2-hydroxyphenyl)-4,5-dihydro-1*H*-pyrazole (**9**), 75% yield, 332 mg, (white solid). ^{1}H NMR (300.13 MHz; DMSO-d_6): δ = 2.98 (dd, 1H, *J* 10.7, 16.6 Hz, H-4), 3.62 (dd, 1H, *J* 10.7, 16.6 Hz, H-4), 4.87 (dt, 1H, *J* 2.1, 10.7 Hz, H-5), 6.89 - 6.93 (m, 2H, H-3', 5'), 7.20 (t, 2H, *J* 8.8 Hz, H-3'', 5''), 7.17-7.27 (m, 1H, H-4'), 7.30 (dd, 1H, *J* 1.3, 7.6 Hz, H-6'), 7.45 (dd, 2H, *J* 5.6, 8.8 Hz, H-2'',6''), 10.23 (s, 1H, N*H*), 11.14 (s, 1H, O*H*) ppm. ^{13}C NMR (75.47 MHz; $CDCl_3$): δ = 40.9 (C-4), 61.4 (C-5), 115.3 (d, 2C, *J* 21.4 Hz, C-3'',5''), 115.8 (C-3'), 119.2 (C-5'), 127.9 (C-6'), 128.8 (d, 2C, *J* 8.1 Hz, C-2'',6''), 129.9 (C-4'), 138.4 (C-1"), 152.7 (C-3), 156.8 (C-2'), 162.0 (d, 1C, *J* 209.1 Hz, C-4"). ^{19}F NMR (300.13 MHz; $CDCl_3$): δ = -138.6 to -138.5 (m, 4''-F) ppm. MS (ESI$^+$) m/z (%): 257.1 (100) $[M+H]^+$.

5.2.6 Synthesis of 5(3)-(4-fluorophenyl)-3(5)-(2-hydroxyphenyl)-1*H*-pyrazole (10)

To a solution of 5-(4-fluorophenyl)-3-(2-hydroxyphenyl)-4,5-dihydro-1*H*-pyrazole (**9**) (200 mg, 0.780 mmol) in toluene (40 mL) were added 3.0 equiv. of chloranil (575 mg,

2.34 mmol). The reaction was stirred and heated at reflux for 23 hours. After that period, the toluene was evaporated to dryness and the compound was isolated after purification by TLC using DCM as eluent. Then it was crystallized from DCM and cyclohexane.

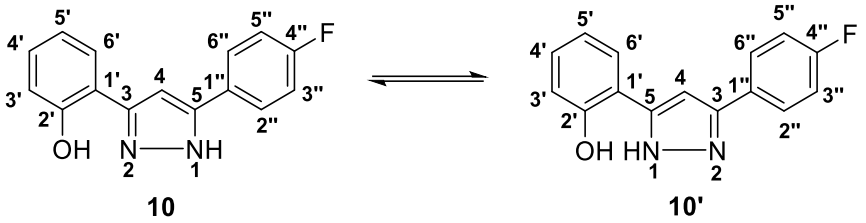

5(3)-(4-Fluorophenyl)-3(5)-(2-hydroxyphenyl)-1*H*-pyrazole (**10**), 64%, 131.6 mg (white solid), m.p. 171.5 – 172.4 ºC. ^{1}H NMR (300.13 MHz; DMSO-d_6): δ = 6.89 - 6.99 (m, 2H, H-3',5'), 7.13 - 7.38 (m, 4H, H-4, 4', 3'', 5''), 7.72 (dd, 1H, *J* 3.7, 7.7 Hz, H-6'), 7.89 (dd, 2H, *J* 5.5, 8.8 Hz, H-2'', 6''), 10.24 (s, 1H, N*H*) and 10.86 (s, 1H, N*H*), 12.90 (s, 1H, O*H*) and 13.64 (s, 1H, O*H*) ppm. MS (ESI$^+$) m/z (%): 255.2 (100) $[M+H]^+$, 277.2 (18) $[M+Na]^+$. HRMS (ESI$^+$) m/z calcd for $C_{15}H_{12}FN_2O$ $[M+H]^+$, 255.2654; found: 255.0922.

5.2.7 Synthesis of (*E*)-5(3)-(4-fluorostyryl)-3(5)-(2-hydroxyphenyl)-1*H*-pyrazole (11)

To a solution of (*E*)-5-(4-fluorophenyl)-1-(2-hydroxyphenyl)pent-4-ene-1,3-dione (**4**) (0.6815 g, 2.40 mmol) in methanol (180 mL) were added 8.0 equiv. of hydrazine hydrate (55%) (1.69 mL, 19.18 mmol). The reaction was stirred under nitrogen at room temperature for 3h30 min. The methanol was evaporated to dryness and the same amount of chloroform was added. Then, the solution was washed with acid water to remove the remaining hydrazine. The chloroform was evaporated to dryness and the solid residue was dissolved in DCM and purified by TLC using DCM as eluent). The solid residue isolated after purification was crystallized from DCM and cyclohexane.

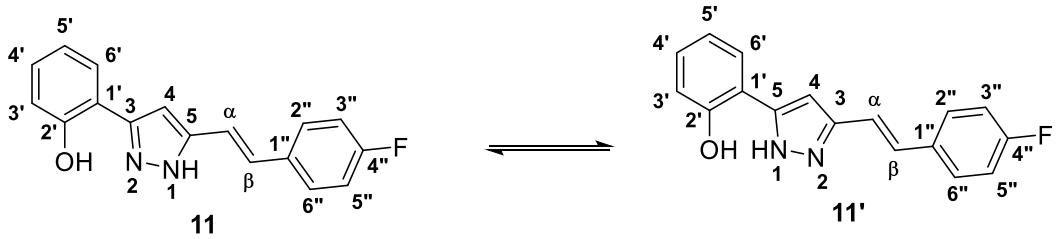

(*E*)-5(3)-(4-fluorostyryl)-3(5)-(2-hydroxyphenyl)-1*H*-pyrazole (**11**), 26% yield, 177.7 mg (brown solid), m.p. 130 - 132 ºC. ^{1}H NMR (300.13 MHz, $CDCl_3$): δ = 6.79 (br s,

1H, H-4), 6.94 (t, 2H, *J* 8.1 Hz, H-3'',5''), 7.03-7.09 (m, 4H, H-3',5', α, β), 7.23 (t, 1H, *J* 7.5 Hz, H-4'), 7.44 (dd, 2H, *J* 5.2 , 8.1 Hz, H-2'',6''), 7.59 (dd, 1H, *J* = 1.5, 7.7 Hz, H-6'), 10.55 (br s, 2H, N*H* and 2'-O*H*) ppm. MS (ESI^+) m/z (%): 281.1 (100) $[M+H]^+$.

5.2.8 Synthesis of (*E*)-4-(4-fluorostyryl)-3(5)-(2-hydroxyphenyl)-1*H*-pyrazole (12)

To a solution of (*E*)-3-(4-fluorostyryl)-4*H*-chromen-4-one (**7**) (1.537 g, 5.77 mmol) in methanol (385 mL) were added 2.0 equiv. of hydrazine hydrate (55%) (1.02 mL, 11.54 mmol). The reaction was stirred under nitrogen at room temperature for 2 hours. The methanol was evaporated to dryness and the same amount of chloroform was added. Then, the solution was washed with acid water to remove any remaining hydrazine. The chloroform was evaporated to dryness and the solid residue was dissolved in DCM and purified by TLC with using DCM: acetone (9:1) as eluent. The solid residue obtained after purification was crystallized with DCM and cyclohexane.

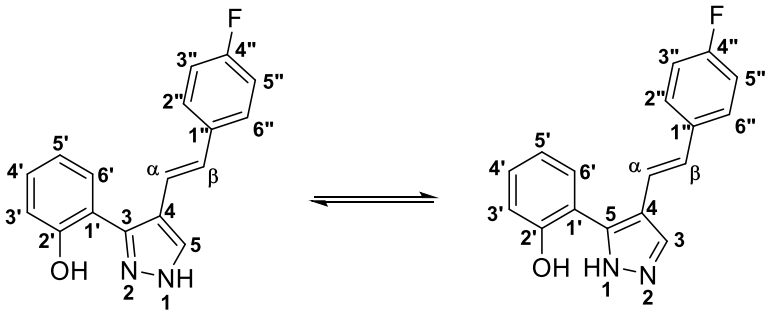

(*E*)-4-(4-fluorostyryl)-3(5)-(2-hydroxyphenyl)-1*H*-pyrazole (**12**), 85% yield, 1.38 g (white solid), m.p. 165 - 167 ºC. ^{1}H NMR (300.13 MHz, $CDCl_3$): δ = 6.85 (d, 1H, *J* = 16.9 Hz, H-β), 6.96 (dt, 1H, *J* = 1.3, 7.4 Hz, H-5'), 7.05 (t, 2H, *J* = 8.7 Hz, H-3'', 5''), 7.06 (d, 1H, *J* = 16.9 Hz, H-α), 7.31 (ddd, 1H, *J* = 1.7, 7.4, 8.6 Hz, H-4'), 7.44 (dd, 2H, *J* = 5.4, 8.7 Hz, H-2'',6''), 7.60 (dd, 1H, *J* = 1.7, 7.4 Hz, H-6'), 7.83 (s, 1H, H-5) ppm. ^{13}C NMR (75.47 MHz, $CDCl_3$): δ = 115.7 (d, 2C, *J* = 21.5 Hz, C-3'',5''), 117.0 (C-3'), 117.2 (C-1'), 118.4 (C-4), 118.6 (C-α), 119.6 (C-5'), 127.7 (C-5), 127.8 (d, 2C, *J* 8.0 Hz, C-2'',6''), 128.6 (C-6'), 128.8 (C-β), 129.6 (C-4'), 133.5 (C-1"), 147.5 (C-3), 155.6 (C-2'), 162.3 (d, 1C, *J* 247.1 Hz, C-4") ppm. ^{19}F NMR (300.13 MHz, $CDCl_3$): δ = -138.7 (m, 4'-F) ppm. MS (ESI^+) m/z (%): 281.1 (100) $[M+H]^+$.

5.2.9 Synthesis of 5-(4-fluorophenyl)-1-(6-hydroxyhexyl)-3-(2-hydroxyphenyl)-1*H*-pyrazole (13a) and 5(3)-(4-fluorophenyl)-3(5)-[2-(6-hydroxyhexyloxy)phenyl]-1*H*-pyrazole (13b)

To a solution of 5(3)-(4-fluorophenyl)-3(5)-(2-hydroxyphenyl)-1*H*-pyrazole (**10**) (94.7 mg, 0.372 mmol) in acetone (30 mL) were added 3.0 equiv. of K_2CO_3 (154.2 mg, 1.116 mmol) and 1.5 equiv of 6-bromohexanol (73 µL, 0.558 mmol). The reaction was stirred under nitrogen at reflux for 71 hours. Then, the potassium carbonate was filtered, and acetone was evaporated to dryness. The solid residue was dissolved in DCM and purified by TLC using ethyl acetate:hexane (3:2) as eluent. Two compounds were isolated; the compound with lower RF corresponding to 5(3)-(4-fluorophenyl)-3(5)-[2-(6-hydroxyhexyloxy)phenyl]-1*H*-pyrazole (**13b**) and that with high RF corresponding to 5-(4-fluorophenyl)-1-(6-hydroxyhexyl)-3-(2-hydroxyphenyl)-1*H*-pyrazole (**13a**)

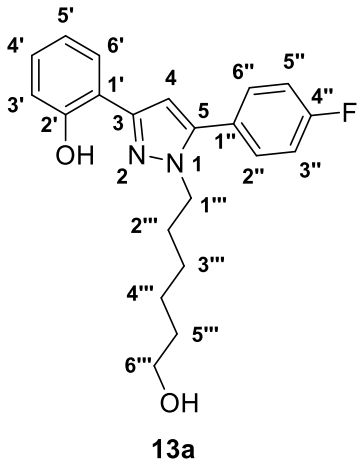

13a

5-(4-Fluorophenyl)-1-(6-hydroxyhexyl)-3-(2-hydroxyphenyl)-1*H*-pyrazole (**13a**), (orange oil). ^{1}H NMR (300.13 MHz; $CDCl_3$): δ = 1.22 - 1.26 (m, 4H, 3’’’-CH_2, 4’’’-CH_2), 1.51 (quint, 2H, *J* 6.0 Hz, 5’’’-CH_2), 1.85 (quint, 2H, *J* 7.2 Hz, 2’’’-CH_2), 3.58 (t, 2H, *J* 6.0 Hz, 6’’’-CH_2), 4.11 (t, 2H, *J* 7.2 Hz, 1’’’-CH_2), 6.62 (s, 1H, H-4), 6.91 (dt, 1H, *J* 1.3, 7.6 Hz, H-5’), 7.03 (dd, 1H, *J* 1.2, 8.2 Hz, H-3’), 7.19 (t, 2H, *J* 8.7 Hz, H-3’’, 5’’), 7.24 - 7.28 (m, 1H, H-4’), 7.42 (dd, 2H, *J* 5.3, 8.7 Hz, H-2’’, 6’’), 7.57 (dd, 1H, *J* 1.7, 7.6 Hz, H-6’) ppm. ^{13}C NMR (75.47 MHz; $CDCl_3$): δ = 25.2 (C-4’’’), 26.2 (C-3’’’), 30.0 (C-2’’’), 32.5 (C- 5’’’), 49.3 (C-1’’’), 62.6 (C-6’’’), 102.7 (C-4), 116.0 (d, 2C, *J* 21.8 Hz, C-3’’,5’’), 116.5 (C-1’), 117.0 (C-3’), 119.3 (C-5’), 126.1 (C-6’), 126.2 (C-1”), 129.1 (C-4’), 130.9 (d, 2C, *J* 8.3 Hz, C-2’’, 6’’), 143.6 (C-5), 150.5 (C-3), 155.9 (C-2’), 163.1 (d, 1C, *J* 249.6 Hz, C-4”) ppm. ^{19}F NMR (300.13 MHz; $CDCl_3$): δ = -108.3 to -108.2 (m, 4’’-F) ppm. MS (ESI$^+$) m/z (%): 355.3 (100) $[M+H]^+$, 377.3 (28) $[M+Na]^+$.

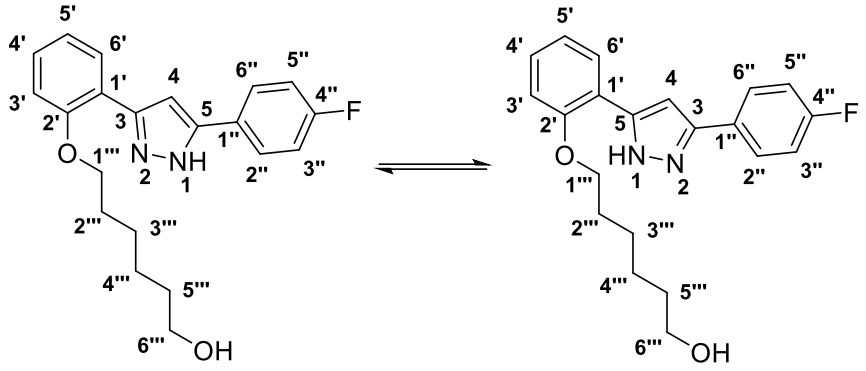

13b **13b'**

5(3)-(4-fluorophenyl)-3(5)-[2-(6-hydroxyhexyloxy)phenyl]-1*H*-pyrazole (**13b**), 37% yield, 48.3 mg, (orange oil). ^{1}H NMR (300.13 MHz; $CDCl_3$): δ = 1.50 - 1.67 (m, 6H, 3’’’-CH_2, 4’’’-CH_2, 5’’’-CH_2), 1.95 (quint, 2H, *J* 6.4 Hz, 2’’’-CH_2), 3.66 (t, 2H, *J* 6.2 Hz, 6’’’-CH_2), 4.17 (t, 2H, *J* 6.4 Hz, 1’’’-CH_2), 6.89 (s, 1H, H-4), 7.00 - 7.06 (m, 2H, H-3’, 5’), 7.11 (t, 2H, *J* 8.5 Hz, H-3’’, 5’’), 7.30 (ddd, 1H, *J* 1.6, 7.9, 8.9 Hz, H-4’), 7.72 (dd, 1H, *J* 1.6, 7.7 Hz, H-6’), 7.83 (dd, 2H, *J* 5.5, 8.5 Hz, H-2’’, 6’’) ppm. ^{13}C NMR (75.47 MHz; $CDCl_3$): δ = 25.5 (C-4’’’), 25.9 (C-3’’’), 29.2 (C-2’’’), 32.3 (C-5’’’), 62.3 (C-6’’’), 68.8 (C-1’’’), 99.6 (C-4), 112.5 (C-3’), 115.6 (d, 2C, *J* 21.5 Hz, C-3’’, 5’’), 117.3 (C-1’), 121.4 (C-5’), 127.3 (d, 2C, *J* 8.1 Hz, C-2’’, 6’’), 128.0 (C-6’), 129.5 (C-4’ and C-1”), 142.4 (C-3), 150.7 (C-5), 155.4 (C-2’), 162.6 (d, 1C, *J* 249.6 Hz, C-4”) ppm. ^{19}F NMR (300.13 MHz; $CDCl_3$): δ = -111.0 to -110.9 (m, 4’’-F) ppm. MS (ESI$^+$) m/z (%): 355.3 (100) $[M+H]^+$, 377.3 (15) $[M+Na]^+$.

5.2.10 Synthesis of (*E*)-4-(4-fluorostyryl)-1-(2-hydroxyethyl)-3-(2-hydroxyphenyl)-1*H*-pyrazole (14a)

To a solution of (*E*)-4-(4-fluorostyryl)-3(5)-(2-hydroxyphenyl)-1*H*-pyrazole (**12**) (112 mg, 0.401 mmol) in acetone (30 mL) were added 3.0 equiv. of K_2CO_3 (166.4 mg, 1.204 mmol) and 1.2 equiv of 2-bromoethanol (34 µL, 0.482 mmol). The reaction was stirred under nitrogen at 50ºC for more than 4 days. Then, potassium carbonate was filtered, and acetone was evaporated to dryness. The solid residue was dissolved in DCM and purified by TLC using DCM: methanol (9.5:0.5) as eluent. One compound was isolated corresponding to (*E*)-4-(4-fluorostyryl)-1-(2-hydroxyethyl)-3-(2-hydroxyphenyl)-1*H*-pyrazole (**14a**).

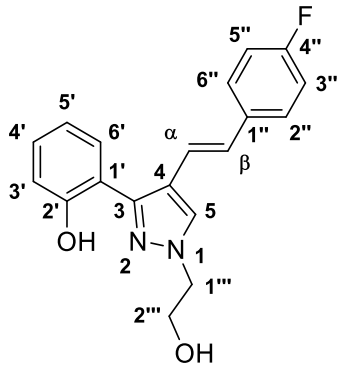

14a

(*E*)-4-(4-Fluorostyryl)-1-(2-hydroxyethyl)-3-(2-hydroxyphenyl)-1*H*-pyrazole (**14a**), 34% yield, 44.8 mg (white oil). ^{1}H NMR (300.13 MHz, $CDCl_3$): δ = 4.05 (t, 2H, *J* 5.0 Hz, 2’’’-CH_2), 4.30 (t, 2H, *J* 5.0 Hz, 1’’’-CH_2), 6.81 (d, 1H *J* 16.2 Hz, H-β), 6.94 (dt, 1H, *J* 1.2, 7.7 Hz, H-5’), 6.99-7.08 (m, 4H, H-3’, α, 3’’,5’’), 7.23-7.29 (m, 1H, H-4’), 7.41 (dd, 2H, *J* 5.4, 8.6 Hz, H-2’’,6’’), 7.56 (dd, 1H, *J* 1.6, 7.7 Hz, H-6’), 7.74 (s, 1H, H-5) ppm. ^{13}C NMR (75.47 MHz, $CDCl_3$): δ = 54.6 (C-1’’’), 61.5 (C-2’’’), 115.8 (d, 2C, *J* = 22.6 Hz, C-3’’,5’’), 117.1 (C-3’), 117.5 (C-1’), 118.7 (C-α,4), 119.6 (C-5’), 127.8 (d, 2C, *J* = 7.9 Hz, C-2’’,6’’), 128.5 (C-β, 6’), 129.5 and 129.6 (C-4’, 5), 133.6 (C-1”), 148.2 (C-3), 155.6 (C-2’), 162.4 (d, 1C, *J* 247.1 Hz, C-4”) ppm. ^{19}F NMR (300.13 MHz; $CDCl_3$): δ = -110.8 to -110.7 (m, 4’’-F) ppm.

5.2.11 Synthesis of (*E*)-4-(4-fluorostyryl)-3(5)-[2-(2-hydroxyethoxy) phenyl]-1*H*-pyrazole (14b)

To a solution of (*E*)-4-(4-fluorostyryl)-3(5)-(2-hydroxyphenyl)-1*H*-pyrazole (**12**) (150 mg, 0.535 mmol) in acetone (30 mL) were added 3.0 equiv. of K_2CO_3 (221.9 mg, 1.605 mmol) and 1.2 equiv of 2-bromoethanol (46 µL, 0.642 mmol). The reaction was stirred under nitrogen at 50ºC for 24 hours. Then, the potassium carbonate was filtered, and acetone was evaporated to dryness. The solid residue was dissolved in DCM and purified by TLC using DCM: methanol (9.5:0.5) as eluent. One compound was isolated (*E*)-4-(4-fluorostyryl)-3(5)-[2-(2-hydroxyethoxy)phenyl]-1*H*-pyrazole (**14b**).

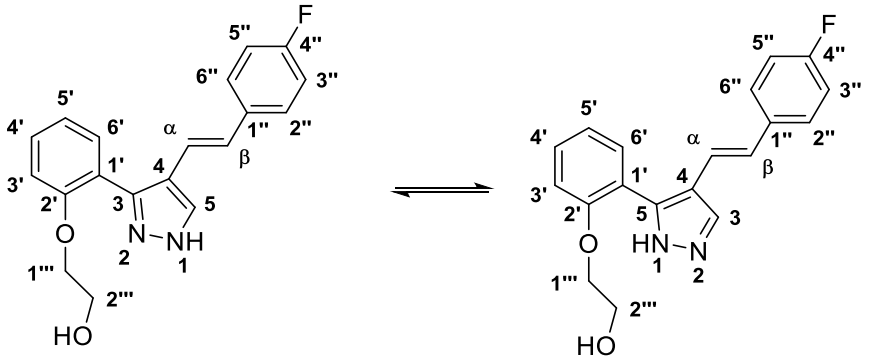

14b 14b'

(*E*)-4-(4-Fluorostyryl)-3(5)-[2-(2-hydroxyethyl)phenyl]-1*H*-pyrazole (**14b**), 17 % yield, 29.7 mg , (white oil). ^{1}H NMR (300.13 MHz; $CDCl_3$): δ = 4.00 (t, 2H, *J* 4.2 Hz, 1’’’-CH_2), 4.27 (t, 2H, *J* 4.2 Hz, 2’’’-CH_2), 6.89 (d, 1H, *J* 16.0 Hz, H-β), 6.97 (d, 1H, *J* 16.0 Hz, H-α), 7.02 (t, 2H, *J* 8.7 Hz, H-3’’,5’’), 7.06-7.13 (m, 2H, H-3’,5’), 7.35-7.41 (m, 3H, H-4’, 2’’,6’’), 7.49 (dd, 1H, *J* 1.5, 7.6 Hz, H-6’), 7.85 (br s, 1H, H-5) ppm.

5.2.12 Synthesis of (*E*)-4-(4-fluorostyryl)-3-(2-hydroxyphenyl)-1-(2-tosylethyl)-1*H*-pyrazole (16)

To a solution of (*E*)-4-(4-fluorostyryl)-1-(2-hydroxyethyl)-3-(2-hydroxyphenyl)-1*H*-pyrazole (**14a**) (28.3 mg, 0.087 mmol) in DCM (2 mL) were added 2.0 equiv. of TEA (24 µL, 0.175 mmol) and 1.2 equiv. of *p*-TsCl (19.9 mg, 0.105 mmol) in an ice bath. The reaction was stirred at room temperature for 22h. After this period, HCl was used to neutralize the reaction. The compound was extracted with DCM and purified by TLC using DCM:methanol (9.5:0.5) as eluent. The tosylate pyrazole stain was extracted with ethyl acetate.

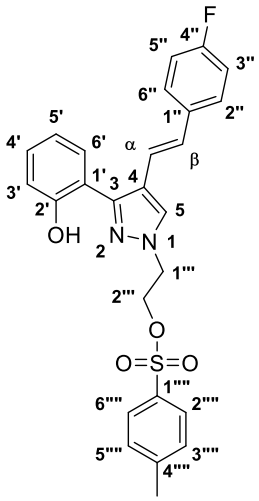

16

(*E*)-4-(4-fluorostyryl)-3-(2-hydroxyphenyl)-1-(6-tosylethyl)-1*H*-pyrazole (**16**), 16% yield, 6.5 mg, (white oil). ^{1}H NMR (300.13 MHz; $CDCl_3$): δ = 2.20 (s, 3H, CH_3), 4.40 (s, 4H, 1’’’-CH_2, 2’’’-CH_2), 6.78 (d, 1H, *J* 16.2 Hz, H-β), 6.95 (dt, 1H, *J* 1.3, 7.5 Hz, H-5’), 7.00-7.10 (m, 4H, H-3’, H-α, H-3’’,5’’), 7.15 (d, 2H, *J* 8.3 Hz, H-3””,5””), 7.23-7.29 (m, 1H, H-4’), 7.45 (dd, 2H, *J* 5.4, 8.7 Hz, H-2’’,6’’), 7.54 (dd, 1H, *J* 1.4, 7.5 Hz, H-6’), 7.60 (d, 2H, *J* 8.3 Hz, H-2””,6””), 7.63 (s, 1H, H-5), 9.84 (s, 1H, O*H*) ppm. ^{13}C NMR (75.47 MHz; $CDCl_3$): δ = 21.4 (*C*H_3), 51.1 ou 67.5 (C-1’’’, C-2’’’), 115.6-115.9 (C-3’’,5’’), 117.0 (C-3’), 117.2 (C-α), 118.4 (C-1’), 118.7 (C-4), 119.4 (C-5’), 127.7 (C-2””,6””), 127.7-127.8 (C-2’’,6’’), 128.2 (C-6’), 128.8 (C-β), 129.5 (C-4’), 129.6 (C-5), 129.9 (C-3””,5””), 131.7 (C-1””), 133.7 (C-1”), 145.4 (C-4””), 148.5 (C-3), 155.6 (C-2’), 161.7 (d, 1C, *J* 249.8 Hz, C-4”) ppm. ^{19}F NMR (300.13 MHz; $CDCl_3$): δ = -110.6 to -110.5 (m, 4’’-F) ppm. MS (ESI$^+$) m/z (%): 479.3 (100) $[M+H]^+$, 501.3 (38) $[M+Na]^+$, 517.3 (6) $[M+K]^+$. HRMS (ESI$^+$) m/z calcd for $C_{26}H_{24}FN_2O_4S$ $[M+H]^+$, 479.5392; found: 479.1429.

5.2.13 Synthesis of (*E*)-4-(4-fluorostyryl)-3(5)-[2-(2-tosylethyl)phenyl]-1*H*-pyrazole (17)

To a solution of (*E*)-4-(4-fluorostyryl)-3(5)-[2-(2-hydroxyethoxy)phenyl]-1*H*-pyrazole (**14b**) (29.7 mg, 0.092 mmol) in DCM (2 mL) were added 2.0 equiv. of TEA (26 µL, 0.183 mmol) and 1.2 equiv. of *p*-TsCl (21.0 mg, 0.110 mmol) in an ice bath. The reaction was stirred at room temperature for 24h. After this period, an aqueous solution of HCl was used to neutralize the reaction. The reaction mixture was extracted with DCM and dried over anhydrous sodium sulfate. The product was isolated after purification by TLC using DCM:methanol (9.5:0.5) as eluent.

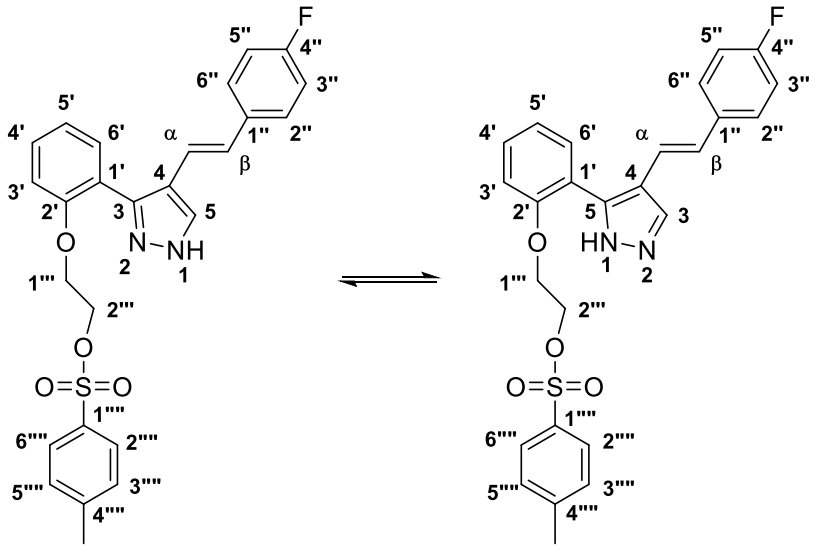

(*E*)-4-(4-Fluorostyryl)-3(5)-[2-(2-tosylethyl)phenyl]-1*H*-pyrazole (**17**), 43% yield, 18.7 mg, (white oil) ^{1}H NMR (300.13 MHz; $CDCl_3$): δ = 2.43 (s, 3H, CH_3), 3.74 (t, 2H, *J* 4.3 Hz, 2’’’-CH_2), 4.12 (t, 2H, *J* 4.3 Hz, 1’’’-CH_2), 6.63 (d, 1H, *J* 16.4 Hz, H-α), 6.85 (d, 1H, *J* 16.4 Hz, H-β), 6.96-7.06 (m, 4H, H-3’’, 5’’, 5’, 3’), 7.29-7.43 (m, 6H, H-2’’, 6’’, 3””, 5””, 6’, 4’), 7.98 (d, 2H, *J* 8.4 Hz, H-2””,6””), 8.32 (s, 1H, H-5) ppm. ^{13}C NMR (75.47 MHz; $CDCl_3$): δ = 21.8 (CH_3), 61.1 (C-2’’’), 71.1 (C-1’’’), 113.9 (C-5’), 115.6-115.9 (C-3’’, 5’’), 117.1 (C-α), 121.0 (C-1’), 121.3 (C-3’), 122.4 (C-4), 127.4 (C-5), 127.8-127.9 (C-2’’, 6’’), 128.4 (C-2””, 6””), 129.3 (C-β), 130.1 (C-3””, 5””), 130.8 (C-4’), 131.7 (C-6’), 132.7 (C-1’’), 133.9 (C-1””), 146.0 (C-4””), 153.3 (C-3), 156.7 (C-2’), 162.5 (d, 1C, *J* 248.0 Hz, C-4’’) ppm. ^{19}F NMR (300.13 MHz; $CDCl_3$): δ = -110.1 to -110.0 (m, 4’’-F) ppm. MS (ESI$^+$)

m/z (%): 479.3 (30) $[M+H]^+$, 501.3 (100) $[M+Na]^+$, 979.5 (10) $[2M+Na]^+$. HRMS (ESI^+) m/z calcd for $C_{26}H_{24}FN_2O_4S$ $[M+H]^+$, 479.5392; found: 479.1426.

5.2.14 Synthesis of (*E*)-4-(4-fluorostyryl)-1-(6-hydroxyhexyl)-3-(2-hydroxyphenyl)-1*H*-pyrazole (15a) and (*E*)-4-(4-fluorostyryl)-3(5)-[2-(6-hydroxyhexyloxy)phenyl]-1*H*-pyrazole (15b)

To a solution of (*E*)-4-(4-fluorostyryl)-3(5)-(2-hydroxyphenyl)-1*H*-pyrazole (**12**) (50 mg, 0.178 mmol) in acetone (30 mL) were added 3.0 equiv. of K_2CO_3 (74.0 mg, 0.535 mmol) and 1.5 equiv of 6-bromohexanol (35 µL, 0.268 mmol). The reaction was stirred under nitrogen at reflux for 48 hours. Then, the potassium carbonate was filtered, and acetone was evaporated to dryness. The solid residue was dissolved in DCM and purified by TLC using ethyl acetate:hexane (3:2) as eluent. Two compounds were isolated; the compound with the lower RF corresponding to (*E*)-4-(4-fluorostyryl)-3(5)-[2-(6-hydroxyhexyloxy)phenyl]-1*H*-pyrazole (**15b**) and that with the high RF corresponding to (*E*)-4-(4-fluorostyryl)-1-(6-hydroxyhexyl)-3-(2-hydroxyphenyl)-1*H*-pyrazole (**15a**).

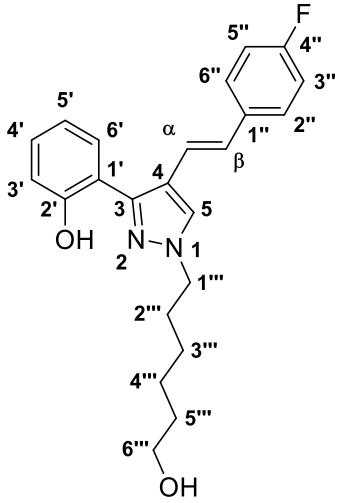

15a

(*E*)-4-(4-fluorostyryl)-1-(6-hydroxyhexyl)-3-(2-hydroxyphenyl)-1*H*-pyrazole (**15a**), 50% yield, 34.2 mg, (white oil) ^1H NMR (300.13 MHz; $CDCl_3$): δ = 1.32-1.43 (m, 4H, 3'''-CH_2, 4'''-CH_2), 1.53 (quint, 2H, *J* 6.5 Hz, 5'''-CH_2), 1.88 (quint, 2H, *J* 7.0 Hz, 2'''-CH_2), 3.58 (t, 2H, *J* 6.5 Hz, 6'''-CH_2), 4.07 (t, 2H, *J* 7.0 Hz, 1'''-CH_2), 6.75 (d, 1H, *J* 16.2 Hz, H-β), 6.93 (dt, *J* 1.4, 7.6 Hz, 1H, H-5'), 6.99-7.07 (m, 4H, H-3', H-α, H-3'',5''), 7.23-7.26 (dt, *J* 1.4, 7.6 Hz, 1H, H-4'), 7.38 (dd, 2H, *J* 5.5, 8.1 Hz, H-2'',6''), 7.56 (br s, 1H, H-5), 7.57 (dd, 1H, *J* 1.4, 7.2 Hz, H-6') ppm. ^{13}C NMR (75.47 MHz; $CDCl_3$): δ = 25.3 (C-4'''), 26.3 (C-3'''), 30.0 (C-2'''), 32.4 (C-5'''), 52.2 (C-1'''), 62.5 (C-6'''), 115.7 (d, 2C, *J* 21.6 Hz, C-3'',5''), 117.0 (C-3'), 118.2 (C-1'), 118.87 and 118.90 (C-α and C-4), 119.5 (C-5'), 127.7 (d, 2C, *J* 7.9 Hz, C-2'',6''), 128.1 (C-β), 128.2 (C-5), 128.3 (C-6'), 129.2 (C-4'), 133.6 (d, 1C, *J* 3.3 Hz, C-1"), 147.4 (C-3), 155.7 (C-2'), 162.2 (d, 1C, *J* 246.9 Hz, C-4'') ppm. ^{19}F NMR (300.13 MHz; $CDCl_3$): δ = -110.9 to -110.8 (m, 4''-F) ppm. MS (ESI^+) m/z (%): 381.3 (100) $[M+H]^+$, 403.3 (6) $[M+Na]^+$.

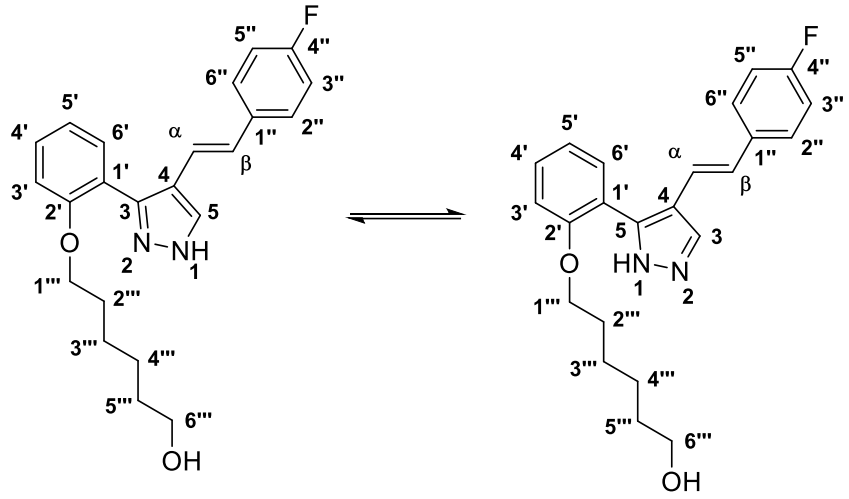

(*E*)-4-(4-Fluorostyryl)-1-(6-hydroxyhexyl)-3-(2-hydroxyphenyl)-1*H*-pyrazole (**15b**), 20% yield, 13.5 mg, (white oil). ^{1}H NMR (300.13 MHz; $CDCl_3$): δ = 1.40-1.46 (m, 4H, 3’’’-CH_2, 4’’’-CH_2), 1.54 (quint, 2H, *J* 6.2 Hz, 5’’’-CH_2), 1.82 (quint, 2H, *J* 6.4 Hz, 2’’’-CH_2), 3.62 (t, 2H, *J* 6.2 Hz, 6’’’-CH_2), 4.07 (t, 2H, *J* 6.4 Hz, 1’’’-CH_2), 6.88 (d, 1H, *J* 16.3 Hz, H-β), 6.95 (d, 1H, *J* 16.3 Hz, H-α), 7.01 (t, 2H, *J* 8.8 Hz, H-3”,5”), 7.02-7.10 (m, 2H, H-3’,5’), 7.35-7.41 (m, 1H, H-4’), 7.39 (dd, 2H, *J* 5.3, 8.8 Hz, H-2’’,6’’), 7.49 (dd, 1H, *J* 1.6, 7.6 Hz, H-6’), 7.88 (s, 1H, H-5) ppm. ^{13}C NMR (75.47 MHz; $CDCl_3$): δ = 25.3 (C-4’’’), 25.8 (C-3’’’), 29.0 (C-2’’’), 32.3 (C-5’’’), 62.4 (C-6’’’), 68.7 (C-1’’’), 112.5 (C-3’), 115.5 (d, 2C, *J* 21.7 Hz, C-3’’,5’’), 118.1 (C-1’), 118.7 (C-4), 119.0 (C-α), 121.1 (C-5’), 126.7 (C-β), 127.5 (d, 2C, *J* 7.9 Hz, C-2’’,6’’), 130.0 (C-4’), 130.8 (C-6’), 133.9 (d, 1C, *J* 3.3 Hz, C-1’’), 137.1 (C-5), 156.1 (C-2’), 162.0 (d, 1C, *J* 246.5 Hz, C-4”) ppm. ^{19}F NMR (300.13 MHz; $CDCl_3$): δ = -111.6 to -111.5 (m, 4’’-F) ppm.

5.2.15 Synthesis of (*E*)-4-(4-fluorostyryl)-3-(2-hydroxyphenyl)-1-(6-tosylhexyl)-1*H*-pyrazole (18)

To a solution of (*E*)-4-(4-fluorostyryl)-1-(6-hydroxyhexyl)-3-(2-hydroxyphenyl)-1*H*-pyrazole (**15a**) (32.7 mg, 0.086 mmol) in DCM (2 mL) were added 2.0 equiv. of TEA (24 µL, 0.172 mmol) and 1.2 equiv. of *p*-TsCl (19.7 mg, 0.103 mmol) in an ice bath. The reaction was stirred at room temperature for 22h. After this period, an aqueous HCl solution was used to neutralize the reaction. The reaction mixture was extracted with DCM, dried

over anhydrous sodium sulfate and the tosylated pyrazole was isolated after purification by TLC using ethyl acetate:hexane (3:2) as eluent.

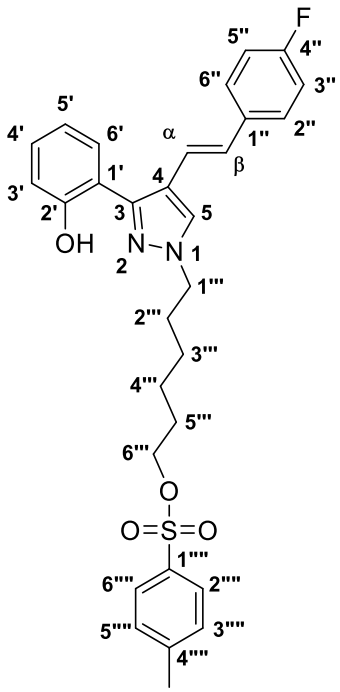

18

(*E*)-4-(4-fluorostyryl)-3-(2-hydroxyphenyl)-1-(6-tosylhexyl)-1*H*-pyrazole (**18**), 22% yield, 9.9 mg, (white oil) ^{1}H NMR (300.13 MHz; $CDCl_3$): δ = 1.25-1.40 (m, 4H, 3'''-CH_2, 4'''-CH_2), 1.58 – 1.68 (m, 2H, 5'''-CH_2), 1.90 (quint, 2H, *J* 6.8 Hz, 2'''-CH_2), 2.43 (s, 3H, CH_3), 4.01 (t, 2H, *J* 6.3 Hz, 6'''-CH_2), 4.13 (t, 2H, *J* 7.0 Hz, 1'''-CH_2), 6.81 (d, 1H, *J* 16.2 Hz, H-β), 6.94 (dt, *J* 1.3, 7.6 Hz, 1H, H-5'), 7.02-7.08 (m, 4H, H-3', H-α, H-3'',5''), 7.22-7.28 (m, 1H, H-4'), 7.33 (d, 2H, *J* 7.9 Hz, H-3a,5a), 7.42 (dd, 2H, *J* 5.6, 8.1 Hz, H-2'',6''), 7.58 (dt, 1H, *J* 1.3, 7.8 Hz, H-6'), 7.63 (s, 1H, H-5), 7.77 (d, 2H, *J* 7.9 Hz, H-2a,6a) ppm. ^{13}C NMR (75.47 MHz; $CDCl_3$): δ = 21.6 (CH_3), 25.0 (C-4'''), 25.9 (C-3'''), 28.6 (C-5'''), 29.7 (C-2'''), 52.2 (C-1'''), 70.3 (C-6'''), 115.7 (d, 2C, *J* 21.7 Hz, C-3'',5''), 117.0 (C-3'), 117.6 (C-1'), 118.3 (C-4), 118.9 (C-α), 119.4 (C-5'), 127.7 (d, 2C, *J* 8.0 Hz, C-2'',6''), 127.9 (C-2a, 6a), 128.2 (C-5, β, 6'), 129.2 (C-4'), 129.8 (C-3a, 5a), 133.1 (C-1a), 133.6 (C-1''), 144.7 (C-4a), 147.6 (C-3), 155.7 (C-2'), 162.2 (d, 1C, *J* 247.5 Hz, C-4") ppm. ^{19}F NMR (300.13 MHz; $CDCl_3$): δ = -110.9 to -110.8 (m, 4''-F) ppm.

5.2.16 Synthesis of [^{19}F]-(*E*)-4-(4-fluorostyryl)-1-(6-fluorohexyl)-3-(2-hydroxyphenyl)-1*H*-pyrazole (19)

To a solution of (*E*)-4-(4-fluorostyryl)-3-(2-hydroxyphenyl)-1-(6-tosylhexyl)-1*H*-pyrazole (**18**) (9.9 mg, 0.019 mmol) in THF (1 mL) were added 2.0 equiv. of TBAF (37 µL, 0.037 mmol). The reaction was stirred at reflux for 30 minutes. After this period, the solvent was evaporated to dryness. The obtained residue was dissolved in DCM and was purified by TLC using DCM as eluent. It was not possible to calculate the yield given the small amount of compound obtained. However, the formation of the expected compound was confirmed based on the analysis of the NMR spectrum.

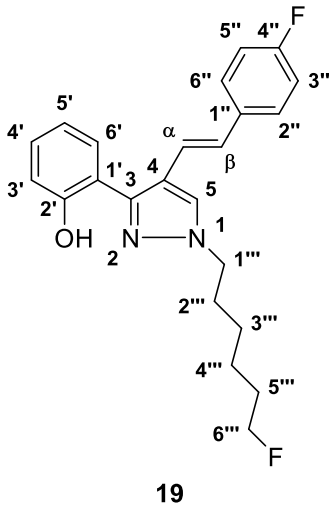

19

[^{19}F]-(*E*)-4-(4-fluorostyryl)-1-(6-fluorohexyl)-3-(2-hydroxyphenyl)-1*H*-pyrazole (**19**), (white oil). ^{1}H NMR (500 MHz; $CDCl_3$): δ = 1.28-175 (m, 6 H, H-3’’’, 4’’’, 5’’’), 1.96 (quint, 2H, *J* 7.1 Hz, H-2’’’), 4.40 (t, 2H, *J* 6.0 Hz, H-6’’’), 4.49 (t, 2H, *J* 6.0 Hz, H-1’’’), 6.81 (d, 1H, *J* 16.1 Hz, H-β), 6.91-6.97 (ddd, 1H, *J* 1.3, 7.7, 8.8 Hz, H-5’), 7.03-7.09 (m, 4H, H-3’, H-α, H-3’’,5’’), 7.23-7.26 (m, 1H, H-4’), 7.43 (dd, 2H, *J* 5.4, 8.6 Hz, H-2’’,6’’), 7.58 (dt, 1H, *J* 1.6, 7.7 Hz, H-6’), 7.64 (s, 1H, H-5) ppm. ^{13}C NMR (75.47 MHz; $CDCl_3$): δ = 25.0 (C-4’’’), 26.1 (C-3’’’), 29.9 (C-2’’’), 30.3 (C-5’’’), 83.3 (C-1’’’), 84.6 (C-6’’’), 115.7 (d, 2C, *J* 21.8 Hz, C-3’’,5’’), 117.0 (C-3’), 117.6 (C-1’), 118.3 (C-4), 118.9 (C-α, 4’’), 119.4 (C-5’), 127.7 (d, 2C, *J* 8.1 Hz, C-2’’,6’’), 128.1-128.2 (C-5, β, 6’), 129.2 (C-4’), 133.6 (C-1’’), 147.6 (C-3), 155.7 (C-2’), ppm. ^{19}F NMR (300.13 MHz; $CDCl_3$): δ = -215.1 (tt, 6’’’-F), -110.9 to -110.8 (m, 4’’-F) ppm.

5.2.17 Synthesis of (*E*)-3(5)-(2-hydroxyphenyl)-4-(4-nitrostyryl)-1*H*-pyrazole (21)

To a solution of (*E*)-3-(4-nitrostyryl)-4*H*-chromen-4-one (**7b)** (199 mg, 0.679 mmol) in methanol (45 mL) were added 2.0 equiv of hydrazine hydrate (55%) (120 µL, 1.357 mmol). The reaction was stirred under nitrogen at room temperature for 3 hours. The methanol was evaporated to dryness and the same amount of chloroform was added. Then, the solution was washed with acid water to remove any remaining hydrazine. The chloroform was evaporated to dryness and the solid residue was dissolved in methanol and cooled down to 6ºC overnight and the pyrazol was isolated after filtration.

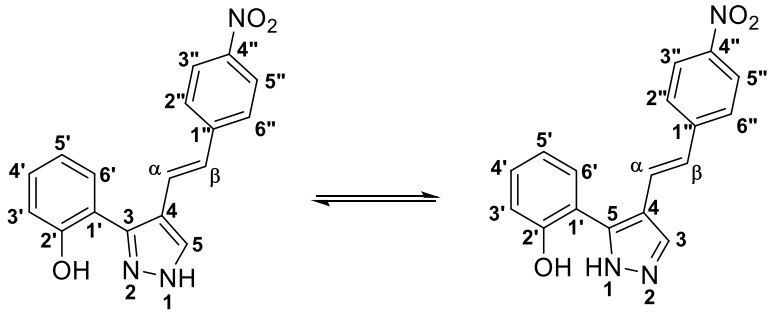

21 **21'**

(*E*)-3(5)-(2-hydroxyphenyl)-4-(4-nitrostyryl)-1*H*-pyrazole (**21**), 60%, 124.9 mg, yellow solid. NMR data for this compound are already reported in the literature. [109] MS (ESI^+) m/z (%): 308.2 (55) $[M+H]^+$. HRMS (ESI+) m/z calcd for $C_{17}H_{14}N_3O_3$ [M+H]+, 308.3088; found: 308.1025.

5.2.18 Synthesis of (*E*)-4-(4-aminostyryl)-3(5)-(2-hydroxyphenyl)-1*H*-pyrazoles (22a)

To a solution of (*E*)-3(5)-(2-hydroxyphenyl)-4-(4-nitrostyryl)-1*H*-pyrazole (**21a**) (174 mg, 0.565 mmol) in chloroform (22 mL) were added 100.0 equiv of tin (6.707 g, 56.5 mmol) and HCl (13 mL). The reaction mixture was vigorously stirred at room temperature for 2 hours. After this period, the reaction mixture was filtered using celite and neutralized using $NaHCO_3$. The expected compound was isolated after purification by TLC, using chloroform:methanol (9.5:0.5) as eluent.

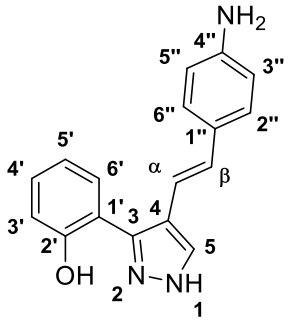

22a

(*E*)-4-(4-aminostyryl)-3(5)-(2-hydroxyphenyl)-1*H*-pyrazoles (23a), 10% yield, 15.6 mg, (orange solid). ^1H NMR (300.13 MHz; $CDCl_3$): δ = 6.68 (d, 2H, *J* 8.6 Hz, H-3'',5''), 6.79 (d, 1H, *J* 16.1 Hz, H-β), 6.92 - 6.98 (m, 2H, H-α, 5'), 7.07 (dd, 1H, *J* 1.2, 8.2 Hz, H-3'), 7.23 - 7.26 (m, 1H, H-4'), 7.30 (d, 2H, *J* 8.6 Hz, H-2'', 6''), 7.66 (dd, 1H, *J* 1.6, 7.8 Hz, H-6'), 7.78 (s, 1H, H-5) ppm. ^{13}C NMR (75.47 MHz; $CDCl_3$): δ = 115.2 (C-3'', 5'', α), 116.9 (C-3'), 117.5 (C-1'), 119.0 (C-4), 119.4 (C-5'), 127.3 (C-5), 127.5 (C-2'', 6''), 128.0 (C-1''), 128.5 (C-6'), 129.3 (C-4'), 130.1 (C-β), 146.1 (C-4''), 147.5 (C-3), 155.6 (C-2') ppm. MS (ESI^+) m/z (%): 278.2 (100) $[M+H]^+$, 300.2 (10) $[M+Na]^+$. HRMS (ESI^+) m/z calcd for $C_{17}H_{16}N_3O$ $[M+H]^+$, 278.3264; found: 278.1282

5.2.19 Synthesis of (*E*)-4-(4-aminostyryl)-3(5)-(2-hydroxy-6-methoxyphenyl)-1*H*-pyrazoles (22b)

To a solution of (*E*)-3(5)-(2-hydroxy-6-methoxyphenyl)-4-(4-nitrostyryl)-1*H*-pyrazole (**21b**) (150.5 mg, 0.440 mmol) in chloroform (15 mL) were added 100.0 equiv of tin (5.274 g, 44.4 mmol) and HCl (8 mL). The reaction was stirred at room temperature for 2 hours. After this period, the reaction mixture was filtered using celite and neutralized using $NaHCO_3$. The (*E*)-4-(4-aminostyryl)-3(5)-(2-hydroxy-6-methoxyphenyl)-1*H*-pyrazole (**22b**), was obtained in 65% (88.5 mg) after purification by column chromatography, using DCM:acetone (9:1) as eluent.

5.2.20 Synthesis of a glycine derivative of pyrazole (23b)

To a solution of (*E*)-3(5)-(2-hydroxy-6-methoxyphenyl)-4-(4-nitrostyryl)-1*H*-pyrazole (**23b**) (70 mg, 0.228 mmol), in methanol (2 mL), were added 2.0 equiv of sodium acetate (37.4 mg, 0.456 mmol), 4.0 equiv of glacial acetic acid (52 µL, 0.911 mmol), 1.01 equiv of sodium cyanoborohydride (14.45 mg, 0.230 mmol) and 1.5 equv of glyoxylic acid monohydrate (31.45 mg, 0.342 mmol). The reaction was stirred at room temperature for 4 hours. After this period, the reaction mixture was washed with brine and extracted with ethyl acetate. After purification by TLC using DCM:acetone (9:1) as eluent, the expected pyrazole **24** was isolated with 12% yield.

5.3 Evaluation of antioxidant activity

5.3.1 $ABTS^{+\bullet}$ radical scavenging assay

A stock solution of $ABTS^{+\bullet}$ was prepared by reacting the ABTS-NH_4 aqueous solution (7 mM) with 2.45 mM potassium persulfate (final concentration) and stored in the dark at room temperature for 12–16 h to allow the completion of radical generation. This solution was then diluted with ethanol so that its absorbance was adjusted to 0.70±0.02 at 734 nm. To determine the scavenging activity, stock solutions with concentrations of 1.0 mM of compound **10-12**, 2-4 mM for **13a**, **13b**, **14a**, **14b** and **15a** and 0.4 mM for **15b** were prepared using DMSO as solvent. Then in a 96-well plate, 50 µL of sample or standard were added as well as 250 µL of $ABTS^{+\bullet}$, previously prepared. Then, the microplate was placed in an environment without light for 20 minutes. After this period, the absorbance was

measured at 734 nm in a spectrophotometer (UVmini-1240 UV-VIS Spectrophotometer, SHIMADZU, Japan) against DMSO (used as blank).[110] The percentage of inhibition of $ABTS^{+\bullet}$ was calculated using the method of Yen & Duh as follows: [111]

$$\% \ ABTS^{+\bullet} \text{ scavenging} = \frac{(Ac\text{-}As)}{Ac} \times 100$$

Where Ac = Absorbance of the control (without addition of compounds) and As = Absorbance of sample/compounds.

5.3.2 $NO^{\bullet}$ radical scavenging assay

The scavenging activity of $NO^{\bullet}$ was estimated by the Griess Ilosvay reaction. [112] In this method, sodium nitroprusside (SNP) decomposes at physiological pH spontaneously generates nitric oxide, that then reacts with oxygen and produces nitrite ions. The amount of these formed products can be quantified through the use of the Griess reagent that reacts with nitrite ions and develops a pink color, formed as a consequence of diazotation of the nitrite with sulfanilamide and subsequent coupling with *N*-(1-naphthyl)ethylenediamine dihydrochloride. In the presence of nitric oxide scavengers, they compete with the oxygen, culminating in a lower production of nitrite ions and subsequently the production of the azo-cromophores, reducing the color tonality. The 3.33 mM SNP solution was made by diluting 5 mg of SNP in 10 mL of potassium buffer 100 mM (pH=7.4). To prepare Griess reagent equal volumes of Griess A (1g of sulfanilamide to 100 mL of phosphoric acid 5%) and Griess B (0.1 g of N-(1-naphthyl)ethylenediamine dihydrochloride to 100 mL of water) had to be added. These solutions were then placed in the fridge and protected from the light. To determine the scavenging activity, stock solutions with concentrations of 0.8-2.0 mM of compound **10-12** and 1-5 mM for **13a**, **13b**, **14a**, **14b**, **15a** and **15b** were prepared using DMSO as solvent. Then in a 96-well plate, 100 µL of standard or sample and 100 µL of 3.33 mM SNP solution were added in this order and then left incubating under fluorescent lamp for 15 minutes. After this period 100 µL of Griess reagent were added. The plate was left in a dark place for 10 minutes. The absorbance of the plate was measured at 562 nm.

Chapter 6 - References

6.1 References

[1] V. L. M. Silva, A. M. S. Silva, D. C. G. A. Pinto, N. Jagerovic, L. F. Callado, J. A. S. Cavaleiro, and J. Elguero, "Synthesis and pharmacological evaluation of chlorinated *N*-alkyl-3- and -5-(2-hydroxyphenyl)pyrazoles as CB_1 cannabinoid ligands", *Monatsh. Chem.*, vol. 138, pp. 797–811, 2007.

[2] V. L. M. Silva, A. M. S. Silva, D. C. G. A. Pinto, P. Rodríguez, M. Gómez, N. Jagerovic, L. F. Callado, J. A. S. Cavaleiro, J. Elguero, and J. Fernández-Ruiz, "Synthesis and pharmacological evaluation of new (*E*)- and (*Z*)-3-aryl-4-styryl-1*H*-pyrazoles as potential cannabinoid ligands", *Arkivoc*, vol. 2010, pp. 226–247, 2010.

[3] C. Patterson, "World Alzheimer Report 2018 - The state of the art of dementia research: New frontiers", *Alzheimer's Dis. Int.*, pp. 1–48, 2018.

[4] X. Wang, W. Wang, L. Li, G. Perry, H. gon Lee, and X. Zhu, "Oxidative stress and mitochondrial dysfunction in Alzheimer's disease", *Biochim. Biophys. Acta - Mol. Basis Dis.*, vol. 1842, pp. 1240–1247, 2014.

[5] V. García-Escudero, P. Martín-Maestro, G. Perry, and J. Avila, "Deconstructing mitochondrial dysfunction in Alzheimer's disease", *Oxid. Med. Cell. Longev.*, vol. 2013, 2013.

[6] H. Sies, "Physiological society symposium: Impaired endothlial and smooth muscle cell function in oxidative stress - oxidative stress: Oxidants and antioxidants", *Exp. Physiol.*, vol. 82, pp. 291–295, 1997.

[7] K. Dasuri, L. Zhang, and J. N. Keller, "Oxidative stress, neurodegeneration, and the balance of protein degradation and protein synthesis", *Free Radic. Biol. Med.*, vol. 62, pp. 170–185, 2013.

[8] B. Halliwell and M. Whiteman, "Measuring reactive species and oxidative damage in vivo and in cell culture : how should you do it and what do the results mean?", *Br. J. Pharmacol.*, vol. 142, pp. 231–255, 2004.

[9] C. G.-R. Selva Rivas-Arancibia, E. F.-G. Nancy Gomez-Crisostomo, and L. N. and E. R.-M. Dulce Flores Briseño, "Oxidative Stress and Neurodegenerative Disease", *Oxidative Stress Neurodegener. Dis.*, pp. 53–88, 2011.

[10] S. I. Liochev and I. Fridovich, "Superoxide and iron: partners in crime", *Life*, vol. 48, pp. 157–161, 1999.

[11] S. S. Liang, Y. L. Shiue, C. J. Kuo, S. E. Guo, W. T. Liao, and E. M. Tsai, "Online monitoring oxidative products and metabolites of nicotine by free radicals generation with fenton reaction in tandem mass spectrometry", *Sci. World J.*, vol. 2013, pp. 1–8, 2013.

[12] R. Radi, A. Cassina, R. Hodara, C. Quijano, and L. Castro, "Peroxynitrite reactions and formation in mitochondria", *Free Radic. Biol. Med.*, vol. 33, pp. 1451–1464, 2002.

[13] M. B. Grisham, D. Jourd'Heuil, and D. A. Wink, "Nitric oxide. I. Physiological chemistry of nitric oxide and its metabolites:implications in inflammation", *Am. J. Physiol.*, vol. 276, pp. G315–G321, 1999.

[14] R. Radi, A. Cassina, and R. Hodara, “Nitric oxide and peroxynitrite interactions with mitochondria”, *Biol. Chem.*, vol. 383, pp. 401–409, 2002.

[15] S. B. Nimse and D. Pal, “Free radicals, natural antioxidants, and their reaction mechanisms”, *RSC Adv.*, vol. 5, pp. 27986–28006, 2015.

[16] B. Halliwell, “Oxidative stress and neurodegeneration: Where are we now?”, *J. Neurochem.*, vol. 97, pp. 1634–1658, 2006.

[17] S. Mondragón-Rodríguez, G. Perry, X. Zhu, P. I. Moreira, M. C. Acevedo-Aquino, and S. Williams, “Phosphorylation of tau protein as the link between oxidative stress, mitochondrial dysfunction, and connectivity failure: Implications for Alzheimer’s disease”, *Oxid. Med. Cell. Longev.*, vol. 2013, 2013.

[18] C. Cheignon, M. Tomas, D. Bonnefont-Rousselot, P. Faller, C. Hureau, and F. Collin, “Oxidative stress and the amyloid beta peptide in Alzheimer’s disease”, *Redox Biol.*, vol. 14, pp. 450–464, 2018.

[19] R. Jakob Roetne and H. Jacobsen, “Alzheimer’s disease: From pathology to therapeutic approaches”, *Angew. Chemie - Int. Ed.*, vol. 48, pp. 3030–3059, 2009.

[20] N. N. Nalivaeva and A. J. Turner, “The amyloid precursor protein: A biochemical enigma in brain development, function and disease”, *FEBS Lett.*, vol. 587, pp. 2046–2054, 2013.

[21] V. W. Chow, M. P. Mattson, P. C. Wong, and M. Gleichmann, “An overview of APP processing enzymes and products”, *Neuromolecular Med.*, vol. 12, pp. 1–12, 2010.

[22] R. C. Barber, “The genetics of Alzheimer’s disease”, *Scientifica (Cairo).*, 2012.

[23] J. A. Hardy and G. A. Higgins, “Alzheimer’s disease: The amyloid cascade hypothesis”, *Science*, vol. 256, pp. 184–185, 1992.

[24] A. Tiiman, P. Palumaa, and V. Tõugu, “The missing link in the amyloid cascade of Alzheimer’s disease-metal ions”, *Neurochem. Int.*, vol. 62, pp. 367–378, 2013.

[25] M. Ono, “Development of positron-emission tomography/single-photon emission computed tomography imaging probes for in vivo detection of β-amyloid plaques in Alzheimer’s brains”, *Chem. Pharm. Bull. (Tokyo).*, vol. 57, pp. 1029–1039, 2009.

[26] K. L. Xiong, Q. W. Yang, S. G. Gong, and W. G. Zhang, “The role of positron emission tomography imaging of β-amyloid in patients with Alzheimer’s disease”, *Nucl. Med. Commun.*, vol. 31, pp. 4–11, Jan. 2010.

[27] A. S. Pithadia and M. H. Lim, “Metal-associated amyloid-β species in Alzheimer’s disease”, *Curr. Opin. Chem. Biol.*, vol. 16, pp. 67–73, 2012.

[28] H. N. Wagner, “A Brief History of Positron Emission Tomography (PET)”, *Nucl. Med.*, vol. 18, pp. 213–220, 1998.

[29] P. A. M. Dirac, “A Theory of electrons and protons”, *Proc. R. Soc. A Math. Phys. Eng. Sci.*, vol. 126, pp. 360–365, 1930.

[30] C. D. Anderson, “Energies of cosmic-ray particles”, *Phys. Rev.*, vol. 41, pp. 405–421, 1932.

[31] E. O. Lawrence and S. Livingston, “The production of high speed light ions without the use of high voltages”, *Phys. Rev.*, vol. 40, pp. 19–37, 1932.

[32] D. E. Kuhl and R. Q. Edwards, “Reorganizing data from transverse section scans of the brain using digital processing”, *Radiology*, vol. 91, pp. 975–983, 1968.

[33] M. M. Ter-Pogossian, M. E. Phelps, E. J. Hoffman, and N. A. Mullani, "A Positron-emission transaxial tomograph for nuclear imaging (PETT)", *Radiology*, vol. 114, pp. 89–98, 1975.

[34] Z. Li and P. S. Conti, "Radiopharmaceutical chemistry for positron emission tomography", *Adv. Drug Deliv. Rev.*, vol. 62, pp. 1031–1051, 2010.

[35] R. E. Coleman, "Clinical PET in oncology", *Clin. Positron Imaging*, vol. 1, pp. 15–30, 1998.

[36] C. J. Anderson, J. W. M. Bulte, K. Chen, X. Chen, B. Khaw, M. Shokeen, K. L. Wooley, H. F. VanBrocklin, "Design of targeted cardiovascular molecular imaging probes", *J. Nucl. Med.*, vol. 51, pp. 3S-17S, 2010.

[37] P. S. Murphy, T. J. McCarthy, and A. S. K. Dzik-Jurasz, "The role of clinical imaging in oncological drug development", *Br. J. Radiol.*, vol. 81, pp. 685–692, Sep. 2008.

[38] R. L. Cazzato, J. Garnon, B. Shaygi, G. Koch, G. Tsoumakidou, J. Caudrelier, P. Addeo, P. Bachellier, I. J. Namer, A. Gangi, "PET/CT-guided interventions: Indications, advantages, disadvantages and the state of the art", *Minim. Invasive Ther. Allied Technol.*, vol. 27, pp. 27–32, 2018.

[39] A. Damont, D. Roeda, and F. Dollé, "The potential of carbon-11 and fluorine-18 chemistry: Illustration through the development of positron emission tomography radioligands targeting the translocator protein 18 kDa", *J. Label. Compd. Radiopharm.*, vol. 56, pp. 96–104, 2013.

[40] S. I. Ziegler, "Positron emission tomography: Principles, technology, and recent developments", *Nucl. Phys. A*, vol. 752, pp. 679–687, 2005.

[41] J. Pacák, Z. Tocik, and M. Cerny, "Synthesis of 2 -deoxy-2-fluoro-D-glucose", *Chem. Commun.*, p. 1969, 1969.

[42] T. Ido, C-N. Wan, V. Casella, J. S. Fowler, A. P. Wolf, M. Reivich and D. E. Khul, "Labeled 2-deoxy-D-glucose analogs. ^{18}F-Labeled 2-deoxy-2-fluoro-D-glucose, 2-deoxy-2-fluoro-D-mannose and ^{14}C-2-deoxy-2-fluoro-D-gluocose", *J. Label. Compd. Radiopharm.*, vol. 14, pp. 175–183, 1977.

[43] G. D. Femminella, T. Thayanandan, V. Calsolaro, K. Komici, G. Rengo, G. Corbi and N. Ferrara, "Imaging and molecular mechanisms of Alzheimer's disease: A review", *Int. J. Mol. Sci.*, vol. 19, p. 3702, 2018.

[44] V. Calsolaro and P. Edison, "Alterations in glucose metabolism in Alzheimer's disease", *Recent Pat. Endocr. Metab. Immune Drug Discov.*, vol. 10, pp. 31–39, 2016.

[45] G. Laking and P. Price, "18-Fluorodeoxyglucose positron emission tomography (FDG-PET) and the staging of early lung cancer", *Thorax*, vol. 56, pp. 38–44, 2001.

[46] G. D. Femminella and P. Edison, "Evaluation of neuroprotective effect of glucagon-like peptide 1 analogs using neuroimaging", *Alzheimer's Dement.*, vol. 10, pp. S55–S61, 2014.

[47] Y-Z. Dang, X. Li, Y-X. Ma, X-L. Li, T. Yang, W-L. Lu and S-G. Huang, "^{18}F-FDG-PET/CT-guided intensity-modulated radiotherapy for 42 FIGO III/IV ovarian cancer: A retrospective study", *Oncol. Lett.*, vol. 17, pp. 149–158, 2018.

[48] G. J. Kelloff, J. M. Hoffman, B. Johnson, H. I. Scher, B. A. Siegel, E. Y. Cheng, B. D. Cheson, J. O'shaughnessy, K. Z. Guyton, D. A. Mankoff, L. Shankar, S. M. Larson, C. C. Sigman, R. L. Schilsky and D. C. Sullivan, "Progress and promise of FDG-PET imaging for cancer patient management and oncologic drug development", *Clin Cancer Res*, vol. 11, pp. 2785–2809, 2005.

[49] R. Kloiber, I. L. Koslowsky, I. Tchajkov, and H. R. Rabin, "Pattern-based interpretation criteria for ^{18}F-fludeoxyglucose positron emission tomography/computed tomography in the assessment of pyogenic spine infection", *Can. Assoc. Radiol. J.*, vol. 69, pp. 397–408, Nov. 2018.

[50] C. A. Mathis, B. J. Bacskai, S. T. Kajdasz, M. E. McLellan, M. P. Frosch, B. T. Hyman, D. P. Holt, Y. Wang, G. F. Huang, M. L. Debnath, W. E. Klunk, "A lipophilic thioflavin-T derivative for positron emission tomography (PET) imaging of amyloid in brain", *Bioorg. Med. Chem. Lett.*, vol. 12, pp. 295–298, 2002.

[51] W. E. Klunk, H. Engler, A. Nordberg, Y. Wang, G. Blomqvist, D. P. Holt, M. Bergstrom, I. Savitcheva, G. F. Huang, S. Estrada, B. Ausén, M. L. Debnath, J. Barletta, J. C. Price, J. Sandell, B. J. Lopestri, A. Wall, P. Koivisto, G. Antoni, C. H. Mathis, B. Langstrom, "Imaging brain amyloid in Alzheimer's disease with Pittsburgh Compound-B", *Ann. Neurol.*, vol. 55, pp. 306–319, 2004.

[52] C. C. Rowe, U. Ackerman, W. Browne, R. Mulligan, K. L. Pike, G. O'Keefe, H. Tochon-Danguy, G. Chan, S. U. Berlangieri, G. Jones, K. L. Dickinson-Rowe, H. P. Kung, W. Zhang, M. P. Kung, D. Skovronsky, T. Dyrks, G. Holl, S. Krause, M. Friebe, L. Lehman, S. Lindemann, L. M. Dinkelborg, C. L. Masters and V. L. Villemagne, "Imaging of amyloid β in Alzheimer's disease with 18F-BAY94-9172, a novel PET tracer: proof of mechanism", *Lancet Neurol.*, vol. 7, pp. 129–135, 2008.

[53] J. Lister-James, M. J. Pontecorvo, C. Clark, A. D. Joshi, M. A. Mintun, W. Zhang, N. Lim, Z. Zhuang, G. Golding, S. R. Choi, T. E. Benedum, P. Kennedy, F. Hefti, A. P. Carpenter, H. F. Kung and D. M. Skovronsky, "Florbetapir F-18: A histopathologically validated beta-amyloid positron emission tomography imaging agent", *Semin. Nucl. Med.*, vol. 41, pp. 300–304, 2011.

[54] G. Martínez, R. Vernooij, P. F. Padilla, J. Zamora, X. B. Cosp, and L. Flicker, "^{18}F PET with florbetapir for the early diagnosis of Alzheimer's disease dementia and other dementias in people with mild cognitive impairment (MCI)", *Cochrane Database Syst. Rev.*, pp. 1–64, 2017.

[55] W. Zhang, S. Oya, M. P. Kung, C. Hou, D. L. Maier, and H. F. Kung, "F-18 polyethyleneglycol stilbenes as PET imaging agents targeting Aβ aggregates in the brain", *Nucl. Med. Biol.*, vol. 32, pp. 799–809, 2005.

[56] D. A. Wolk, I. D. Grachev, C. Buckley, H. Kazi, M. S. Grady, J. Q. Trojanowski, R. H. Hamilton, P. Sherwin, R. McLain and S. E. Arnold, "Association between in vivo [^{18}F]-flutemetamol amyloid PET imaging and in vivo cerebral cortical histopathology", *Arch Neurol.*, vol. 68, pp. 1398–1403, 2011.

[57] E. D. Hostetler, S. Sanabria-Bohórquez, H. Fan, Z. Zeng, L. Gammage, P. Miller, S. O'Malley, B. Connolly, J. Mulhearn, S. T. Harrison, S. E. Wolkenberg, J. C. Barrow, D. L. Williams Jr., R. J. Hargreaves, C. Sur and J. J. Cook, "[^{18}F]Fluoroazabenzoxazoles as potential amyloid plaque PET tracers: Synthesis and in vivo evaluation in rhesus monkey", *Nucl. Med. Biol.*, vol. 38, pp. 1193–1203, 2011.

[58] Z. Cselenyi, M. E. Jonhagen, A. Forsberg, C. Halldin, P. Julin, M. Schou, P. Johnstrom, K. Varnas, S. Svensson and L. Farde, "Clinical validation of ^{18}F-AZD4694, an amyloid-beta-specific PET radioligand", *J. Nucl. Med.*, vol. 53, pp. 415–424, 2012.

[59] M. Goedert and M. G. Spillantini, "Propagation of Tau aggregates Tim Bliss", *Mol. Brain*, vol. 10, pp. 1–9, 2017.

[60] L. Knorr, “Einwirkung substituirter Acetessigester auf Phenylhydrazin,” *Ber. Dtsch. Chem. Ges.*, vol. 16, pp. 2597–2599, 1883.

[61] F. Abrigach and R. Touzani, “Pyrazole derivatives with NCN junction and their biological activity: A review”, *Med Chem (Los Angeles)*, vol. 6, pp. 292–298, 2016.

[62] M. Suri, T. Jousseaume, J. J. Neumann, and F. Glorius, “An efficient copper-catalyzed formation of highly substituted pyrazoles using molecular oxygen as the oxidant”, *Green Chem.*, vol. 14, pp. 2193–2196, 2012.

[63] F. F. Noe and L. Fowden, “alpha-Amino-beta-(pyrazolyl-*N*) propionic acid: a New amino-acid from Citrullus vulgaris (Water Melon)”, *Nature*, vol. 183, pp. 1813–1814, 1959.

[64] V. Kumar, K. Kaur, G. K. Gupta, and A. K. Sharma, “Pyrazole containing natural products: Synthetic preview and biological significance”, *Eur. J. Med. Chem.*, vol. 69, pp. 735–753, 2013.

[65] V. L. M. Silva, J. Elguero, and A. M. S. Silva, “Current progress on antioxidants incorporating the pyrazole core”, *Eur. J. Med. Chem.*, vol. 156, pp. 394–429, 2018.

[66] M. S. Abdel-Maksoud, M. I. El-Gamal, M. M. Gamal El-Din, and C. H. Oh, “Design, synthesis, *in vitro* anticancer evaluation, kinase inhibitory effects, and pharmacokinetic profile of new 1,3,4-triarylpyrazole derivatives possessing terminal sulfonamide moiety”, *J. Enzyme Inhib. Med. Chem.*, vol. 34, pp. 97–109, 2019.

[67] B. N. Chowdary, M. Umashankara, B. Dinesh, K. Girish, and A. R. Baba, “Development of 5-(Aryl)-3-phenyl-1*H*-pyrazole derivatives as potent antimicrobial compounds”, *Asian J. Chem.*, vol. 31, pp. 45–50, 2019.

[68] A. Ansari, A. Ali, M. Asif, and Shamsuzzaman, “Review: biologically active pyrazole derivatives”, *New J. Chem.*, vol. 41, pp. 16–41, 2016.

[69] V. V. Prabhu, N. Kannan, and C. Guruvayoorappan, “1,2-Diazole prevents cisplatin-induced nephrotoxicity in experimental rats”, *Pharmacol. Reports*, vol. 65, pp. 980–990, 2013.

[70] N. Alam, J. Bristi, and Rafiquzzaman, “Review on in vivo and in vitro methods evaluation of antioxidant activity”, *Saudi Pharm. J.*, vol. 21, pp. 143–152, 2013.

[71] F. Giornal, S. Pazenok, L. Rodefeld, N. Lui, J. P. Vors, and F. R. Leroux, “Synthesis of diversely fluorinated pyrazoles as novel active agrochemical ingredients”, *J. Fluor. Chem.*, vol. 152, pp. 2–11, 2013.

[72] J. Li, R. S. Daughtersa, C. Bullisb, R. Bengiamina, M. W. Stuckyc, J. Brennanb and D. A. Simone “The cannabinoid receptor agonist WIN 55,212-2 mesylate blocks the development of hyperalgesia produced by capsaicin in rats”, *Pain*, vol. 81, pp. 25–33, 1999.

[73] F. Gonzalez-Rosales and D. Walsh, “Intractable nausea and vomiting due to gastrointestinal mucosal metastases relieved by tetrahydrocannabinol (Dronabinol)”, *J. Pain Symptom Manage.*, vol. 14, pp. 311–314, 1997.

[74] C. M. Williams and T. C. Kirkham, “Anandamide induces overeating: Mediation by central cannabinoid (CB1) receptors”, *Psychopharmacology (Berl).*, vol. 143, pp. 315–317, 1999.

[75] W. B. Mathews, U. Scheffel, P. Finley, H. T. Ravert, R. A. Frank, M. Rinaldi-Carmona, F. Barth and R. F. Dannals, “Biodistribution of [^{18}F] SR144385 and [^{18}F] SR147963: Selective radioligands for

positron emission tomographic studies of brain cannabinoid receptors", *Nucl. Med. Biol.*, vol. 27, pp. 757–762, 2000.

[76] M. Rinaldi-Carmona, F. Barth, M. Hkaulme, D. Shireb, B. Calandrab, C. Congy, S. Martinez, J. Maruani, G. Néliat", D. Caputb, P. Ferrarab, P. Soubrié, J. C. Brelike and G. Le Fura, "SR141716A, a potent and selective antagonist of the brain cannabinoid receptor", *FEBS Lett.*, vol. 350, pp. 240–244, 1994.

[77] F. A. Moreira and J. A. S. Crippa, "The psychiatric side-effects of rimonabant", *Rev. Bras. Psiquiatr.*, vol. 31, pp. 145–153, 2009.

[78] Y. Nojiri, K. Ishiwata, Qinggeletu, S. Tobiishi, T. Sasada, F. Yamamoto, T. Mukai and M. Maeda, "Radiosynthesis and biodistribution in mice of a ^{18}F-labeled analog of O-1302 for use in cerebral CB1 cannabinoid receptor imaging", *Biol Pharm Bull*, vol. 31, pp. 1274–1278, 2008.

[79] Z. Li, A. Gifforda, Q. Liub, R. Thotapallyb, Y.S. Dinga, A. Makriyannisb and S. J. Gatley, "Candidate PET radioligands for cannabinoid CB1 receptors: [^{18}F]AM5144 and related pyrazole compounds", *Nucl. Med. Biol.*, vol. 32, pp. 361–366, 2005.

[80] D. Tang, E. T. McKinley, M. R. Hight, Md. I. Uddin, J. M. Harp, A. Fu, M. L. Nickels, J. R. Buck and H. Charles Manning, "Synthesis and structure-activity relationships of 5,6,7-substituted pyrazolopyrimidines: Discovery of a novel TSPO PET ligand for cancer imaging", *J. Med. Chem.*, vol. 56, pp. 3429–3433, 2013.

[81] J. Zheng, A. Winkeler, M. A. Peyronneau, F. Dollé, and R. Boisgard, "Evaluation of PET imaging performance of the TSPO radioligand [^{18}F]DPA-714 in mouse and rat models of cancer and inflammation", *Mol. Imaging Biol.*, vol. 18, pp. 127–134, 2016.

[82] S. Lavisse, K. Inoue, C. Jan, M. A. Peyronneau, F. Petit, S. Goutal, J. Dauguet, M. Guillermier, F. Dollé, L. Rbah-Vidal, N. Van Camp, R. Aron-Badin, P. Remy and P. Hantraye, "[^{18}F]DPA-714 PET imaging of translocator protein TSPO (18 kDa) in the normal and excitotoxically-lesioned nonhuman primate brain", *Eur. J. Nucl. Med. Mol. Imaging*, vol. 42, pp. 478–494, 2015.

[83] T. Keller, A. Krzyczmonik, S. Forsback, F. R. L. Picón, A. K. Kirjavainen, J. Takkinen, J. Rajander, F. Cacheux, A. Damont, F. Dollé, J. O. Rinne, M. Haaparanta-Solin and O. Solin, "Radiosynthesis and preclinical evaluation of [^{18}F]F-DPA, A novel pyrazolo[1,5-*a*]pyrimidine acetamide TSPO radioligand, in healthy sprague dawley rats", *Mol. Imaging Biol.*, vol. 19, pp. 736–745, 2017.

[84] A. Damont, V. Médran-Navarrete, F. Cacheux, B. Kuhnast, G. Pottier, N. Bernards, F. Marguet, F. Puech, R. Boisgard and F. Dollé "Novel pyrazolo[1,5-*a*]pyrimidines as translocator protein 18 kDa (TSPO) ligands: Synthesis, in vitro biological evaluation, [^{18}F]-labeling, and in vivo neuroinflammation PET images", *J. Med. Chem.*, vol. 58, pp. 7449–7464, 2015.

[85] F. Chauveau, N. Van Camp, F. Dollé, B. Kuhnast, F. Hinnen, A. Damont, H. Boutin, M. James, M. Kassiou and B. Tavitian, "Comparative evaluation of the translocator protein radioligands ^{11}C-DPA-713, ^{18}F-DPA-714, and ^{11}C-PK11195 in a rat model of acute neuroinflammation", *J. Nucl. Med.*, vol. 50, pp. 468–476, 2009.

[86] A. Martín, R. Boisgard, M. Kassiou, F. Dollé, and B. Tavitian, "Reduced PBR/TSPO expression after minocycline treatment in a rat model of focal cerebral ischemia: A PET study using [18F]DPA-714",

Mol. Imaging Biol., vol. 13, pp. 10–15, 2011.

[87] J. Doorduin, H. C. Klein, R. A. Dierckx, M. James, M. Kassiou, and E. F. J. de Vries, "[^{11}C]-DPA-713 and [^{18}F]-DPA-714 as new PET tracers for TSPO: A comparison with [^{11}C]-(R)-PK11195 in a rat model of herpes encephalitis", *Mol. Imaging Biol.*, vol. 11, pp. 386–398, 2009.

[88] L. Sarda-Mantel, J. M. Alsac, R. Boisgard, F. Hervatin, F. Montravers, B. Tavitian, J. B. Michel and D. Le Guludec, "Comparison of ^{18}F-fluoro-deoxy-glucose, ^{18}F-fluoro-methyl-choline, and ^{18}F-DPA714 for positron-emission tomography imaging of leukocyte accumulation in the aortic wall of experimental abdominal aneurysms", *J. Vasc. Surg.*, vol. 56, pp. 765–773, 2012.

[89] G. Pottier, N. Bernards, F. Dollé, and R. Boisgard, "[^{18}F]DPA-714 as a biomarker for positron emission tomography imaging of rheumatoid arthritis in an animal model", *Arthritis Res. Ther.*, vol. 16, pp. 1–10, 2014.

[90] Y. Y. J. Gent, K. Weijers, C. F. M. Molthoff, A. D. Windhorst, M. C. Huisman, M. Kassiou, G. Jansen, A. A. Lammertsma and C. J. van der Laken, "Promising potential of new generation translocator protein tracers providing enhanced contrast of arthritis", *Embase Arthritis Res. Ther.*, vol. 16, pp. 1–9, 2014.

[91] S. Sridharan, F. X. Lepelletier, W. Trigg, S. Banister, T. Reekie, M. Kassiou, A. Gerhard, R. Hinz and H. Boutin, "Comparative evaluation of three TSPO PET radiotracers in a LPS-induced model of mild neuroinflammation in rats", *Mol. Imaging Biol.*, vol. 19, pp. 77–89, 2017.

[92] S. Celen, M. Koole, M. D. Angelis, I. Sannen, S. K. Chitneni, J. Alcazar, S. Dedeurwaerdere, D. Moechars, M. Schmidt, A. Verbruggen, X. Langlois, K. Van Laere, J. I. Andrés and G. Bormans, "Preclinical Evaluation of ^{18}F-JNJ41510417 as a radioligand for PET imaging of phosphodiesterase-10A in the brain," *J. Nucl. Med.*, vol. 51, pp. 1584–1591, 2010.

[93] K. Van Laere, R. U. Ahmad, H. Hudyana, S. Celen, K. Dubois, M. E. Schmidt, G. Bormans and M. Koole, "Human biodistribution and dosimetry of ^{18}F-JNJ42259152, a radioligand for phosphodiesterase 10A imaging", *Eur. J. Nucl. Med. Mol. Imaging*, vol. 40, pp. 254–261, 2013.

[94] S. Khanapur, S. Paul, A. Shah, S. Vatakuti, M. J. B. Koole, R. Zijlma, R. A. J. O. Dierckx, G. Luurtsema, P. Garg, A. van Waarde and P. H. Elsinga, "Development of [^{18}F]-labeled pyrazolo[4,3-*e*]-1,2,4-triazolo[1,5-*c*]pyrimidine (SCH442416) analogs for the imaging of cerebral adenosine A_{2A} receptors with positron emission tomography", *J. Med. Chem.*, vol. 57, pp. 6765–6780, 2014.

[95] S. Khanapur, A. van Waarde, R. A. J. O. Dierckx, P. H. Elsinga, and M. J. B. Koole, "Preclinical evaluation and quantification of ^{18}F-fluoroethyl and ^{18}F-fluoropropyl analogs of SCH442416 as radioligands for PET imaging of the adenosine A_{2A} receptor in rat brain", *J. Nucl. Med.*, vol. 58, pp. 466–472, 2017.

[96] J. Xu, H. Liu, G. Li, Y. He, R. Ding, X. Wang, M. Feng, S. Zhang, Y. Chen, S. Li, M. Zhao, Y. Li, C. Qi and Y. Dang, "^{18}F-labeled pyrazolo[1,5-*a*]pyrimidine derivatives: Synthesis from 2,4-dinitrobenzamide and tosylate precursors and comparative biological evaluation for tumor imaging with positron emission tomography," *Molecules*, vol. 17, pp. 3774–3793, 2012.

[97] E. Chang, H. Liu, K. Unterschemmann, P. Ellinghaus, S. Liu, V. Gekeler, Z. Cheng, D. Berndorff, S. S. Gambhir, "^{18}F-FAZA PET imaging response tracks the reoxygenation of tumors in mice upon

treatment with the mitochondrial complex I inhibitor bay 87-2243", *Clin. Cancer Res.*, vol. 21, pp. 335–346, 2015.

[98] V. J. Majo, V. Arango, N. R. Simpson, J. Prabhakaran, S. A. Kassir, M. D. Underwood, M. Bakalian, P. Canoll, J. J. Mann, J. S. D. Kumar, "Synthesis and in vitro evaluation of [^{18}F]BMS-754807: A potential PET ligand for IGF-1R", *Bioorg. Med. Chem. Lett.*, vol. 23, pp. 4191–4194, 2013.

[99] M. J. Uddin, B. C. Crews, K. Ghebreselasie, I. Huda, P. J. Kingsley, M. S. Ansari, M. N. Tantawy, J. Reese and L. J. Marnett, "Fluorinated COX-2 inhibitors as agents in PET imaging of inflammation and cancer", *Cancer Prev. Res.*, vol. 4, pp. 1536–1545, 2011.

[100] O. Prante, R. Tietze, C. Hocke, S. Löber, H. Hübner, T. Kuwert, P. Gmeiner, "Synthesis, radiofluorination, and in vitro evaluation of pyrazolo[1,5-*a*]pyridine-based dopamine D4receptor ligands: Discovery of an inverse agonist radioligand for PET", *J. Med. Chem.*, vol. 51, pp. 1800–1810, 2008.

[101] A. C. Tomé. Introdução à nomenclatura dos compostos orgânicos. *Editora UA ed* **2004**.

[102] V. L. M. Silva, A. M. S. Silva, D. C. G. A. Pinto, J. A. S. Cavaleiro, A. Vasas, T. Patonay, " Syntheses of (*E*)- and (*Z*)-3-styrylchromones", *Monatsh. Chem.* vol. 139, pp.1307–1315, 2008.

[103] A. Sandulache, A. M. S. Silva, D. C. G. A. Pinto, J. A. S. Cavaleiro, L. M. P. M. Almeida, Wittig reactions of chromone-3-carboxaldehydes with benzylidenetriphenyl phosphoranes: a new synthesis of 3-styrylchromones, *New J. Chem*., vol. 27, pp. 1592-1598, 2003.

[104] V. L. M. Silva, A. M. S. Silva, Diana C. G. A. Pinto, José A. S. Cavaleiro and J. Elguero, "3(5)-(2-Hydroxyphenyl)-5(3)-styrylpyrazoles: Synthesis and Diels-Alder transformations", *Eur. J. Org. Chem.* pp. 4348-4356, 2004.

[105] V. L. M. Silva, A. M. S. Silva, D. C. G. A. Pinto, J. A. S. Cavaleiro, J. Elguero, Synthesis of (*E*)- and (*Z*)-3(5)-(2-hydroxyphenyl)-4-styrylpyrazoles, *Monatsh. Chem.*, vol. 140, pp. 87–95, 2009.

[106] A. Cano, "An end-point method for estimation of the total antioxidant activity in plant material", *Phytochem. Anal.*, vol. 9, pp. 196–202, 1998.

[107] J. A. Friederich and J. Butterworth, "Sodium nitroprusside: Twenty years and counting", *Anesth. Analg.*, vol. 81, pp. 152–162, Aug. 1995.

[108] W. M. Partridge, "Peptide Drug Delivery to the Brain", Raven Press: New York, 2001

[109] V. L. M. Silva, "Síntese e transformação de 3-estirilcromonas e 3-(2-hidroxifenil)pirazóis com potencial actividade analgésica", Tese de Doutoramento, Universidade de Aveiro, pp. 148, 2006.

[110] M. D. Catarino, A. M. S. Silva, M. T. Cruz, S. M. Cardoso, "Antioxidant and anti-inflammatory activities of Geranium robertianum L. decoctions", *Food Funct.*, vol. *8*, pp. 3355-3365, 2017.

[111] G. Yen, P. Duht, "Scavenging Effect of Methanolic Extracts of Peanut Hulls on Free-Radical and Active-Oxygen Species", *J. Agric. Food Chem.* vol. 42, pp. 629-632, 1994.

[112] P. Griess, "Bemerkungen zu der Abhandlung der HH. Weselsky und Benedikt, Ueber einige Azoverbindungen", *Ber. Dtsch Chem. Ges.* vol.12, pp. 426-428, 1879.